UNIVERSITAT POLITÈCNICA DE CATALUNYA BARCELONATECH

Analysis of the cardiovascular response to autonomic nervous system modulation in Brugada syndrome patients

Mireia Calvo González

UNIVERSITAT POLITÈCNICA DE CATALUNYA

Ph.D. program in Biomedical Engineering

Analysis of the cardiovascular response to autonomic nervous system modulation in Brugada syndrome patients

Mireia Calvo González

Supervisors:
Dr. Pedro Gomis
Dr. Alfredo Hernández

Thesis submitted for the joint Ph.D. degree in Biomedical Engineering by the Universitat Politècnica de Catalunya and in Signal Processing by the Université de Rennes 1

Acknowledgements

I would like to express my deepest sense of gratitude to my supervisors: *Alfredo Hernández*, for his enthusiasm, immense knowledge and brilliant ideas; *Pedro Gomis*, for his valuable guidance not only throughout this thesis, but since my academic studies from which we still enjoy fruitful collaborations, for having encouraged me to pursue a doctoral degree in France; and *Virginie Le Rolle*, for her constant support, valuable advice, continuous availability and infinite patience for deeply revising this thesis and all the associated scientific publications. I would also like to express my sincere appreciation to *Daniel Romero*, the last, but not least, component of the Brugada team. I thank them all for our stimulating discussions, as well as for their kindness and priceless advice both on my PhD research, but also on my professional career.

I gratefully acknowledge the financial support allowing this research, provided by the *Fédération Hospitalo-Universitaire de Technologies pour la Santé*, in France, and by the *Obra social la Caixa*, in Spain; being part of such a brilliant and inspiring community is a tremendous privilege.

I am indebted to all students and staff members of the LTSI, for making me feel at home in my daily work. Special thanks to *Lotfi Senhadji* for warmly welcoming me in his research laboratory, and to *Patricia*, *Muriel*, and *Soizic* for their logistic support, organizational skills and cheerful disposition. To my *bureau* 508 colleagues *Nadine*, *Matthieu* and, again, *Daniel*, for being the best labmates to share the final sprint with. For their help and support, the long afternoons spent working together, and for all the fun we have had in the last year. But also to *Juan*, *Héctor* and *David*, for the great moments shared at the beginning of this journey.

A huge thank you to my friends outside the laboratory, to the new ones, for the experiences shared in this wonderful country and to elders, for staying present and continuously supporting me despite the distance. Special thanks to my beloved *Elena* and *Estefanía*, for being the best examples of friendship anyone could ever dream of.

Y a mi querida familia, para la que no existen suficientes palabras de agradecimiento; por entender mis ausencias y ser mi mayor apoyo a pesar de la distancia. En especial a mi madre y a mi hermano, por ser mi pilar y ejemplo a seguir en la vida, por proporcionarme todas las facilidades que me han permitido lograr mis objetivos y por vivir mis logros con la misma intensidad e ilusión que los suyos propios. Pero también a mi cuñada, a mi abuelo, a mis primos, tíos y familia venezolana, por su cariño y apoyo incondicional. A *Diego*, por haberse convertido en mi principal apoyo en todos los sentidos, contagiándome su energía y afán de superación. Y a mi padre, ya que nada de esto habría sido posible sin su ejemplar esfuerzo y contagiosa perseverancia a lo largo de su vida.

Abstract

Brugada syndrome (BS) is a genetic arrhythmogenic disease characterized by a distinctive electrocardiographic pattern, associated with a high risk for sudden cardiac death (SCD) due to ventricular fibrillation (VF) in absence of structural cardiopathies. Its complex and multifactorial nature turns risk stratification into a major challenge. Although variations in autonomic modulation are commonly related to arrhythmic events in this population, novel markers with higher predictive values are still needed so as to identify those patients at high risk.

The autonomic function can be better characterized through the application of standardized maneuvers stimulating the autonomic nervous system (ANS), such as exercise testing or the head-up tilt (HUT) test. This PhD thesis is based on the hypothesis that a thorough analysis of the ANS response of BS patients may provide additional information to improve risk stratification in this population. The main objective is thus to evaluate the cardiovascular response to ANS modulations on a clinical database composed of BS patients with different levels of risk (symptomatic and asymptomatic subjects), using different autonomic maneuvers, in order to identify novel potential markers for risk stratification.

In this context, the autonomic function was assessed by three main approaches. First, through the characterization and comparison of previously described methods capturing heart rate complexity, baroreflex sensitivity, and non-stationary heart rate variability, never before studied in the context of BS patients; in order to identify new markers capable of distinguishing between symptomatic and asymptomatic patients. According to the results, a lower variability and complexity overnight, as well as a higher vagal tone and a lower sympathetic activity both during exercise and HUT testing, was observed in the symptomatic group.

In a second analysis, in order to address the multifactorial nature of the disease, a multivariate approach based on a step-based machine learning method was introduced. By employing features extracted at signal-processing analysis, robust classifiers capable of identifying patients at high risk were proposed. The classifier based on autonomic features extracted during nighttime analysis presented the best performance ($AUC = 95\%$), improving previously reported predictive models of risk in BS based on non-invasive parameters.

Finally, the third part of this work was focused on the implementation of novel mathematical models and the associated model analysis methods, so as to study the autonomic mechanisms regulating the mechanical and circulatory functions of the cardiovascular system in this population. First, by the integration and evaluation of a computational model capturing the cardiovascular system's dynamics and its autonomic regulation in response to HUT testing. Likewise, a second

model-based approach based on a recursive identification of the sympathetic and parasympathetic contributions to ANS regulation was proposed in order to estimate the time-varying autonomic response to exertion and subsequent recovery. The results showed a reduced contractility function, as well as a significantly greater parasympathetic activity during exercise, in symptomatic patients. Finally, in order to combine characteristics extracted from model-based approaches, a prospective study introduced a multivariate classifier based on estimated model parameters.

Overall, the obtained results indicate significant trends of clinical relevance that provide new insights into the underlying autonomic mechanisms regulating the cardiovascular system in BS, improving physiopathology and prognosis interpretation, with a potential future impact on diagnostic and therapeutic strategies. The proposed approach may be used as an instrument for the identification of those asymptomatic patients at high risk who may benefit from a cardioverter defibrillator implantation.

Resumen

El síndrome de Brugada (SB) es una enfermedad genética asociada a un patrón electrocardiográfico característico y a un elevado riesgo de muerte súbita cardíaca (MSC), causada por fibrilación ventricular (FV) en ausencia de cardiopatías estructurales. Debido a su naturaleza compleja y multifactorial, la estratificación del riesgo supone, en la actualidad, uno de los aspectos más controvertidos. Ciertas alteraciones en la modulación del sistema nervioso autónomo (SNA) se han relacionado con eventos arrítmicos en esta población; no obstante, nuevos marcadores con valores predictivos más elevados que permitan identificar a aquellos pacientes con un alto riesgo de sufrir MSC son todavía necesarios.

El uso de maniobras estandarizadas con el objetivo de estimular el SNA permite una mejor caracterización de la función autonómica. El principal objetivo de esta tesis doctoral es, por tanto, la evaluación exhaustiva de la respuesta cardiovascular a la modulación del SNA en una serie de pacientes con SB y diferentes niveles de riesgo (sujetos sintomáticos y asintomáticos), a través de diferentes maniobras autonómicas, con la finalidad de identificar nuevos marcadores potencialmente útiles para la estratificación de riesgo en esta población.

En este contexto, la evaluación de la función autonómica se llevó a cabo mediante tres estrategias principales. En primer lugar, se caracterizaron y compararon la variabilidad y complejidad del ritmo cardíaco, así como la sensibilidad barorrefleja, en pacientes sintomáticos y asintomáticos, con el objetivo de identificar nuevos marcadores capaces de distinguir entre grupos de pacientes. Los resultados mostraron, en el grupo sintomático, una menor variabilidad y complejidad durante la noche, así como un mayor tono vagal y una menor actividad simpática tanto durante el ejercicio como en respuesta a la prueba de mesa inclinada.

En un segundo análisis, se abordó la etiología multifactorial del síndrome mediante un enfoque multivariado basado en un método de aprendizaje automático por etapas. A partir de marcadores extraídos en la etapa anterior, se propusieron modelos predictivos capaces de clasificar pacientes diagnosticados con SB en función de su nivel de riesgo. El mejor clasificador ($AUC = 95\,\%$) fue diseñado a partir de marcadores autonómicos obtenidos durante la noche, superando modelos predictivos previamente descritos para la estratificación del riesgo en el SB a partir de la combinación de parámetros no invasivos.

Finalmente, se analizaron las interacciones entre las funciones mecánica, circulatoria y autonómica de estos pacientes a partir de modelos fisiológicos. En primer lugar, mediante la implementación y evaluación de un modelo computacional integrando la dinámica del sistema cardiovascular y su respuesta autonómica a la prueba de mesa inclinada. Asimismo, se propuso la

identificación recursiva de un modelo implementado para el análisis de la evolución temporal de las contribuciones simpática y parasimpática del SNA durante una prueba de esfuerzo. Los resultados mostraron una menor contractilidad, así como una actividad parasimpática significativamente mayor durante el ejercicio, en pacientes sintomáticos. Con el objetivo de combinar características extraídas del modelado fisiológico, un último estudio prospectivo propuso el diseño de un clasificador multivariado integrando los parámetros estimados en esta última etapa.

Los resultados obtenidos indican importantes tendencias de relevancia clínica que aportan nuevos conocimientos sobre los mecanismos autonómicos encargados de regular el sistema cardiovascular en el SB. Su interpretación permite mejorar la estratificación del riesgo en estos pacientes y, por tanto, optimizar las estrategias terapéuticas aplicadas. La metodología propuesta se presenta como un instrumento para la identificación de aquellos pacientes con alto riesgo de MSC que podrían beneficiarse de la implantación de desfibriladores automáticos.

Résumé

Le syndrome de Brugada (BS) est une maladie cardiaque caractérisée par la survenue d'une syncope ou mort subite, provoquées par une arythmie cardiaque, chez les patients avec un cœur structurellement normal, mais présentant des altérations électrocardiographiques spécifiques. Cependant, ces modifications sont intermittentes et varient avec la température ou les traitements appliqués, ce qui rend particulièrement difficile le diagnostic chez un patient donné. En outre, elles sont fortement modulées par le système nerveux autonome (SNA), partie du système nerveux périphérique responsable de la régulation des organes internes. Les défibrillateurs implantables (DI) sont le traitement principal pour les patients symptomatiques, c'est-à-dire les patients documentés d'arythmie ventriculaire, syncope ou ayant survécu à un épisode de mort subite. Cependant, la décision d'implanter un DI peut être très difficile pour des patients asymptomatiques sans antécédents familiaux de morte subite.

Dans ce contexte, l'objectif de la thèse était d'améliorer la compréhension de l'influence du SNA chez les patients souffrant du BS. Une méthodologie globale fusionnant traitement du signal, *machine learning* et modélisation a été proposée durant la thèse. Cette chaine de traitement originale a pu être mise en œuvre sur trois bases de données de patients BS symptomatiques et asymptomatiques. Les bases de données cliniques utilisées dans ce travail sont le résultat d'une étude prospective, multicentrique dont l'objectif était de provoquer des modifications de l'activité du SNA chez les patients BS. L'acquisition des données s'est déroulée entre 2009 et 2013 dans le service de cardiologie du CHU de Rennes et les participants provenaient de 8 hôpitaux français situés à La Rochelle, Angers, Bordeaux, Brest, Nantes, Rennes, Poitiers et Tours. Afin de caractériser les patients présentant différents niveaux de risque, les participants ont été classés en patients symptomatiques et asymptomatiques, selon leurs historiques cliniques. Les patients symptomatiques devaient présenter les symptômes documentés suivants : arrêt cardiaque dû à une fibrillation ventriculaire, syncopes, vertiges, palpitations et convulsions nocturnes.

La base de données est constituée des ECG (12 dérivations) de 87 patients, collectés pendant 24 heures, incluant un test d'orthostatisme (tilt-test) et une épreuve d'effort. L'acquisition était réalisée à l'aide d'un moniteur Holter (ELA medical, Sorin Group, Le Plessis Robinsson, France) à une fréquence d'échantillonnage de 1000 Hz. Par ailleurs, des tilt-tests ont été réalisés sur 32 patients en mesurant de manière non-invasive la pression artérielle et l'ECG avec le moniteur Task Force (CN Systems, Graz, Autriche) à une fréquence d'échantillonnage de 100 Hz et 1000 Hz, respectivement. Des signaux ECG à 12 dérivations échantillonnés à 1000 Hz ont été acquis chez 36 autres patients BS lors d'un test d'exercice avec le moniteur ECG (Cardionics, Webster,

Texas). Par conséquent, l'analyse de l'activité du système nerveux autonome est basée sur 3 périodes différentes : 1) une épreuve d'effort, 2) un test d'orthostatisme (tilt-test) et 3) un recueil de données pendant la nuit.

La réponse du système nerveux autonome, à ces trois tests, a tout d'abord été évaluée avec des méthodes d'estimation du gain du baroréflexe, de variabilité et de complexité cardiaque. L'une des difficultés du traitement des signaux associés à l'épreuve d'effort et au test d'orthostatisme réside dans leurs natures non-stationnaires. L'analyse spectrale de ces signaux nécessite la mise en œuvre d'outils spécifiques permettant de décrire une évolution temporelle des caractéristiques fréquentielles. Des analyses temps-fréquence, basées sur la transformée de Wigner-Ville, ont ainsi été utilisées afin d'étudier conjointement, le contenu spectral des signaux, et leurs évolutions temporelles. Cependant, ces méthodes classiques d'analyse de la variabilité cardiaque ne permettent pas de capturer la non-linéarité de la dynamique cardiovasculaire. Ainsi, des méthodes spécifiques d'analyse de la complexité des séries cardiaques ont pu être utilisées. La sensibilité du baroréflexe de ces patients a été évaluée à partir de différentes méthodes proposées dans la littérature. Une série d'indices a ainsi été déduite des signaux avant d'être analysée pour trouver des différences significatives entre les patients symptomatiques et asymptomatiques. Les résultats ont mis en évidence que les indices calculés chez les patients symptomatiques sont associés à une baisse de la variabilité et de la complexité cardiaque pendant la nuit. Par ailleurs, pendant le test d'exercice, les patients symptomatiques ont montré une activité vagale augmentée et un tonus sympathique réduit. Lors de la réponse au tilt-test, les patients symptomatiques ont présenté une augmentation du tonus parasympathique et une réduction de l'équilibre sympatho-vagal par rapport aux patients asymptomatiques.

L'étiologie multifactorielle du BS nécessite l'utilisation d'approches complexes capables de capturer les multiples mécanismes sous-jacents à la maladie. Ainsi, une analyse multivariée a été réalisée à partir de la série d'indices calculés précédemment. L'approche globale, basée sur des méthodes de *machine learning*, permet de combiner de manière optimale les indices autonomiques extraits précédemment, afin de concevoir des classificateurs capables de différencier les patients BS, en fonction de leur symptomatologie. La sélection de ces indicateurs autonomiques, permettant une meilleure caractérisation du BS, peut être difficile surtout lorsque le nombre de sources dépasse la quantité d'observations et que les variabilités entre patients sont significatives. Ainsi, une approche robuste basée sur un processus de sélection de paramètres en deux étapes a été mise en œuvre. La méthodologie proposée a été optimisée, évaluée et comparée sur les données extraites lors de différents tests autonomiques. Les résultats montrent que le meilleur classificateur ($AUC = 95\%$) a été conçu à partir de marqueurs autonomiques obtenus pendant la nuit, améliorant des modèles prédictifs décrits précédemment pour la stratification du risque dans le BS à partir de la combinaison de paramètres non invasifs.

Bien que l'analyse multivariée proposée montre une amélioration des performances de classification par rapport à la littérature, les méthodes utilisées n'intègrent pas de connaissance physiologique dans le traitement des données. Or le BS étant une pathologie complexe et multifactorielle, l'utilisation de modèles mathématiques de connaissance peut s'avérer pertinente car

cela permet l'intégration d'information physiologique dans le traitement des données et l'analyse de mécanismes sous-jacents qui sont difficiles ou impossibles à observer en clinique avec des méthodes non-invasives, comme le tonus vagal ou sympathique. Une analyse à base de modèle a été proposée durant la thèse afin : 1) d'étudier la réponse autonomique et hémodynamique au test d'orthostatisme chez des sujets sains et des patients BS, 2) de simuler les réponses vagales et sympathiques durant l'épreuve d'effort chez les patients BS symptomatiques et asymptomatiques.

Concernant l'étude de la réponse au test d'orthostatisme, un modèle a été proposé de manière à intégrer les représentations : i) de l'activité électrique cardiaque, ii) de la mécanique des ventricules et des oreillettes, iii) des circulations systémique et pulmonaire et iv) du baroréflexe incluant les voies vagale et sympathique. Le modèle complet permet de simuler les réponses hémodynamiques et autonomiques au test d'orthostatisme. Des analyses de sensibilité, basées sur des méthodes globales et de criblage, ont mis en évidence l'importance de certains paramètres du baroréflexe et en lien avec la description des propriétés diastoliques des ventricules. Ces paramètres ont pu être identifiés, à l'aide d'algorithmes évolutionnaires, afin de créer des modèles spécifiques-patients de 8 sujets sains et 12 patients BS. Les résultats ont montré des différences significatives concernant la réponse sympathique au tilt-test entre sujets sains et BS. Par ailleurs, les patients symptomatiques et asymptomatiques sont associés des modifications significatives des paramètres diastoliques ventriculaires.

Concernant les simulations de la réponse autonomique durant l'épreuve d'effort, un algorithme d'identification récursif a pu être mis en œuvre sur un modèle composé des cavités cardiaques, des circulations systémique et pulmonaire, couplées au baroréflexe. L'identification récursive réalisée sur le modèle a permis une estimation des activités vagale et sympathique durant l'effort chez 13 patients BS symptomatiques et 31 asymptomatiques. Les patients symptomatiques ont montré une élévation significative de l'activité vagale, spécialement à la fin de l'échauffement. Les analyses réalisées sur les modèles proposés, concernant le test d'orthostatisme et l'épreuve d'effort, ont permis une exploration de variables physiologiques, difficilement observables. Les résultats obtenus avec les modèles mettent en évidence des modifications de la réponse hémodynamique cardiaque et confirment des modifications de la balance sympatho-vagale entre les patients symptomatiques et asymptomatiques.

En résumé, les résultats obtenus mettent en évidence un déséquilibre de la balance sympatho-vagale entre les patients symptomatiques et asymptomatiques et montrent l'utilité des indices de variabilité cardiaque pour la classification des patients en fonction de la symptomatologie. Les résultats obtenus sont cohérents avec la littérature, rapportant un tonus vagal plus élevé, ainsi qu'une activité sympathique, variabilité et complexité cardiaques plus faibles, chez les patients symptomatiques. Des études précédentes ont rapporté que la plupart des événements cardiaques majeurs se produisent au repos et pendant le sommeil, ainsi que l'apparition des altérations électrocardiographiques caractéristiques du BS augmente avec la stimulation vagale. Les résultats obtenus pendant la nuit, lorsque l'activité parasympathique est prédominante, ont montré des résultats particulièrement pertinents pour la différentiation des populations de patients. De plus, étant donnée qu'il existe une activité parasympathique significativement plus élevée chez les

patients symptomatiques pendant les tests d'exercice et d'orthostatisme par rapport aux sujets asymptomatiques, les résultats soulignent le rôle de l'analyse du tonus vagal pour la stratification du risque dans cette population. Enfin, l'analyse basée sur un modèle du système cardiovasculaire a permis de mettre en évidence des différences concernant les propriétés diastoliques cardiaques et la réponse du baroréflexe pendant le test d'orthostatisme. L'ensemble des résultats de la thèse permet une meilleure caractérisation des profils autonomiques des patients atteints du syndrome de Brugada et laisse envisager une amélioration de la sélection des patients pour implantation d'un DI.

Contents

List of acronyms

ANS	Autonomic nervous system
AP	Action potential
ARP	Absolute refractory period
AUC	Area under the ROC curve
AV(N)	Atrioventricular (node)
BRS	Baroreflex sensitivity
BS	Brugada syndrome
CES	Cardiac electrical system
CNS	Central nervous system
CVS	Cardiovascular system
EA	Evolutionary algorithms
ECG	Electrocardiogram
EDPVR	End Diastolic Pressure-Volume Relationship
EDR	ECG-derived respiration
EPS	Electrophysiological study
ESPVR	End Systolic Pressure-Volume Relationship
HF	High frequency
HIP	Hydrostatic indifference point
HR	Heart rate
HRC	Heart rate complexity
HRV	Heart rate variability

HUT(T) Head-up tilt (test)

ICD Implantable cardioverter defibrillator

k-NN k nearest neighbors

LA Left atrium

LBB Left bundle branch

LBH Lower bundle of His

LDA Linear discriminant analysis

LF Low frequency

LP Late potentials

LV Left ventricle

NE Norepinephrine

PNS Peripheral nervous system

PSD Power spectral density

PV Pressure-Volume

PVS Programmed ventricular stimulation

RA Right atrium

RBB(B) Right bundle branch (block)

RRP Relative refractory period

RV Right ventricle

RVOT Right ventricular outflow tract

SA(N) Sinoatrial (node)

(S)BP (Systolic) blood pressure

SCD Sudden cardiac death

SDD Slow diastolic depolarization

SNS Somatic nervous system

SPWVD Smoothed Pseudo Wigner Ville distribution

SUNDS Sudden unexplained nocturnal death syndrome

SW Stroke work

TF Time-frequency

UBH Upper bundle of His

UDP Upstroke depolarization period

ULF Ultra low frequency

VA Ventricular arrhythmias

VF Ventricular fibrillation

VLF Very low frequency

VT Ventricular tachycardia

CHAPTER 1

Introduction

Brugada syndrome (BS) is a genetic arrhythmogenic disorder presenting an abnormal pattern on the electrocardiogram (ECG), characterized by a distinctive ST-segment elevation in right precordial leads; associated with a high risk for unexpected sudden cardiac death (SCD) due to ventricular fibrillation (VF) in absence of structural cardiopathies (Priori et al., 2015; Priori et al., 2013). Since its first description in 1992 as a distinct clinical entity (Brugada et al., 1992), BS continues to spark research interest due to its high incidence, particularly in Southeast Asia, and due to its association with SCD in young adults and, less frequently, in children and infants. The syndrome is estimated to be responsible for at least 4% of the total amount of SCD and for 20% of SCD in structurally normal hearts (Antzelevitch, 2005; Brugada et al., 1998).

After diagnosis, implantable cardioverter defibrillators (ICD) are the only proven effective treatment thus far. These devices can detect and revert most life-threatening ventricular arrhythmias by delivering electrical shocks. However, they can present some complications, such as inappropriate discharges or risks related to surgery (Miyazaki et al., 2013). According to international guidelines (Priori et al., 2015), ICD implantation is recommended in BS patients having survived from an SCD and/or having a history of spontaneous sustained ventricular arrhythmias (VA), and should be considered in subjects with a spontaneous type 1 Brugada-like ECG pattern presenting documented syncopes of ventricular origin. However, the decision of implanting an ICD on asymptomatic patients is still complex, since they present a relatively low risk for cardiac events, estimated at less than 1% (Probst et al., 2010).

Although the prognostic value for VF occurrence of several methods has been evaluated, studies based on the largest clinical series have only confirmed two reliable predictors: spontaneous type 1 Brugada-like ECG pattern and documented symptoms (Antzelevitch, 2005; Probst et al., 2010). As a consequence, risk stratification in order to determine the best therapeutic strategy for asymptomatic patients still remains challenging, even if they represent around 60% of diagnosed patients.

The autonomic nervous system (ANS) plays a determinant role in the pathophysiology, arrhythmogenesis and prognosis of the disease. Major cardiac events in BS most commonly occur during parasympathetic dominance at rest or during sleep (KIES et al., 2004; MATSUO et al., 1999) and studies based on positron emission tomography have confirmed autonomic dysfunctions in this population (KIES et al., 2004; PAUL et al., 2011; WICHTER et al., 2002). Thus, indicators capturing changes in ANS modulation may provide useful knowledge for the prediction of VF occurrence at follow-up. However, previous studies on the autonomic function of BS patients have lead to conflicting results when based on long-term measurements (BEHAR et al., 2016; HERMIDA et al., 2003; KOSTOPOULOU et al., 2010; KRITTAYAPHONG et al., 2003; NAKAZAWA et al., 2003; PIERRE et al., 2007; TOKUYAMA et al., 2014). In order to better characterize autonomic modulation, standard maneuvers, such as physical stress testing or the head-up tilt (HUT) test, can be applied. Indeed, some studies have already reported the potential of exercise testing (AMIN et al., 2009; MAKIMOTO et al., 2010; SUBRAMANIAN et al., 2017), among other autonomic tests (BIGI et al., 2008; IKEDA et al., 2006), for the prediction of cardiac events in BS.

Nevertheless, the multifactorial etiology of BS requires complex approaches capable of capturing multiple mechanisms underlying the pathology. Accordingly, previous works based on multivariate analysis have proposed predictive models combining several indicators in order to assess VF risk in BS patients (DELISE et al., 2014, 2011; KAWAZOE et al., 2016; OKAMURA et al., 2015). Moreover, since experimental data represent indirect estimations of the regulatory mechanisms involved in the cardiovascular system, the selection of those indicators best explaining the syndrome can be challenging, especially when the number of sources exceeds the amount of observations, in a biomedical context where intra- and inter-patient variabilities are significant.

Another limitation of previous methods applied to study the autonomic response in BS patients is that they are based on generic models assuming strong hypotheses about data statistical properties, and do not integrate explicit biological and/or physiological *a priori* knowledge. Although some approaches based on the simulation of Brugada syndrome through mathematical models have been proposed (CLANCY et al., 2002; HOOGENDIJK et al., 2011; MIYOSHI et al., 2003; XIA et al., 2006), they are focused on an electrophysiological perspective. The description of computational models integrating physiological knowledge on interactions between the cardiac function, the circulatory system and the ANS could be a step forward towards the understanding of autonomic modulation in BS.

In this contex, the main objective of this work is the assessment of the autonomic function in Brugada syndrome through the application of previously described methods and the development of novel approaches better accounting for the complexity and multifactorial nature of biomedical signals. These methods include signal processing, machine learning and model-based techniques evaluated on clinical databases composed of cardiovascular signals from subjects at different levels of risk (symptomatic and asymptomatic BS patients), acquired for 24 hours including exercise testing and a head-up tilt test. The description of new biomarkers capable of identifying a high-risk group of patients could provide new insights into the underlying autonomic mechanisms regulating the cardiovascular system in BS, improving physiopathology and prognosis interpretation, with a

potential future impact on therapeutic strategies for these patients. Figure 1.1 represents the global methodological approach developed in this thesis, decomposed in four main chapters.

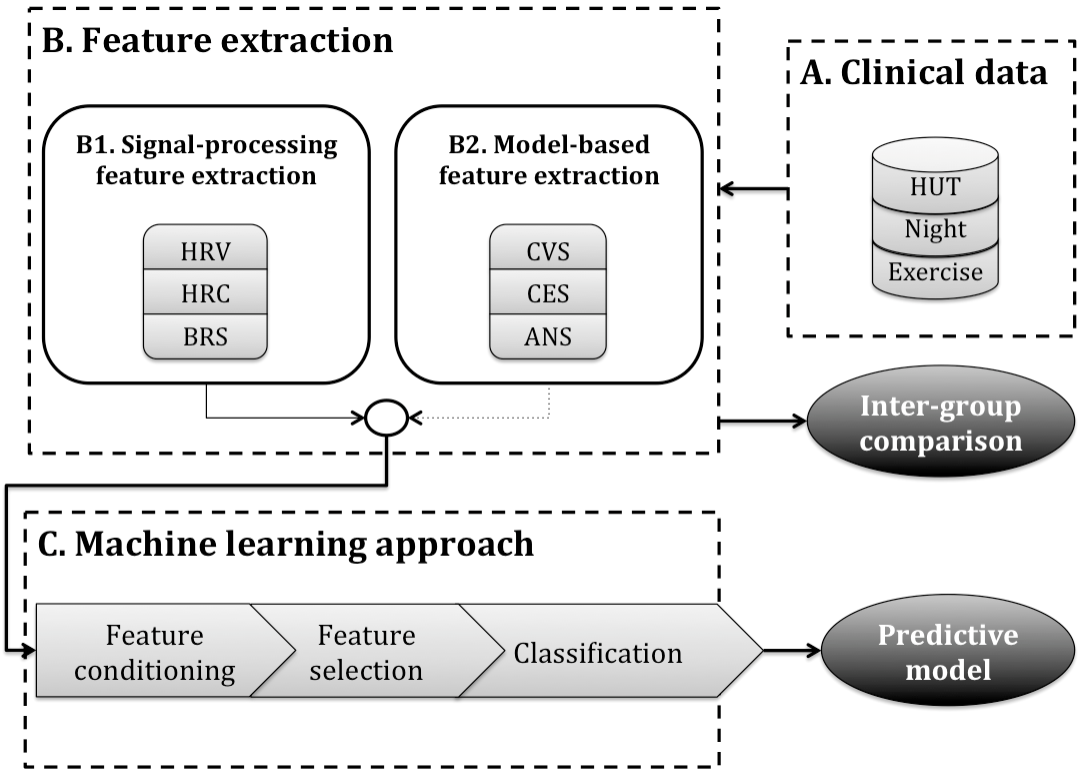

FIGURE 1.1– Global methodological approach to study the autonomic function of BS patients. A) Cardiovascular signals are obtained from clinical databases acquired overnight and during exercise and head-up tilt (HUT) testing on BS patients. B) Feature extraction is divided in two major blocks: B1) signal-processing feature extraction, where heart rate variability (HRV), heart rate complexity (HRC) and baroreflex sensitivity (BRS) parameters are estimated; and B2) model-based feature extraction, where patient-specific models integrating the cardiovascular system (CVS), the cardiac electrical system (CES) and the autonomic nervous system (ANS) are identified. First, extracted features are compared between symptomatic and asymptomatic groups of patients. C) In a second phase, these same parameters are included in a step-based machine learning approach in order to design predictive models capable of identifying patients at high risk of SCD.

The next chapter provides the clinical context in which this thesis is framed. After a brief review about cardiovascular physiology and its regulation through the autonomic nervous system, a general overview of the BS, including diagnostic criteria, epidemiology, genetic basis, risk stratification, clinical management, as well as a state-of-the-art review of the autonomic function in this population, is presented. Finally, the clinical databases exploited in this research, containing cardiovascular signals overnight and during different autonomic tests (Figure 1.1A), are described.

Chapter 3 focuses on the application of signal processing methods to evaluate the autonomic function of BS patients (Figure 1.1B1), by estimating their heart rate variability (HRV), heart rate complexity (HRC) and baroreflex sensitivity (BRS). Symptomatic and asymptomatic groups

of patients are characterized and compared in order to identify markers presenting significant differences between groups that could provide useful information for the detection of patients at high risk for major cardiac events.

However, since univariate analyses are unable to capture the multifactorial nature of the syndrome, chapter 4 proposes a multivariate approach based on a step-based machine learning method (Figure 1.1C) exploiting the features extracted in the previous chapter, in order to improve classification performance.

In chapter 5, a system-level model-based approach is developed so as to study not only the autonomic function of BS patients, but also their underlying mechanic and circulatory characteristics (Figure 1.1B2). By means of a thorough sensitivity analysis and model-parameter identifications, patient-specific models integrating the cardiovascular response to the autonomic modulation during HUT testing are implemented. Moreover, a recursive model to estimate the time-varying autonomic response to exercise is introduced. Finally, a prospective application based on a multivariate classifier combining features extracted from model-based approaches is introduced (dotted arrow in Figure 1.1).

References

AMIN, A. S., E. A. DE GROOT, J. M. RUIJTER, A. A. WILDE, and H. L. TAN (2009). "Exercise-Induced ECG Changes in Brugada Syndrome". In: *Circulation: Arrhythmia and Electrophysiology* 2.5, pp. 531–539.

ANTZELEVITCH, C. (2005). "Heart Rhythm Society; European Heart Rhythm Association. Brugada syndrome: report of the second consensus conference: endorsed by the Heart Rhythm Society and the European Heart Rhythm Association". In: *Circulation* 111.5, pp. 659–670.

BEHAR, N., B. PETIT, V. PROBST, F. SACHER, G. KERVIO, J. MANSOURATI, P. BRU, A. HERNANDEZ, and P. MABO (2016). "Heart rate variability and repolarization characteristics in symptomatic and asymptomatic Brugada syndrome". In: *Europace*, euw224.

BIGI, M. A. B., A. ASLANI, and A. ASLANI (2008). "Significance of cardiac autonomic neuropathy in risk stratification of Brugada syndrome". In: *Europace* 10.7, pp. 821–824.

BRUGADA, J., R. BRUGADA, and P. BRUGADA (1998). "Right bundle-branch block and st-segment elevation in leads V1 through V3 a marker for sudden death in patients without demonstrable structural heart disease". In: *Circulation* 97.5, pp. 457–460.

BRUGADA, P. and J. BRUGADA (1992). "Right bundle branch block, persistent ST segment elevation and sudden cardiac death: a distinct clinical and electrocardiographic syndrome: a multicenter report". In: *Journal of the American College of Cardiology* 20.6, pp. 1391–1396.

CLANCY, C. E. and Y. RUDY (2002). "Na+ channel mutation that causes both Brugada and long-QT syndrome phenotypes". In: *Circulation* 105.10, pp. 1208–1213.

DELISE, P., G. ALLOCCA, N. SITTA, and P. DI STEFANO (2014). "Event rates and risk factors in patients with Brugada syndrome and no prior cardiac arrest: a cumulative analysis of the

largest available studies distinguishing ICD-recorded fast ventricular arrhythmias and sudden death". In: *Heart Rhythm* 11.2, pp. 252–258.

Delise, P., G. Allocca, E. Marras, C. Giustetto, F. Gaita, L. Sciarra, L. Calo, A. Proclemer, M. Marziali, L. Rebellato, et al. (2011). "Risk stratification in individuals with the Brugada type 1 ECG pattern without previous cardiac arrest: usefulness of a combined clinical and electrophysiologic approach". In: *European heart journal* 32.2, pp. 169–176.

Hermida, J.-S., A. Leenhardt, B. Cauchemez, I. Denjoy, G. Jarry, F. Mizon, P. Milliez, J.-L. Rey, P. Beaufils, and P. Coumel (2003). "Decreased nocturnal standard deviation of averaged NN intervals". In: *European heart journal* 24.22, pp. 2061–2069.

Hoogendijk, M. G., M. Potse, A. Vinet, J. M. de Bakker, and R. Coronel (2011). "ST segment elevation by current-to-load mismatch: an experimental and computational study". In: *Heart Rhythm* 8.1, pp. 111–118.

Ikeda, T., A. Abe, S. Yusu, K. Nakamura, H. Ishiguro, H. Mera, M. Yotsukura, and H. Yoshino (2006). "The full stomach test as a novel diagnostic technique for identifying patients at risk of Brugada syndrome". In: *Journal of cardiovascular electrophysiology* 17.6, pp. 602–607.

Kawazoe, H., Y. Nakano, H. Ochi, M. Takagi, Y. Hayashi, Y. Uchimura, T. Tokuyama, Y. Watanabe, H. Matsumura, S. Tomomori, et al. (2016). "Risk stratification of ventricular fibrillation in Brugada syndrome using noninvasive scoring methods". In: *Heart Rhythm* 13.10, pp. 1947–1954.

Kies, P., T. Wichter, M. Schäfers, M. Paul, K. P. Schäfers, L. Eckardt, L. Stegger, E. Schulze-Bahr, O. Rimoldi, G. Breithardt, et al. (2004). "Abnormal myocardial presynaptic norepinephrine recycling in patients with Brugada syndrome". In: *Circulation* 110.19, pp. 3017–3022.

Kostopoulou, A., M. Koutelou, G. Theodorakis, A. Theodorakos, E. Livanis, T. Maounis, A. Chaidaroglou, D. Degiannis, V. Voudris, D. Kremastinos, et al. (2010). "Disorders of the autonomic nervous system in patients with Brugada syndrome: a pilot study". In: *Journal of cardiovascular electrophysiology* 21.7, pp. 773–780.

Krittayaphong, R., G. Veerakul, K. Nademanee, and C. Kangkagate (2003). "Heart rate variability in patients with Brugada syndrome in Thailand". In: *European Heart Journal* 24.19, pp. 1771–1778.

Makimoto, H., E. Nakagawa, H. Takaki, Y. Yamada, H. Okamura, T. Noda, K. Satomi, K. Suyama, N. Aihara, T. Kurita, et al. (2010). "Augmented ST-segment elevation during recovery from exercise predicts cardiac events in patients with Brugada syndrome". In: *Journal of the American College of Cardiology* 56.19, pp. 1576–1584.

Matsuo, K., T. Kurita, M. Inagaki, M. Kakishita, N. Aihara, W. Shimizu, A. Taguchi, K. Suyama, S. Kamakura, and K. Shimomura (1999). "The circadian pattern of the development of ventricular fibrillation in patients with Brugada syndrome". In: *European heart journal* 20.6, pp. 465–470.

MIYAZAKI, S., T. UCHIYAMA, Y. KOMATSU, H. TANIGUCHI, S. KUSA, H. NAKAMURA, H. HACHIYA, M. ISOBE, K. HIRAO, and Y. IESAKA (2013). "Long-term complications of implantable defibrillator therapy in Brugada syndrome". In: *The American journal of cardiology* 111.10, pp. 1448–1451.

MIYOSHI, S., H. MITAMURA, K. FUJIKURA, Y. FUKUDA, K. TANIMOTO, Y. HAGIWARA, M. ITA, and S. OGAWA (2003). "A mathematical model of phase 2 reentry: role of L-type Ca current". In: *American Journal of Physiology-Heart and Circulatory Physiology* 284.4, H1285–H1294.

NAKAZAWA, K., T. SAKURAI, A. TAKAGI, R. KISHI, K. OSADA, T. NANKE, F. MIYAKE, N. MATSUMOTO, and S. KOBAYASHI (2003). "Autonomic imbalance as a property of symptomatic Brugada syndrome". In: *Circulation journal* 67.6, pp. 511–514.

OKAMURA, H., T. KAMAKURA, H. MORITA, K. TOKIOKA, I. NAKAJIMA, M. WADA, K. ISHIBASHI, K. MIYAMOTO, T. NODA, T. AIBA, et al. (2015). "Risk stratification in patients with Brugada syndrome without previous cardiac arrest". In: *Circulation Journal* 79.2, pp. 310–317.

PAUL, M., M. MEYBORG, P. BOKNIK, U. GERGS, W. SCHMITZ, G. BREITHARDT, T. WICHTER, and J. NEUMANN (2011). "Autonomic dysfunction in patients with Brugada syndrome: further biochemical evidence of altered signaling pathways". In: *Pacing and Clinical Electrophysiology* 34.9, pp. 1147–1153.

PIERRE, B., D. BABUTY, P. PORET, C. GIRAUDEAU, O. MARIE, P. COSNAY, and L. FAUCHIER (2007). "Abnormal nocturnal heart rate variability and QT dynamics in patients with Brugada syndrome". In: *Pacing and clinical electrophysiology* 30.s1, S188–S191.

PRIORI, S. G., C. BLOMSTRÖM-LUNDQVIST, A. MAZZANTI, N. BLOM, M. BORGGREFE, J. CAMM, P. ELLIOTT, D. FITZSIMONS, R. HATALA, G. HINDRICKS, et al. (2015). "Task Force for the Management of Patients with Ventricular Arrhythmias and the Prevention of Sudden Cardiac Death of the European Society of Cardiology (ESC). 2015 ESC guidelines for the management of patients with ventricular arrhythmias and the prevention of sudden cardiac death: the Task Force for the Management of Patients with Ventricular Arrhythmias and the Prevention of Sudden Cardiac Death of the European Society of Cardiology (ESC) endorsed by: Association for European Paediatric and Congenital Cardiology (AEPC)". In: *Europace* 17, pp. 1601–1687.

PRIORI, S. G., A. A. WILDE, M. HORIE, Y. CHO, E. R. BEHR, C. BERUL, N. BLOM, J. BRUGADA, C.-E. CHIANG, H. HUIKURI, et al. (2013). "Executive summary: HRS/EHRA/APHRS expert consensus statement on the diagnosis and management of patients with inherited primary arrhythmia syndromes". In: *Europace* 15.10, pp. 1389–1406.

PROBST, V., C. VELTMANN, L. ECKARDT, P. MEREGALLI, F. GAITA, H. TAN, D. BABUTY, F. SACHER, C. GIUSTETTO, E. SCHULZE-BAHR, et al. (2010). "Long-term prognosis of patients diagnosed with Brugada syndrome results from the FINGER Brugada Syndrome Registry". In: *Circulation* 121.5, pp. 635–643.

SUBRAMANIAN, M., M. A. PRABHU, M. S. HARIKRISHNAN, S. S. SHEKHAR, P. G. PAI, and K. NATARAJAN (2017). "The Utility of Exercise Testing in Risk Stratification of Asymptomatic

Patients with type 1 Brugada Pattern". In: *Journal of Cardiovascular Electrophysiology* 28, pp. 677–683.

Tokuyama, T., Y. Nakano, A. Awazu, Y. Uchimura-Makita, M. Fujiwra, Y. Watanabe, A. Sairaku, K. Kajihara, C. Motoda, N. Oda, et al. (2014). "Deterioration of the circadian variation of heart rate variability in Brugada syndrome may contribute to the pathogenesis of ventricular fibrillation". In: *Journal of cardiology* 64.2, pp. 133–138.

Wichter, T., P. Matheja, L. Eckardt, P. Kies, K. Schäfers, E. Schulze-Bahr, W. Haverkamp, M. Borggrefe, O. Schober, G. Breithardt, et al. (2002). "Cardiac autonomic dysfunction in Brugada syndrome". In: *Circulation* 105.6, pp. 702–706.

Xia, L., Y. Zhang, H. Zhang, Q. Wei, F. Liu, and S. Crozier (2006). "Simulation of Brugada syndrome using cellular and three-dimensional whole-heart modeling approaches". In: *Physiological measurement* 27.11, pp. 1125–1142.

CHAPTER 2

Brugada syndrome and autonomic nervous system modulation

This chapter describes the clinical context in which this thesis is framed. First, a brief review on the physiological basis of the cardiovascular system and its modulation through the autonomic nervous system is introduced. Then, a general overview of the disease under study, the Brugada syndrome, is presented. This genetic disorder is characterized by a distinctive electrocardiographic pattern, associated with an elevated risk for sudden cardiac death due to malignant ventricular arrythmias in patients having structurally normal hearts. The complexity and multifactorial nature of its prognosis turns risk stratification into a major challenge nowadays. Since autonomic nervous system (ANS) modulation plays a significant role in the pathophysiology, arrhythmogenesis and prognosis of the disease, the application of specific maneuvers stimulating the ANS, such as exercise or the head-up tilt (HUT) test, could improve autonomic assessment and, thus, risk stratification in BS. Therefore, the last section is dedicated to the description of the clinical databases applied in this research, containing cardiovascular signals overnight and during exercise and HUT testing, in order to assess the autonomic function of BS patients at different levels of risk.

2.1. Neural regulation of the cardiovascular system

2.1.1. The cardiovascular system

The cardiovascular system (CVS) is a closed circulatory system mainly composed of the heart, blood vessels and blood. Its function is to transport nutrients, oxygen, carbon dioxide, hormones, and blood cells throughout the organism in order to provide nourishment, protect from diseases, regulate body temperature and pH, and maintain homeostasis.

2.1.1.1. Circulatory physiology

The CVS is divided in two circulatory paths: pulmonary and systemic circulations (GUYTON et al., 2006). In the former, oxygen-deprived blood is pumped from the heart to the lungs, via the pulmonary artery, and returns, oxygenated, back into the heart through the pulmonary vein. On the other hand, systemic circulation transports oxygenated blood from the heart to the rest of the body, via the aorta, and returns oxygen-poor blood back into the heart through the venae cavae.

Arteries, which are vessels with muscular and elastic thick walls, branch into smaller structures called arterioles and then into capillaries, which are tiny extremely thin-walled vessels connecting arterial and venous systems. After their passage through body tissues to exchange gases and nutrients, capillaries merge again into venules and then into veins, which are thin-walled vessels resisting lower pressures than arteries. Figure 2.1 illustrates the cardiovascular system, where blue represents oxygen-poor and CO_2-rich blood circulation, whereas red refers to oxygen-rich and CO_2-poor blood.

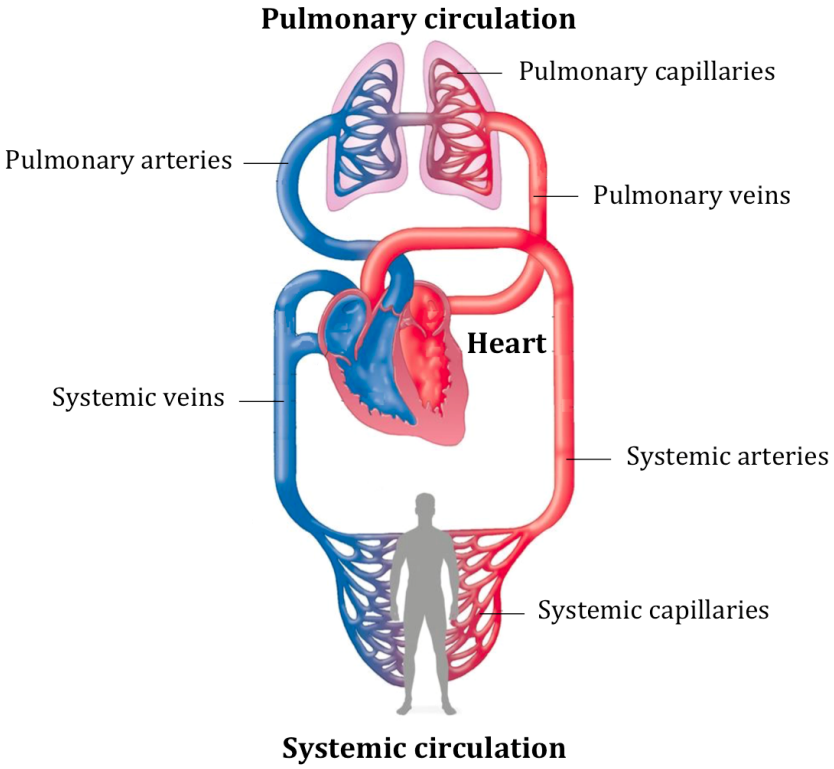

FIGURE 2.1– Cardiovascular system, composed of the heart and the pulmonary and systemic circulations.

Blood pressure reflects the force exerted by circulating blood on the walls of blood vessels, usually refering to systemic arterial pressure. In most clinical applications, it is expressed by the systolic and diastolic pressures, which account for the pressure measured during ventricular contraction (systole), and during ventricular relaxation (diastole), respectively.

2.1.1.2. Anatomy of the heart

The heart is a muscular organ pumping blood through the circulatory system. It is composed of four chambers: two atria and two ventricles. The right atrium (RA) receives deoxygenated blood from the systemic circulation, through the superior and inferior venae cavae; while oxygenated blood arrives to the left atrium (LA) back from the lungs, through the pulmonary veins (Whitaker, 2014).

Atrioventricular valves connect atria and ventricles, ensuring unidirectional blood flows. The tricuspid valve separates the RA from the right ventricle (RV), whereas the mitral valve separates the left heart. Two additional semilunar valves are located at the exit of each ventricle to prevent blood backflow: the pulmonary valve between the RV and the pulmonary artery, and the aortic valve between the left ventricle (LV) and the aorta. Both atria and ventricles are separated by the interatrial and interventricular septums, respectively. Figure 2.2 displays the main anatomical structures of the heart.

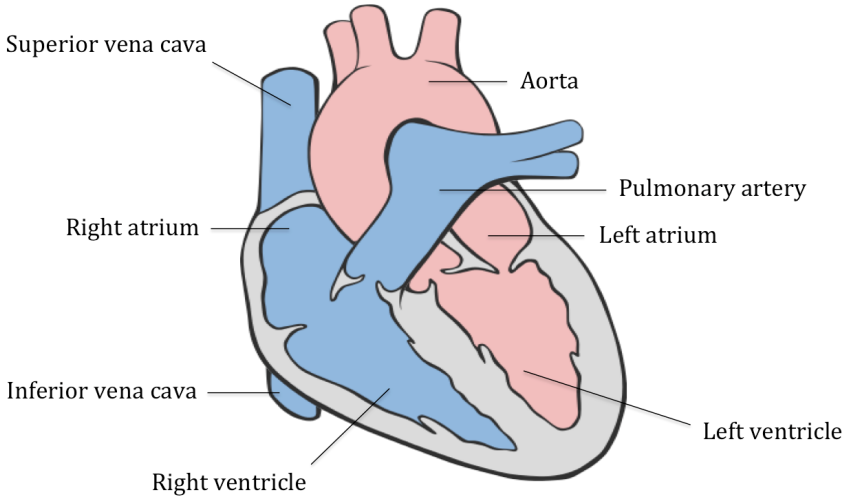

Figure 2.2– Anatomical structure of the heart.

Each cardiac cycle begins with both atria and ventricles relaxed. Since blood circulates from areas of higher to lower pressures, atria begin to fill until pressure rises and blood moves into the ventricles. Likewise, this causes ventricular pressure to rise, which leads to the contraction of ventricles in order to pump blood from the RV into the pulmonary artery, as well as from the LV into the aorta. This mechanical cardiac cycle is controlled by the electrical activity generated at the cellular level.

2.1.1.3. Cardiac electrical conduction

In normal conditions, the heart rhythm is established by the sinoatrial (SA) node, the heart's pacemaker, where an electrical impulse causing heart muscles to contract is generated and propagated through the heart (Anderson et al., 2009).

This electrical impulse, known as the action potential (AP), excites the RA and travels through Bachmann's bundle to simultaneously excite the LA. Then, it propagates through internodal pathways in the RA to the atrioventricular (AV) node. From this node, the impulse travels through the bundle of His and down the bundle branches on either side of the interventricular septum: the right bundle branch (RBB) and the left bundle branch (LBB). Both branches lead into the Purkinje fibers that finally transmit the electrical impulse to the muscle tissue (myocardium) of the ventricles. Figure 2.3 illustrates the cardiac electrical conduction pathway.

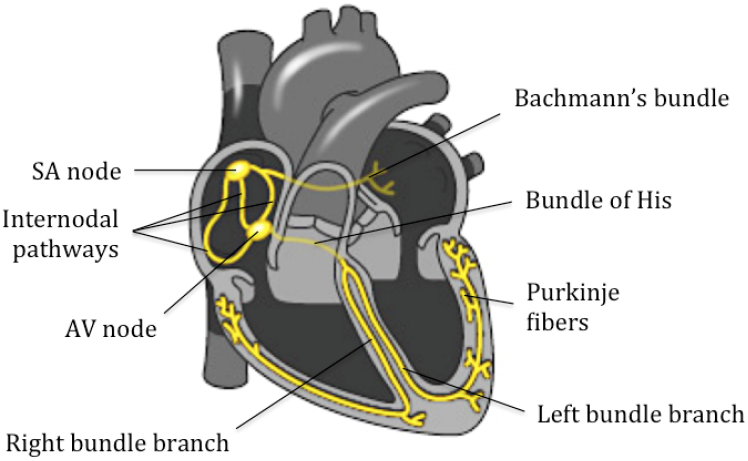

FIGURE 2.3– Cardiac electrical conduction system.

In the cellular level, the cardiac AP is composed of the following 5 phases (NERBONNE et al., 2005), represented in Figure 2.4 for both nodal and myocardial cell types:

- **Phase 0.** When cardiac cells are in resting state, their membranes are negatively charged. However, a rapid influx of sodium (Na^+) ions causes the membrane potential to become positive. This phenomenon is called depolarization and, in pacemaker cells, occurs spontaneously. In ventricular cells, though, this fast depolarization or fast flow of Na^+ ions into the cell is caused by the electrical excitation of nearby cells.

- **Phase 1.** Only in non-pacemaker cells, the rapid inactivation of Na^+ channels followed by an outgoing flow of potassium (K^+) ions causes a brief repolarization where the membrane potential slightly becomes more negative. This is referred to as a *notch* on the AP waveform.

- **Phase 2.** Known as the *plateau* phase due to a nearly balanced charge caused by the influx of calcium (Ca^{2+}) ions and the outgoing flow of K^+ ions, the membrane potential of non-pacemaker cells remains relatively constant.

- **Phase 3.** When Ca^{2+} channels close, the positive outward current of K^+ ions that remains causes a negative change in the membrane potential and, thus, a rapid repolarization. Once

the cell is sufficiently negatively charged, K^+ channels close and membrane potential is restored to a resting value.

- **Phase 4.** It refers to the resting state, when the cell is more easily excitable.

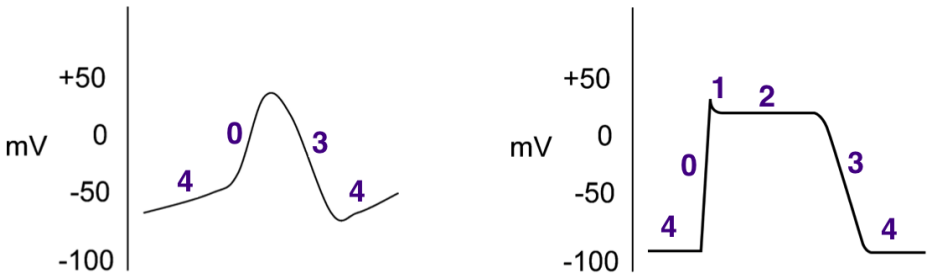

FIGURE 2.4– Phases of the action potential from a SA node (left) and a ventricular (right) cell.

Depolarization causes Na^+ channels to close and inactivate. The refractory period of a cardiac cell is the time from phase 0 until the next possible depolarization. Indeed, different degrees of refractoriness are encountered during an AP, depending on the amount of Na^+ channels no longer inactivated and capable of reopening. During the absolute refractory period (ARP), which starts with phase 0 until halfway of phase 3, channels cannot be opened regardless of the strength of the stimulus received. The ARP is immediately followed, until the end of phase 3, by the relative refractory period (RRP), during which a stronger-than-usual stimulus can initiate another AP. This is due to the membrane potential's hyperpolarization caused by the leaking of K^+ ions at the end of phase 3, which opens the inactivation gates of Na^+ channels, but still leaves those channels closed.

2.1.1.4. The electrocardiogram

The electric currents generated during the depolarization and repolarization phases of myocardial cells can be detected and recorded by placing surface electrodes on the thorax. This measurable cardiac electrical activity is known as the electrocardiogram (ECG) and is composed of three main parts: the P wave (atrial depolarization), the QRS complex (ventricular depolarization) and the T wave (ventricular repolarization).

From the time difference between consecutive QRS complex locations (RR intervals), heart rate can be estimated. In addition, from the heartbeart waveform, the following segments and intervals can be measured (Figure 2.5):

- **PR interval**. It is the time between P-wave onset and the beginning of the QRS complex, and it represents the time the electrical impulse takes to travel from the SA node through the AV node.
- **PR segment**. It is measured between the end of P wave and QRS-complex onset, and it reflects the duration of depolarization through the AV node.

- **ST segment**. It is the time between the end of the QRS complex and T-wave onset, and it represents the time during which the ventricles are depolarized. In normal conditions, it should be isoelectric. The J wave is a positive deflection occurring at the junction between the QRS complex and the ST segment (MARUYAMA et al., 2004), where the S point, also known as the J point, has a myocardial infarction-like, or Brugada-like, elevation.

- **QT interval**. It is measured between QRS-complex onset and the end of the T wave and indicates the duration of ventricular depolarization and repolarization.

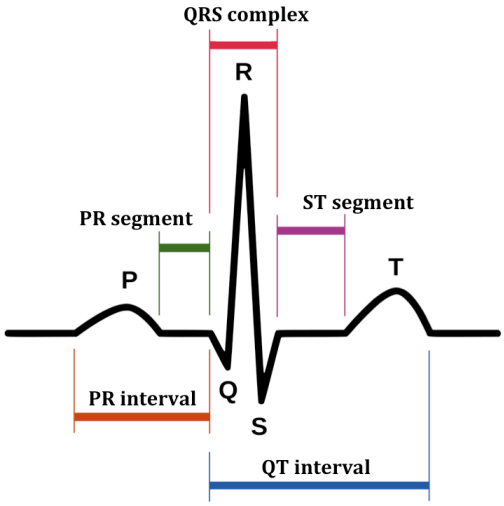

FIGURE 2.5– Main waves, intervals and segments measured in a normal ECG waveform.

In a conventional 12-lead ECG, 10 electrodes are placed on the patient's limbs and chest, their locations being specified in Table 2.1. The overall magnitude of the heart's electrical potential is then measured from 12 different angles or leads: three bipolar limb leads (I, II, III), three augmented limb leads (aVL, aVR, aVF) and six precordial leads (V1-V6).

Limb leads are bipolar measures calculated by comparing two electrodes located at different sides of the heart, in this case, on different limbs: right arm (RA), left arm (LA) and left leg (LL). These locations define the Einthoven's triangle, drawn around the area of the heart (Figure 2.6a). Lead I is recorded by placing the negative terminal of the electrocardiograph on the RA and the positive terminal on the LA. In lead II, the negative terminal is connected to the RA and the positive terminal to the LL; and in lead III, the positive terminal stays in the LL, while the negative terminal is placed on the LA. Einthoven's law states that if the electrical potentials of any two of the three bipolar limb leads are known at any given instant, the third one can be determined mathematically (GUYTON et al., 2006).

The second group of typically used leads consists of the unipolar augmented limb leads. In this case, two limbs are connected to the negative terminal of the electrocardiograph, and the third limb is connected to the positive terminal. When this positive terminal is on the RA, the

TABLE 2.1– Electrodes placement on a conventional 12-lead ECG recording.

Electrode name	**Electrode placement**
RA	Right arm
LA	Left arm
RL	Right leg
LL	Left leg
V1	Fourth intercostal space, at the right border of the sternum
V2	Fourth intercostal space, at the left border of the sternum
V3	Midway between V2 and V4
V4	Fifth intercostal space, at the mid-clavicular line
V5	Horizontally even with V4, at the anterior axillary line
V6	Horizontally even with V4 and V5, at the mid-axillary line

lead is known as the aVR lead; when on the LA, the aVL lead; and when on the LL, the aVF lead. Based on Einthoven's law, they can be determined mathematically from bipolar limb leads as follows:

- Lead aVL $= -\mathrm{I} - \dfrac{\mathrm{II}}{2}$
- Lead aVR $= \dfrac{-\mathrm{I} + \mathrm{II}}{2}$
- Lead aVF $= -\mathrm{II} - \dfrac{\mathrm{I}}{2}$

Finally, precordial leads (Figure 2.6b) are unipolar measures compared to a reference lead, typically the Wilson's central terminal (WCT), calculated as the centroid of the Einthoven's triangle: WCT$= \dfrac{1}{3}(\mathrm{RA} + \mathrm{LA} + \mathrm{LL})$.

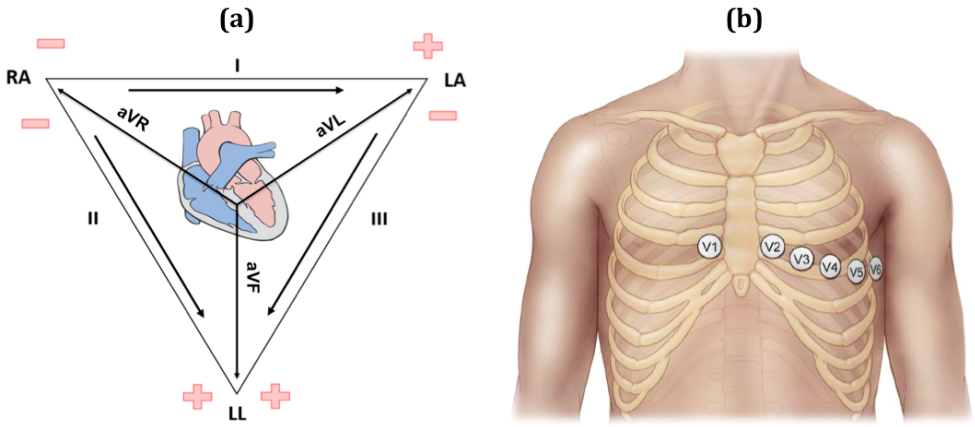

FIGURE 2.6– a) Einthoven's triangle and representation of the bipolar (I, II , III) and augmented (aVL, aVR, aVF) limb leads. b) Precordial leads placement on the thorax.

2.1.2. The nervous system

The nervous system is a complex network of billions of nerve cells called neurons that, together with the brain and spinal cord, monitor and control body functions by sending, receiving and interpreting information from the entire organism (Guyton et al., 2006). It is subdivided in the following subsystems:

- **The Central Nervous System (CNS)**, composed of the brain and spinal cord, and responsible for the supervision and coordination of the entire nervous system.
- **The Peripheral Nervous System (PNS)**, which consists of glands and nerves, in order to connect and transport information between the CNS and any part of the body. Nerves transmitting signals from the brain are called motor or efferent nerves, while those transmitting information from the body to the CNS are sensory or afferent nerves. The PNS is likewise divided into:
  - **The somatic nervous system (SNS)**, which is composed of the nerves that mediate voluntary movement, and thus that innervate skeletal muscles and external sensory organs such as the skin.
  - **The autonomic nervous system (ANS)**, which innervates internal organs and glands, in order to regulate involuntary body functions. It is further divided in the enteric, sympathetic and parasympathetic nervous systems. The former regulates bowel motility in digestion; the sympathetic nervous system is generally activated in cases of stress such as exercise to mobilize energy; and the parasympathetic nervous system is activated when organisms are in a relaxed state, in order to save energy.

2.1.2.1. Autonomic nervous system

The ANS regulates internal body functions such as the heart rate or respiration. It is mainly divided in two complementary branches: the sympathetic and the parasympathetic systems.

In general, each effector organ is connected with its respective sympathetic and/or parasympathetic system through preganglionic and postganglionic neurons, synapsed together in the autonomic ganglia (Figure 2.7). All preganglionic neurons are cholinergic, since they release a neurotransmitter called acetylcholine (Ach). In the parasympathetic system and in some cases of the sympathetic system, postganglionic neurons are also cholinergic. However, most sympathetic postganglionic neurons are adrenergic, since they release norepinephrine (NE).

Both sympathetic and parasympathetic systems can cause excitatory or inhibitory responses, depending on the effector organ's receptors. Moreover, for those organs having both sympathetic and parasympathetic innervations, their respective functions are typically opposed and it is the balance of the relative sympathetic to parasympathetic tone which dictates the organ action. For example, sympathetic stimulation of the SA node increases heart rate (HR), while parasympathetic stimulation does the contrary. Thus, the actual heart rate depends on the relative balance between these two systems.

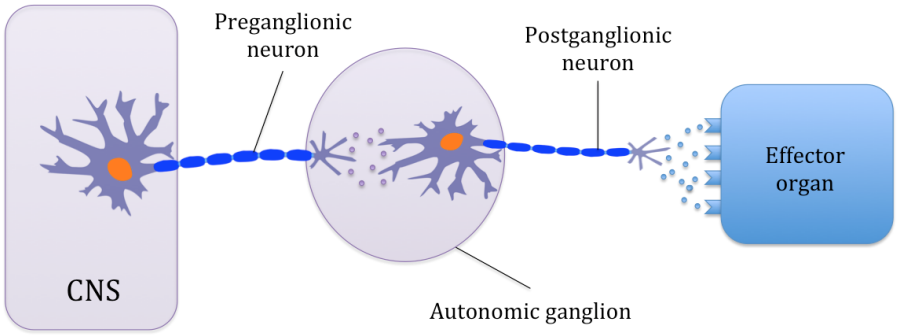

FIGURE 2.7– Neural connection between the central nervous system (CNS) and effector organs by the sympathetic and parasympathetic branches, through preganglionic and postganglionic neurons, synapsed together in the autonomic ganglia.

2.1.2.2. Autonomic regulation of the cardiovascular system

Autonomic nervous system controls the cardiovascular system by innervating the heart with both sympathetic and parasympathetic neurons, as well as blood vessels through the sympathetic system, in order to regulate heart rate and blood pressure (THOMAS, 2011).

On the one hand, parasympathetic neurons release acetylcholine, a cholinergic hormone that activates muscarinic M2-receptors on the heart, causing HR to decrease by slowing down nodal conduction. This phenomenon is known as the negative chronotropic effect. Hyperstimulation of the parasympathetic influence on the heart promotes bradyarrhythmias, predisposing to conduction block at the AV node. Since parasympathetic innervation is mainly provided by the vagus nerve, parasympathetic tone is commonly referred to as vagal tone. At rest, although both sympathetic and parasympathetic tones are exerted on the heart, vagal tone predominates.

On the other hand, sympathetic neurons release norepinephrine (NE), a catecholamine, which activates β_1 receptors on the heart, causing the following effects:

- **Chronotropic.** It increases heart rate, by rising SA node discharge rate.
- **Dromotropic.** It speeds up conduction through the AV node.
- **Inotropic.** It increases cardiac contractility.
- **Lusitropic.** It causes a faster relaxation after contraction.

Regarding blood vessels, sympathetic neurons also cause vasoconstriction and, thus, a blood pressure rise through the increase of peripheral resistance. In the closed-loop system formed by both autonomic and cardiovascular systems, the short-term regulation of blood pressure is known as the baroreflex arc (Figure 2.8). The nervous signals coming from arterial baroreceptors are transmitted to the ANS centers, which modulate heart rate, cardiac contractility and blood vessels resistance through the sympathetic and parasympathetic systems.

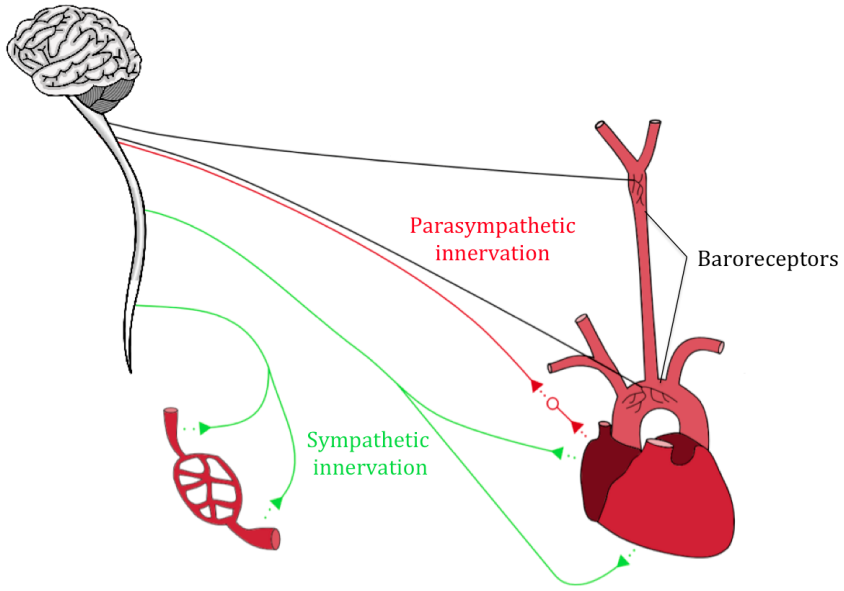

FIGURE 2.8– Autonomic and cardiovascular closed-loop system regulating blood vessels resistance, heart rate and cardiac contractility based on the pressure detected at arterial baroreceptors.

Arterial baroreceptors are stretch receptors mainly located in the carotid sinus and in the aortic arch, firing at a rate proportional to their stretch state and related to blood pressure in a sigmoid manner. When blood pressure is close to the point of maximum sensitivity and increases, stretch and, thus, baroreceptors firing rate rise, making cardiac centers to decrease sympathetic stimulation and increase parasympathetic tone.

2.2. Brugada syndrome

In 1992, eight individuals having resuscitated from sudden cardiac death (SCD), showing a characteristic ST-segment elevation in the right precordial leads and presenting structurally normal hearts, were reported as a base for a distinct clinical entity (BRUGADA et al., 1992). Nowadays, and since 1996 (MIYAZAKI et al., 1996), the "right bundle branch block, persistent ST-segment elevation, and sudden death syndrome" is known as the Brugada syndrome (BS). Since 1997, several studies have recognized BS as the same disease as the sudden unexplained nocturnal death syndrome (SUNDS), also known as *Bangungut* in Philippines, *Pokkuri* in Japan or *Lai Tai* in Thailand (NADEMANEE et al., 1997; VATTA et al., 2002). In 1998, the genetic basis of BS was established by associating the disease with mutations in the *SCN5A* gene, which encodes the α-subunit of the voltage-gated $Na_v1.5$ cardiac sodium channel (CHEN et al., 1998).

At present, BS is known as a rare, inherited disease caused by alterations on the cardiac electrical conduction system that lead to SCD. It is characterized by a distinct electrocardiographic (ECG) pattern, but variable expressivity and incomplete penetrance complicate the diagnosis (BRUGADA et al., 2013). Since its description, although major advances in clinical and genetic

knowledge have provided valuable information about the disease, risk stratification and clinical management still remain challenging, propeling an extensive research activity on the subject.

2.2.1. Clinical diagnosis

2.2.1.1. Diagnostic criteria

Based on the second BS consensus report (Antzelevitch, 2005), three different abnormal ECG patterns, represented in Figure 2.9, have been associated with the Brugada syndrome:

- **Type 1**, which consists of a coved-type ST-segment elevation > 2 mm (0.2 mV), followed by a negative T wave.
- **Type 2**, defined as a saddleback-shaped pattern, with a high initial increase followed by an ST-segment elevation > 2 mm, a trough displaying > 1 mm ST elevation, and either a positive or biphasic T wave.
- **Type 3**, which refer to saddleback-shaped patterns with a high initial increase followed by an ST-segment elevation < 2 mm.

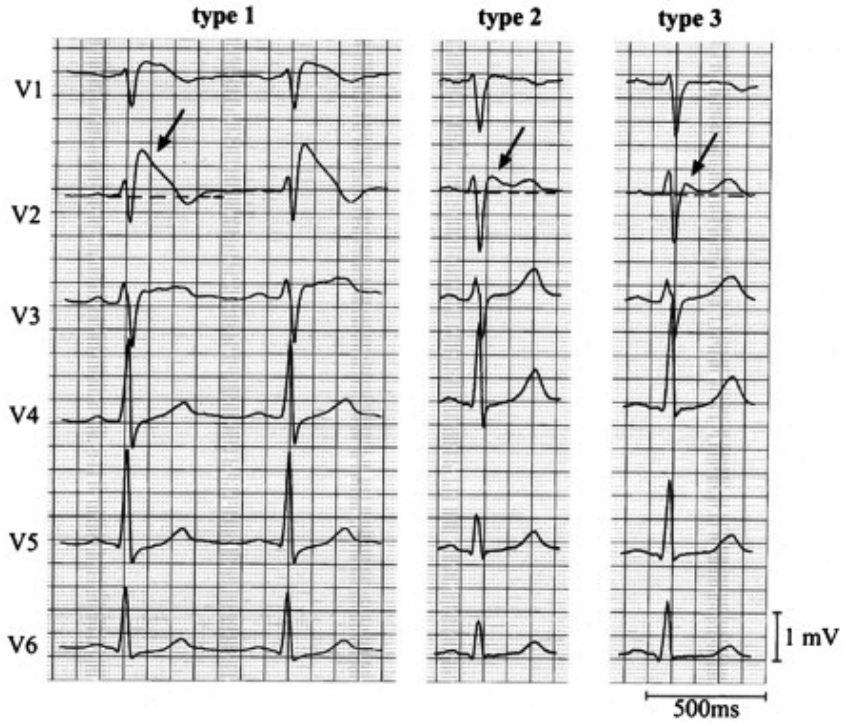

Figure 2.9– ECG patterns in precordial leads (V1-V6) associated with the BS (Nishizaki et al., 2013).

However, according to current guidelines (Priori et al., 2015), BS is only diagnosed in patients presenting the type 1 Brugada-like ECG pattern in at least one right precordial lead;

located in the second, third or fourth intercostal space; and appearing either spontaneously or after provocative drug tests with intravenous administration of sodium channel blockers, when baseline ECG presents a type 2 or type 3 morphology.

Although BS patients present no apparent structural cardiopathy, some microscopic myocardial alterations have been reported, suggesting that the disease may induce cardiomyopathic changes in some patients (Frustaci et al., 2005, 2009).

2.2.1.2. Diagnostic tools

Concealed forms of the disease may be unmasked through the intravenous administration of class IC antiarrhythmic agents, such as ajmaline, flecainide or procainamide. Since these drugs can promote sodium channel blockade, they stimulate the appearance of the diagnostic ECG pattern (Morita et al., 2009). On the basis of comparative studies, though, ajmaline was found to be the most sensitive drug in unmasking the coved-type morphology (Wolpert et al., 2005).

In 2014, the ajmaline drug test was repeated after puberty, in a cohort who showed negative drug tests during childhood (Conte et al., 2014). They were able to unmask a diagnostic ECG pattern in 23% of cases, suggesting a potential role for hormonal, autonomic, and epigenetic factors in the response to antiarrhythmic agents, such as ajmaline, during childhood. Indeed, since nearly 25% of drug-induced tests may lead to false-negative results (Hong et al., 2004), clinical experience suggests that these tests should be repeated.

Moreover, (Calvo et al., 2015a) analyzed the influence of time in the interpretation of drug-induced tests, reporting that longer periods of ECG recording seem to increase the probability of type 1 ECG pattern detection.

2.2.2. Epidemiology

Brugada syndrome is thought to be responsible for 4 to 12% of the total amount of SCD and for up to 20% of SCD in subjects with structurally normal hearts (Antzelevitch, 2005). Its prevalence is estimated at 5 in 10,000 inhabitants, although this rate should be carefully interpreted. First, because many patients present concealed forms of the disease, thus probably underestimating BS prevalence; second, because important ethnic and geographic differences have been reported (Antzelevitch, 2005). Indeed, while the prevalence of BS is estimated at 1 in 10,000 people from western countries, it seems to increment up to 12 in 10,000 in Southest Asia (Fowler et al., 2009), where the syndrome is endemic and, apart from accidents, it is the leading cause of death among young healthy men (Nademanee et al., 1997).

The syndrome is inherited with an autosomal dominant pattern and shows age- and sex-related penetrance. The clinical phenotype is eightfold more frequent in men than in women (Gehi et al., 2006), and it is mainly manifested in adulthood, at a mean age of 41 $\pm$ 15 years, usually during rest or sleep (Priori et al., 2002). Fever, excessive alcohol intake and large meals are triggers that unmask the type 1 ECG pattern and predispose to VF.

2.2.3. Genetic basis

In 1998, the first work relating the syndrome to the gene *SCN5A*, which encodes the α-subunit of the cardiac sodium channel, was published (Chen et al., 1998). To date, nearly 300 pathogenic variations associated with BS have been reported in 22 different genes (Campuzano et al., 2016), which primarily encode for sodium, potassium, and calcium channels, or proteins associated with these channels (Table 2.2). Pathogenic variations in genes encoding desmosomal proteins have also been associated with BS (Cerrone et al., 2014).

Table 2.2– Genes associated with Brugada syndrome.

Channel	**Inheritance**	**Gene**	**Percentage**
Sodium	Autosomal dominant	*SCN5A*	25-35%
		GPD1-L	$< 1\%$
		SCN1B	$< 1\%$
		SCN3B	$< 1\%$
		SCN2B	$< 1\%$
		SCN10A	$< 1\%$
		HEY2	$< 1\%$
		RANGRF	$< 1\%$
		SLMAP	$< 1\%$
		FGF12	$< 1\%$
		PKP2	$< 1\%$
Potassium	Autosomal dominant	*ABCC9*	$< 1\%$
		KCNE3	$< 1\%$
		KCNJ8	$< 1\%$
		HCN4	$< 1\%$
		KCND3	$< 1\%$
		SEMA3A	$< 1\%$
	Chromosome X	*KCNE5*	$< 1\%$
Calcium	Autosomal dominant	*CACNA1C*	$< 1\%$
		CACNB2B	$< 1\%$
		CACNA2D1	$< 1\%$
		TRPM4	$< 1\%$

However, only 30–35% of BS patients are genetically diagnosed, and most of them (25–30%) result from pathogenic alterations in *SCN5A* (Kapplinger et al., 2010). Since this gene directly affects phase 0 of the cardiac AP, pathogenic variants in *SCN5A* lead to sodium channel loss of function due to either: 1) a decreased sodium channel current (I_{Na}); 2) alterations in voltage- and time-dependent I_{Na} activation, inactivation, or reactivation; 3) intermediate state of I_{Na} inactivation from which it recovers more slowly; or 4) early I_{Na} inactivation.

The last mechanism involving an accelerated inactivation of sodium channels has never been observed at room temperature, and it has been proved to be accentuated at temperatures above the physiologic range (Dumaine et al., 1999). Thus, BS patients, and particularly children

(PROBST et al., 2007), may be at an increased risk during febrile periods. Indeed, several BS patients displaying fever-induced polymorphic ventricular tachycardia (VT) have been identified (ANTZELEVITCH et al., 2002).

2.2.4. Cellular mechanisms

Two main cellular mechanisms have been proposed to explain the characteristic Brugada-like ST segment elevation (MEREGALLI et al., 2005): 1) a depolarization hypothesis, based on a conduction delay in the right ventricular outflow tract (RVOT); and 2) a repolarization hypothesis, based on a disequilibrium between Na^+ and K^+ ionic currents.

According to the second theory, during repolarization, a reduced inward Na^+ current (I_{Na}) and a prominent outward K^+ current (I_{to}) lead to an accentuation of the AP notch in the RV epicardium with respect to the endocardium, producing a transmural voltage gradient which manifests electrocardiographically as the Brugada-like ST-segment elevation. At the end of phase 1, some epicardial sites undergo all-or-none repolarizations, losing their AP dome and leading to an heterogenous repolarization environment that facilitates phase 2 re-entry and, thus, the occurrence of VT and VF events (ANTZELEVITCH, 2006; YAN et al., 1999).

In normal conditions (Figure 2.10a), the absence of transmural voltage gradients at the level of the AP plateau leads to isoelectric ST segments. However, under pathophysiological conditions, accentuation of the epicardial RV notch leads to the appereance of voltage gradients and thus of the J-wave (or ST-segment elevation). When epicardial repolarization precedes repolarization in the M and endocardial regions, the T wave remains positive, resulting in a saddleback configuration of the ECG (Figure 2.10b). Further accentuation of the AP notch may lengthen the epicardial AP, reversing transmural voltage and repolarization direction across the RV wall, which leads to an inversion of the T wave and, thus, to the development of a coved-type ST-segment elevation (Figure 2.10c).

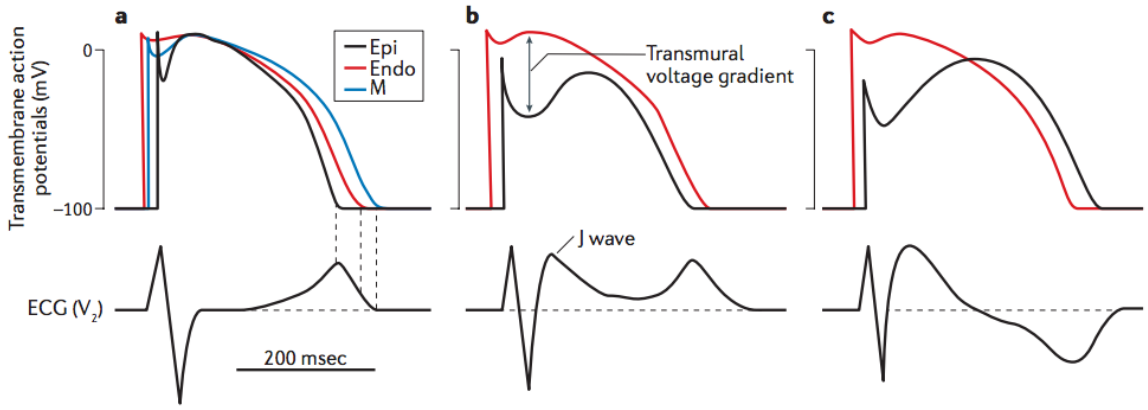

FIGURE 2.10– AP changes in the right ventricular epicardium leading to the Brugada-like ECG pattern. a) Healthy individual, b) Saddleback-shaped BS pattern (type 2/3) and c) Coved-type BS pattern (type 1). Endo: endocardium; Epi: epicardium; M: midmyocardium. Modified from (SIEIRA et al., 2016)

As mentioned before, despite equal genetic transmission of the disease, the clinical phenotype is 8 to 10 times more frequent in men than in women. The basis for this gender-related distinction is thought to be due to a more prominent I_{to}-mediated AP notch in the RV epicardium of males (Di Diego et al., 2002). In this study, RV epicardial AP at the end of phase 1 was found to be more negative in arterially perfused wedge preparations from males; facilitating a loss of the AP dome and, thus, the development of phase 2 re-entry that can lead to polymorphic VT.

2.2.5. Risk stratification

2.2.5.1. Main risk factors

Although the prognostic value for VF occurrence of several variables has been evaluated, only spontaneous type 1 Brugada-like ECG and documented symptoms are recognized as reliable and consistent predictors (Adler et al., 2016). As a consequence, risk stratification in order to determine the best therapeutic strategy for asymptomatic patients still remains challenging.

The risk of major arrhythmic events, such as sustained VT, VF, or SCD, among previously asymptomatic BS patients varies according to the clinical series: 8% recurrence rate at 33 ± 39 months of follow-up reported by (Brugada et al., 2003), 6% recurrence rate at 34 ± 44 months by (Priori et al., 2002); 1% recurrence rate after 40 ± 50 months and 30 ± 21 months of follow-up, respectively, by (Eckardt et al., 2005) and (Giustetto et al., 2009), and 1.5% recurrence rate at 31 months of follow-up reported by (Probst et al., 2010).

Results from a meta-analysis estimated the incidence of arrhythmic events per year at: 13.5% in patients with documented sudden cardiac arrest, 3.2% in patients with history of syncope and 1% in asymptomatic individuals (Fauchier et al., 2013).

A more recent study showed a 0.5% annual incidence rate in asymptomatic patients. Moreover, inducibility of ventricular arrhythmias (VA), spontaneous type 1 ECG pattern and presence of sinus node dysfunction were proposed as risk factors (Sieira et al., 2015a). Another recently published meta-analysis showed that asymptomatic subjects presenting either a spontaneous type 1 ECG pattern or inducible VA seem to be at increased risk for arrhythmic events (Letsas et al., 2015).

From the results, it can be noted that reported rates of events have decreased over time, probably due to the inherent bias during the first years following the description of a novel disorder, in which particularly severe forms of the disease are most likely to be diagnosed.

2.2.5.2. Clinical factors

Male sex has consistently shown a tendency to more frequently present arrhythmic events in all studies, and it has even been defined as an independent predictor for a worse prognosis (Gehi et al., 2006).

Brugada syndrome can also be aggravated by supraventricular arrhythmias (Liu et al., 2015). Spontaneous atrial fibrillation (AF), which can appear in 10% to 53% of cases, has demonstrated to be related to a higher incidence of VF and syncopal episodes (Kusano et al., 2008).

A family history of SCD or the presence of an *SCN5A* mutation have not been proven to be risk markers in any of the large studies conducted thus far (Gehi et al., 2006).

2.2.5.3. Programmed ventricular stimulation

Although large registries agree that VA inducibility during an electrophysiological study (EPS) is greatest among BS patients with documented SCD or syncope, there is no consensus on its prognostic value in asymptomatic BS patients (Priori et al., 2012).

Some published results indicate that inducibility during programmed ventricular stimulation (PVS) is an independent predictor of cardiac events (Brugada et al., 2003). However, other studies stress the negative predictive value of EPS testing (Giustetto et al., 2009), and in those studies performed on the largest clinical series of BS patients published so far, inducibility did not predict arrhythmic events (Probst et al., 2010).

In a recent study including over 400 BS patients, the authors concluded that EPS might be a suitable screening tool to reassure non-inducible asymptomatic individuals (Sieira et al., 2015b).

2.2.5.4. Electrocardiographic variables

In an effort to improve risk stratification in BS, several non-invasive methods have been proposed as predictors of cardiac events (Campuzano et al., 2016). For instance, an S-wave width in V1 $\geq$ 80 ms; an ST-segment elevation $\geq$ 0.18 mV in V2; spontaneous changes in the ST segment; a corrected QT interval (QTc) $>$ 460 ms in V2; a prolonged T_{peak}-T_{end} ($T_{p\text{-}e}$) interval and $T_{p\text{-}e}$ dispersion; the *aVR sign* (R wave $\geq$ 0.3 mV in lead aVR); or a prolonged QRS-complex duration in precordial leads, among others.

Several studies have suggested late potentials (LP), assessed by signal-averaged ECG (SAECG), as a marker of high risk and even a prospective study concluded that LP was an independent predictor of high risk in BS patients (Priori et al., 2012). However, more prospective studies including larger clinical series and longer follow-up periods are still needed in order to prove the usefulness of LP and other non-invasive markers in predicting SCD in the context of BS.

Moreover, previous works based on multivariate analyses have proposed predictive models combining several indicators in order to assess VF risk in BS patients. (Delise et al., 2014, 2011) found that spontaneous type 1 ECG in combination with documented syncope, family history of SCD, and positive EPS were associated with an increased risk. Similarly, (Okamura et al., 2015) reported that the combination of spontaneous type 1 ECG, documented syncope, and positive EPS were relevant for stratifying risk in BS patients. More recently, (Kawazoe et al., 2016) proposed a logistic regression model for VF risk stratification in BS patients based on non-invasive parameters including documented syncope, QRS duration in V6, and T_{peak}-T_{end} dispersion.

2.2.5.5. Autonomic function

There is increasing evidence that autonomic imbalance significantly contributes to the arrhythmogenesis and prognosis of BS patients. Data on cardiac ANS analyzed by positron emission tomography has confirmed that these patients display an autonomic dysfunction, caused by an increased presynaptic norepinephrine (NE) recycling and thus a reduction in the concentration of NE at the synaptic cleft. This imbalance is thought to decrease intracellular levels of 3–5-cyclic adenosine monophosphate (cAMP), thus disrupting the subsequent signaling pathway with potential implications for arrhythmogenesis (Kies et al., 2004; Paul et al., 2011; Wichter et al., 2002). In addition, this autonomic imbalance might be aggravated due to physiological downregulation of the adrenergic activity, justifying the occurrence of VA and SCD during parasympathetic dominance at rest or during sleep (Matsuo et al., 1999; Mizumaki et al., 2004; Yan et al., 1999).

Although several studies on the autonomic function of BS patients have been published, they report conflicting results; particularly when based on long-term measurements obtained from 24-hour analysis. (Krittayaphong et al., 2003) concluded that BS patients showed a decreased HRV and vagal tone at night compared to controls; as well as lower diurnal and higher overnight HR when symptomatic patients were compared to asymptomatic subjects and controls. Likewise, (Hermida et al., 2003) found significantly lower HRV values at night when comparing symptomatic and asymptomatic patients; and (Pierre et al., 2007) also observed a decreased HRV in BS patients, with respect to healthy subjects. Results from (Tokuyama et al., 2014) also showed a significant reduction on the HRV in BS patients with respect to controls, as well as on both sympathetic and parasympathetic tones and on their circadian variation over 24 hours.

However, HRV analysis in (Kostopoulou et al., 2010) did not reveal any significant difference between BS patients and controls; and in (Nakazawa et al., 2003) the results showed higher vagal and reduced sympathetic tones in symptomatic BS patients. Likewise, in a recent work from (Behar et al., 2016), symptomatic subjects showed an increased parasympathetic activity during both daytime and nighttime, when compared to asymptomatic patients.

Thus, although a decreased HRV is commonly related to symptomatic patients with higher risk, there is still no consensus regarding changes on the vagal tone of these patients. In order to better characterize autonomic modulation, standard maneuvers, such as exercise testing or the head-up tilt (HUT) test, can be applied. Indeed, some studies have already reported the potential of exercise testing (Masrur et al., 2015) or the full stomach test (Ikeda et al., 2006), among other autonomic tests (Bigi et al., 2008), for the prediction of cardiac events in BS.

Previous studies on the full stomach test have demonstrated that vagal stimulation induced by a large meal increase distinctive Brugada-like ECG changes (Ikeda et al., 2005). Moreover, patients resulting in a positive full stomach test seem to be more frequently related to life-threatening events than patients with a negative test result (Ikeda et al., 2006).

In a recent study, (Subramanian et al., 2017) proved the usefulness of some ECG markers extracted during exercise testing for risk stratification in asymptomatic BS patients. The work from (Amin et al., 2009), though, was the first large study measuring the autonomic function in

a clinical series of patients suffering from BS during exercise, finding a higher parasympathetic reactivation during early recovery after exertion in individuals with prior VF events. Likewise, (Makimoto et al., 2010) assessed the autonomic function during recovery from treadmill exercise testing. By analyzing the parasympathetic reactivation of BS patients and controls through the Heart Rate Recovery (HRR) after peak exercise, they concluded that a higher vagal activity was related to the occurrence of cardiac events in BS.

2.2.6. Treatment

To date, the only proven effective therapeutic strategy for the prevention of SCD in BS patients is the implantation of cardioverter defibrillators (ICD); therefore the device is recommended in patients with documented VT or VF and in patients presenting with a spontaneous type 1 ECG and a history of syncope (Priori et al., 2015).

However, it is important to remark that ICDs can present several complications, especially in active young individuals, facing a long-lasting coexistence with the device and, thus, needing multiple replacements. Indeed, some series have reported low rates of appropriate shocks (8-15%, from a median follow-up of 45 months) and high rates of complications, mainly consisting of inappropriate shocks (20-36% from 21 to 47 months of follow-up) (Rosso et al., 2008; Sarkozy et al., 2007; Zipes et al., 2006).

Since quinidine may rebalance ionic currents involved in the cardiac AP affected in BS, it has also been proposed as a preventive pharmacologic therapy. Although published reports show that it reduces VA inducibility during EPS testing, there is still no data confirming its ability to reduce the risk of SCD. Therefore, it is currently used in patients carrying an ICD but presenting complications, and it has been suggested for BS treatment in children, as a bridge to ICD implantation or as an alternative treatment approach (Schweizer et al., 99).

Recently, it has been suggested that epicardial catheter ablation over the anterior RVOT may prevent electrical storms in patients with recurring episodes (Nademanee et al., 2011). Although larger studies with longer follow-up periods are still required, a study conducted in a cohort of BS patients demonstrated that epicardial ablation of the arrythmogenic electrical substrate identified in the presence of flecainide could eliminate the BS phenotype and, thus, VF inducibility without complications (Brugada et al., 2015).

2.3. Clinical data

The main clinical database used in this work was acquired during a prospective, multicentric study aimed at inducing autonomic changes in BS patients through the application of standard autonomic tests while a 24-hour ECG was obtained. It was conducted between 2009 and 2013 in the Cardiology department of the Rennes University Hospital, in France, and participants were enrolled in 8 French hospitals located in La Rochelle, Angers, Bordeaux, Brest, Nantes, Rennes, Poitiers and Tours.

Other 2 databases including patients from the Rennes University Hospital, were composed of additional signals during the application of the same autonomic tests. The protocols were approved by each local ethics committee and all patients granted their informed consent to participate in the study.

2.3.1. Study population

In accordance with current guidelines (Priori et al., 2015; Priori et al., 2013), BS was diagnosed when a coved ST-segment elevation ($\geq$ 0.2 mV) was detected in at least one right precordial lead placed in the second to fourth intercostal space, in the presence or absence of sodium-channel-blocking agent.

In order to characterize patients with different levels of risk, participants were classified in symptomatic and asymptomatic patients, based on their clinical history. Patients from the first group could present the following documented symptoms: cardiac arrest due to VF, syncopes, dizziness, palpitations and nocturnal convulsions. Since each substudy was performed with different groups of patients, data are described in detail in the corresponding sections.

2.3.2. Data acquisition

In the first database, the standard 12-lead ECG of 87 patients was collected for 24 hours, including a head-up tilt (HUT) test and a physical exercise test, with the Holter monitor (ELA medical, Sorin Group, Le Plessis Robinsson, France) at a sampling frequency of 1000 Hz. Additionally, HUT tests were performed in 32 patients while non-invasive blood pressure and ECG recordings were acquired with the Task Force monitor (CN Systems, Graz, Austria) at a sampling frequency of 100 Hz and 1000 Hz, respectively. The 12-lead ECG signals sampled at 1000 Hz of other 36 BS patients were acquired during exercise testing with the ECG monitor (Cardionics, Webster, Texas).

Hence, autonomic analysis was focused on 3 different periods: overnight and during the realization of exercise and HUT tests. Figure 2.11 specifies the sources (hereafter named the Holter, Cardionics and Task Force databases) for each autonomic analysis, and the following sections describe in more detail the protocols applied.

2.3.2.1. Overnight analysis

Since major cardiac events in BS typically occur during sleep (Matsuo et al., 1999; Mizumaki et al., 2004; Yan et al., 1999) and some previous studies have already shown significant differences between patients at different levels of risk overnight (Behar et al., 2016; Hermida et al., 2003), the autonomic function during this period was carefully studied. First, by the application of previously reported indicators in order to validate previous results in our clinical series; second, by proposing new approaches never before studied in BS so as to analyze their predictive value.

For autonomic evaluations at night, only the period from midnight to 6 a.m. was identified, so as to make sure that HR was being assessed while patients were asleep.

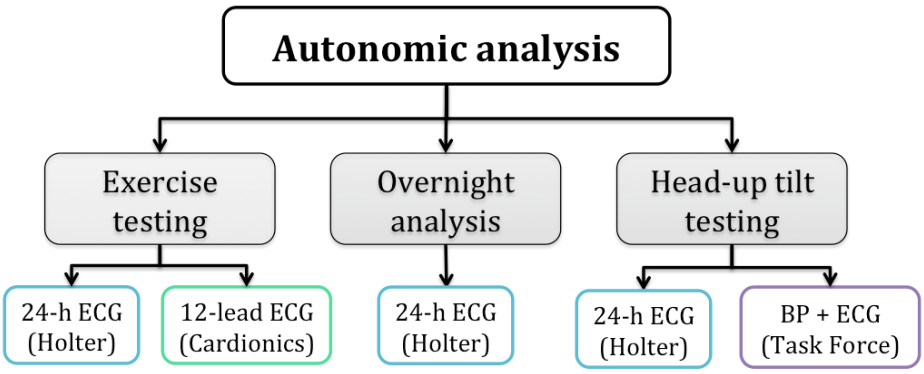

FIGURE 2.11– Autonomic studies were based on 3 different analyses: exercise testing, overnight analysis and head-up tilt testing. Each colour represents the source signals coming from different clinical databases.

2.3.2.2. Exercise testing

Exertion causes a sympathetic activation that, together with a parasympathetic inhibition, increases heart rate, a reliable indicator to evaluate cardiac autonomic function (LAHIRI et al., 2008). Similarly, post-exercise cardiodeceleration is adjusted by parasympathetic activation and sympathetic withdrawal (ARAI et al., 1989), generally expected to accentuate ST-segment elevation in BS (MIZUMAKI et al., 2004).

In contrast to long-term analysis, there are limited data on the role of exercise testing in the autonomic function of BS patients (AMIN et al., 2009; MAKIMOTO et al., 2010). Therefore, patients underwent a triangular stress test recommended by the American Heart Association (GIBBONS et al., 2002), where the load was progressively increased until the patient reached, at least, the 80% of his/her theoretical maximum heart rate (MHR), defined as $MHR = 220 - age$ (FOX 3RD et al., 1968). The test was performed in a cyclo ergometer (Ergoline 900 Egamed, Piestany, Slovakia) and divided in the following phases:

- Exercise phase:
  - Warm-up phase: for men, initial load of 50 W; for women, initial load of 30 W, both for 2 minutes.
  - Incremental exercise phase: for men, initial load of 80 W for 2 minutes and then incrementing 20 W every 2 minutes; for women, initial load of 50 W increasing load 20 W every 2 minutes.
- Recovery phase:
  - Active recovery: for men, fixed load of 50 W; for women, fixed load of 30 W, both for 3 minutes.
  - Passive recovery: total cessation of effort for 3 minutes.

2.3.2.3. Head-up tilt testing

Head-up tilt (HUT) testing provokes hemodynamic changes mainly based on the redistribution of blood volume to the lower part of the body, causing a decrease in both central venous and ventricular filling pressures, as well as in stroke volume (Blomqvist et al., 1983; Smith, 1990). Consequently, cardiovascular regulatory mechanisms such as the arterial baroreceptors stimulate a reflex increase in sympathetic activity and a vagal inhibition, inducing an increase in heart rate, peripheral vascular resistance, venous tone and heart contractility (Kirchheim, 1976).

Although several studies have analyzed the role of HUT testing on BS patients for risk stratification (Behar et al., 2016; Kostopoulou et al., 2010; Letsas et al., 2008), the autonomic function under these conditions has never been analyzed in this population. Therefore, patients also underwent head-up tilt (HUT) tests in the morning in fasting conditions, according to the following protocol:

- Pre-tilt resting phase: 10 minutes in supine position.
- Tilting phase: 45 minutes at 60° of table (Sissel, Sautron, France) inclination.
- Post-tilt resting phase: 10 minutes in supine position.

2.4. Conclusion

The autonomic nervous system (ANS) innervates the heart with both sympathetic and parasympathetic branches, as well as blood vessels through the sympathetic system, in order to regulate heart rate and blood pressure. One of the primary sensory receptors in the closed loop between autonomic and cardiovascular systems are the arterial baroreceptors. Abnormal behavior of the ANS can lead to serious pathological conditions; and in the context of the Brugada syndrome (BS), there is increasing evidence that autonomic imbalance significantly contributes to the arrhythmogenesis and prognosis of this population.

BS is defined as a rare, genetic disease caused by alterations on the cardiac electrical conduction system that lead to sudden cardiac death (SCD) due to ventricular fibrillation (VF), in absence of structural cardiopathies. To date, though, only 22 genes representing the 30%–35% of diagnosed cases have been associated with the disease, being *SCN5A* the most common. It is characterized by a distinct ECG pattern, but variable expressivity and incomplete penetrance complicate clinical diagnosis, risk stratification and treatment. Implantable cardioverter defibrillators (ICD) are the only proven effective therapy for patients at high risk thus far; despite other approaches, such as quinidine or epicardial ablation, have been suggested for patients suffering ICD complications.

Patients presenting spontaneous Brugada-like ECG morphology or having suffered previous symptoms, such as syncopes or SCD, are considered at high risk for major cardiac events. Thus, in an effort to improve risk stratification in asymptomatic BS patients, several non-invasive methods have been proposed as predictors of SCD. However, more prospective studies including

larger clinical series and longer follow-up periods are still needed in order to prove the usefulness of these markers in predicting SCD.

Since ANS modulation plays a significant role in the disease, biomarkers accounting for autonomic differences in BS patients at high risk of SCD could provide valuable information to improve risk stratification and, thus, therapeutic strategies in asymptomatic patients. Moreover, the application of specific maneuvers stimulating the ANS, such as exercise or the head-up tilt (HUT) test, could improve autonomic assessment. Therefore, this research evaluates the autonomic function of a clinical series of BS patients overnight and during exercise and HUT testing. The following chapters will develop the methods applied on the presented databases.

References

Adler, A., R. Rosso, E. Chorin, O. Havakuk, C. Antzelevitch, and S. Viskin (2016). "Risk stratification in Brugada syndrome: clinical characteristics, electrocardiographic parameters, and auxiliary testing". In: *Heart Rhythm* 13.1, pp. 299–310.

Amin, A. S., E. A. de Groot, J. M. Ruijter, A. A. Wilde, and H. L. Tan (2009). "Exercise-Induced ECG Changes in Brugada Syndrome". In: *Circulation: Arrhythmia and Electrophysiology* 2.5, pp. 531–539.

Anderson, R. H., J. Yanni, M. R. Boyett, N. J. Chandler, and H. Dobrzynski (2009). "The anatomy of the cardiac conduction system". In: *Clinical Anatomy* 22.1, pp. 99–113.

Antzelevitch, C. (2005). "Heart Rhythm Society; European Heart Rhythm Association. Brugada syndrome: report of the second consensus conference: endorsed by the Heart Rhythm Society and the European Heart Rhythm Association". In: *Circulation* 111.5, pp. 659–670.

— (2006). "Brugada syndrome". In: *Pacing and Clinical Electrophysiology* 29.10, pp. 1130–1159.

Antzelevitch, C. and R. Brugada (2002). "Fever and Brugada syndrome". In: *Pacing and Clinical Electrophysiology* 25.11, pp. 1537–1539.

Arai, Y., J. P. Saul, P. Albrecht, L. H. Hartley, L. S. Lilly, R. J. Cohen, and W. S. Colucci (1989). "Modulation of cardiac autonomic activity during and immediately after exercise". In: *American Journal of Physiology-Heart and Circulatory Physiology* 256.1, H132–H141.

Behar, N., B. Petit, V. Probst, F. Sacher, G. Kervio, J. Mansourati, P. Bru, A. Hernandez, and P. Mabo (2016). "Heart rate variability and repolarization characteristics in symptomatic and asymptomatic Brugada syndrome". In: *Europace*, euw224.

Bigi, M. A. B., A. Aslani, and A. Aslani (2008). "Significance of cardiac autonomic neuropathy in risk stratification of Brugada syndrome". In: *Europace* 10.7, pp. 821–824.

Blomqvist, C. G. and H. L. Stone (1983). "Cardiovascular adjustments to gravitational stress". In: *Comprehensive Physiology*.

Brugada, J., R. Brugada, and P. Brugada (2003). "Determinants of sudden cardiac death in individuals with the electrocardiographic pattern of Brugada syndrome and no previous cardiac arrest". In: *Circulation* 108.25, pp. 3092–3096.

Brugada, J., C. Pappone, A. Berruezo, G. Vicedomini, F. Manguso, G. Ciconte, L. Giannelli, and V. Santinelli (2015). "Brugada syndrome phenotype elimination by epicardial substrate ablation". In: *Circulation: Arrhythmia and Electrophysiology*.

Brugada, P. and J. Brugada (1992). "Right bundle branch block, persistent ST segment elevation and sudden cardiac death: a distinct clinical and electrocardiographic syndrome: a multicenter report". In: *Journal of the American College of Cardiology* 20.6, pp. 1391–1396.

Brugada, P., J. Brugada, and D. Roy (2013). "Brugada syndrome 1992–2012: 20 years of scientific excitement, and more". In: *European heart journal* 34.47, pp. 3610–3615.

Calvo, D., J. M. Rubín, D. Pérez, J. Gómez, J. P. Flórez, P. Avanzas, J. M. García-Ruíz, J. M. de la Hera, J. Reguero, E. Coto, et al. (2015a). "Time-dependent responses to provocative testing with flecainide in the diagnosis of Brugada syndrome". In: *Heart Rhythm* 12.2, pp. 350–357.

Campuzano, O., G. Sarquella-Brugada, R. Brugada, and J. Brugada (2016). "Brugada syndrome". In: *Clinical Cardiogenetics*. Springer, pp. 175–191.

Cerrone, M. and M. Delmar (2014). "Desmosomes and the sodium channel complex: implications for arrhythmogenic cardiomyopathy and Brugada syndrome". In: *Trends in cardiovascular medicine* 24.5, pp. 184–190.

Chen, Q., G. E. Kirsch, D. Zhang, R. Brugada, J. Brugada, P. Brugada, D. Potenza, A. Moya, M. Borggrefe, G. Breithardt, et al. (1998). "Genetic basis and molecular mechanism for idiopathic ventricular fibrillation". In: *Nature* 392.6673, pp. 293–296.

Conte, G., W. Dewals, J. Sieira, C. De Asmundis, G. Ciconte, G.-B. Chierchia, G. Di Giovanni, G. Baltogiannis, Y. Saitoh, M. Levinstein, et al. (2014). "Drug-induced brugada syndrome in children". In: *Journal of the American College of Cardiology* 63.21, pp. 2272–2279.

Delise, P., G. Allocca, N. Sitta, and P. Di Stefano (2014). "Event rates and risk factors in patients with Brugada syndrome and no prior cardiac arrest: a cumulative analysis of the largest available studies distinguishing ICD-recorded fast ventricular arrhythmias and sudden death". In: *Heart Rhythm* 11.2, pp. 252–258.

Delise, P., G. Allocca, E. Marras, C. Giustetto, F. Gaita, L. Sciarra, L. Calo, A. Proclemer, M. Marziali, L. Rebellato, et al. (2011). "Risk stratification in individuals with the Brugada type 1 ECG pattern without previous cardiac arrest: usefulness of a combined clinical and electrophysiologic approach". In: *European heart journal* 32.2, pp. 169–176.

Di Diego, J. M., J. M. Cordeiro, R. J. Goodrow, J. M. Fish, A. C. Zygmunt, G. J. Pérez, F. S. Scornik, and C. Antzelevitch (2002). "Ionic and cellular basis for the predominance of the Brugada syndrome phenotype in males". In: *Circulation* 106.15, pp. 2004–2011.

Dumaine, R., J. A. Towbin, P. Brugada, M. Vatta, D. V. Nesterenko, V. V. Nesterenko, J. Brugada, R. Brugada, and C. Antzelevitch (1999). "Ionic mechanisms responsible

for the electrocardiographic phenotype of the Brugada syndrome are temperature dependent". In: *Circulation research* 85.9, pp. 803–809.

Eckardt, L., V. Probst, J. P. Smits, E. S. Bahr, C. Wolpert, R. Schimpf, T. Wichter, P. Boisseau, A. Heinecke, G. Breithardt, et al. (2005). "Long-term prognosis of individuals with right precordial ST-segment–elevation Brugada syndrome". In: *Circulation* 111.3, pp. 257–263.

Fauchier, L., M. A. Isorni, N. Clementy, B. Pierre, E. Simeon, and D. Babuty (2013). "Prognostic value of programmed ventricular stimulation in Brugada syndrome according to clinical presentation: an updated meta-analysis of worldwide published data". In: *Int J Cardiol* 168.3, pp. 3027–3029.

Fowler, S. J. and S. G. Priori (2009). "Clinical spectrum of patients with a Brugada ECG". In: *Current opinion in cardiology* 24.1, pp. 74–81.

Fox 3rd, S. and W. Haskell (1968). "Physical activity and the prevention of coronary heart disease". In: *Bulletin of the New York Academy of Medicine* 44.8, pp. 950–965.

Frustaci, A., S. G. Priori, M. Pieroni, C. Chimenti, C. Napolitano, I. Rivolta, T. Sanna, F. Bellocci, and M. A. Russo (2005). "Cardiac histological substrate in patients with clinical phenotype of Brugada syndrome". In: *Circulation* 112.24, pp. 3680–3687.

Frustaci, A., M. A. Russo, and C. Chimenti (2009). "Structural myocardial abnormalities in asymptomatic family members with Brugada syndrome and SCN5A gene mutation". In: *European heart journal* 30.14, p. 1763.

Gehi, A. K., T. D. Duong, L. D. Metz, J. A. Gomes, and D. Mehta (2006). "Risk Stratification of Individuals with the Brugada Electrocardiogram: A Meta-Analysis". In: *Journal of cardiovascular electrophysiology* 17.6, pp. 577–583.

Gibbons, R. J., G. J. Balady, J. T. Bricker, B. R. Chaitman, G. F. Fletcher, V. F. Froelicher, D. B. Mark, B. D. McCallister, A. N. Mooss, M. G. O'Reilly, et al. (2002). "ACC/AHA 2002 guideline update for exercise testing: summary article: a report of the American College of Cardiology/American Heart Association Task Force on Practice Guidelines (Committee to Update the 1997 Exercise Testing Guidelines)". In: *Journal of the American College of Cardiology* 40.8, pp. 1531–1540.

Giustetto, C., S. Drago, P. G. Demarchi, P. Dalmasso, F. Bianchi, A. S. Masi, P. Carvalho, E. Occhetta, G. Rossetti, R. Riccardi, et al. (2009). "Risk stratification of the patients with Brugada type electrocardiogram: a community-based prospective study". In: *Europace* 11.4, pp. 507–513.

Guyton, A. and J. Hall (2006). *Textbook of medical physiology, 11th.* Elsevier Inc.

Hermida, J.-S., A. Leenhardt, B. Cauchemez, I. Denjoy, G. Jarry, F. Mizon, P. Milliez, J.-L. Rey, P. Beaufils, and P. Coumel (2003). "Decreased nocturnal standard deviation of averaged NN intervals". In: *European heart journal* 24.22, pp. 2061–2069.

Hong, K., J. Brugada, A. Oliva, A. Berruezo-Sanchez, D. Potenza, G. D. Pollevick, A. Guerchicoff, K. Matsuo, E. Burashnikov, R. Dumaine, et al. (2004). "Value of

electrocardiographic parameters and ajmaline test in the diagnosis of Brugada syndrome caused by SCN5A mutations". In: *Circulation* 110.19, pp. 3023–3027.

Ikeda, T., A. Abe, S. Yusu, K. Nakamura, H. Ishiguro, H. Mera, M. Yotsukura, and H. Yoshino (2006). "The full stomach test as a novel diagnostic technique for identifying patients at risk of Brugada syndrome". In: *Journal of cardiovascular electrophysiology* 17.6, pp. 602–607.

Ikeda, T., M. Takami, K. Sugi, Y. Mizusawa, H. Sakurada, and H. Yoshino (2005). "Noninvasive Risk Stratification of Subjects with a Brugada-Type Electrocardiogram and No History of Cardiac Arrest". In: *Annals of Noninvasive Electrocardiology* 10.4, pp. 396–403.

Kapplinger, J. D., D. J. Tester, M. Alders, B. Benito, M. Berthet, J. Brugada, P. Brugada, V. Fressart, A. Guerchicoff, C. Harris-Kerr, et al. (2010). "An international compendium of mutations in the SCN5A-encoded cardiac sodium channel in patients referred for Brugada syndrome genetic testing". In: *Heart Rhythm* 7.1, pp. 33–46.

Kawazoe, H., Y. Nakano, H. Ochi, M. Takagi, Y. Hayashi, Y. Uchimura, T. Tokuyama, Y. Watanabe, H. Matsumura, S. Tomomori, et al. (2016). "Risk stratification of ventricular fibrillation in Brugada syndrome using noninvasive scoring methods". In: *Heart Rhythm* 13.10, pp. 1947–1954.

Kies, P., T. Wichter, M. Schäfers, M. Paul, K. P. Schäfers, L. Eckardt, L. Stegger, E. Schulze-Bahr, O. Rimoldi, G. Breithardt, et al. (2004). "Abnormal myocardial presynaptic norepinephrine recycling in patients with Brugada syndrome". In: *Circulation* 110.19, pp. 3017–3022.

Kirchheim, H. R. (1976). "Systemic arterial baroreceptor reflexes". In: *Physiological Reviews* 56.1, pp. 100–177.

Kostopoulou, A., M. Koutelou, G. Theodorakis, A. Theodorakos, E. Livanis, T. Maounis, A. Chaidaroglou, D. Degiannis, V. Voudris, D. Kremastinos, et al. (2010). "Disorders of the autonomic nervous system in patients with Brugada syndrome: a pilot study". In: *Journal of cardiovascular electrophysiology* 21.7, pp. 773–780.

Krittayaphong, R., G. Veerakul, K. Nademanee, and C. Kangkagate (2003). "Heart rate variability in patients with Brugada syndrome in Thailand". In: *European Heart Journal* 24.19, pp. 1771–1778.

Kusano, K. F., M. Taniyama, K. Nakamura, D. Miura, K. Banba, S. Nagase, H. Morita, N. Nishii, A. Watanabe, T. Tada, et al. (2008). "Atrial fibrillation in patients with Brugada syndrome: relationships of gene mutation, electrophysiology, and clinical backgrounds". In: *Journal of the American College of Cardiology* 51.12, pp. 1169–1175.

Lahiri, M. K., P. J. Kannankeril, and J. J. Goldberger (2008). "Assessment of autonomic function in cardiovascular disease". In: *Journal of the American College of Cardiology* 51.18, pp. 1725–1733.

Letsas, K. P., M. Efremidis, G. Gavrielatos, G. S. Filippatos, A. Sideris, and F. Kardaras (2008). "Neurally Mediated Susceptibility in Individuals with Brugada-Type ECG Pattern". In: *Pacing and clinical electrophysiology* 31.4, pp. 418–421.

Letsas, K. P., T. Liu, Q. Shao, P. Korantzopoulos, G. Giannopoulos, K. Vlachos, S. Georgopoulos, A. Trikas, M. Efremidis, S. Deftereos, et al. (2015). "Meta-analysis on risk stratification of asymptomatic individuals with the Brugada phenotype". In: *The American journal of cardiology* 116.1, pp. 98–103.

Liu, B., C. Guo, D. Fang, and J. Guo (2015). "Clinical observations of supraventricular arrhythmias in patients with brugada syndrome". In: *International journal of clinical and experimental medicine* 8.8, pp. 14520–14526.

Makimoto, H., E. Nakagawa, H. Takaki, Y. Yamada, H. Okamura, T. Noda, K. Satomi, K. Suyama, N. Aihara, T. Kurita, et al. (2010). "Augmented ST-segment elevation during recovery from exercise predicts cardiac events in patients with Brugada syndrome". In: *Journal of the American College of Cardiology* 56.19, pp. 1576–1584.

Maruyama, M., Y. Kobayashi, E. Kodani, Y. Hirayama, H. Atarashi, T. Katoh, and T. Takano (2004). "Osborn waves: history and significance". In: *Indian pacing and electrophysiology journal* 4.1, pp. 33–39.

Masrur, S., S. Memon, and P. D. Thompson (2015). "Brugada syndrome, exercise, and exercise testing". In: *Clinical cardiology* 38.5, pp. 323–326.

Matsuo, K., T. Kurita, M. Inagaki, M. Kakishita, N. Aihara, W. Shimizu, A. Taguchi, K. Suyama, S. Kamakura, and K. Shimomura (1999). "The circadian pattern of the development of ventricular fibrillation in patients with Brugada syndrome". In: *European heart journal* 20.6, pp. 465–470.

Meregalli, P. G., A. A. Wilde, and H. L. Tan (2005). "Pathophysiological mechanisms of Brugada syndrome: Depolarization disorder, repolarization disorder, or more?" In: *Cardiovascular research* 67.3, pp. 367–378.

Miyazaki, T., H. Mitamura, S. Miyoshi, K. Soejima, Y. Aizawa, and S. Ogawa (1996). "Autonomic and antiarrhythmic drug modulation of ST segment elevation in patients with Brugada syndrome". In: *Journal of the American College of Cardiology* 27.5, pp. 1061–1070.

Mizumaki, K., A. Fujiki, T. Tsuneda, M. Sakabe, K. Nishida, M. Sugao, and H. Inoue (2004). "Vagal activity modulates spontaneous augmentation of ST elevation in the daily life of patients with Brugada syndrome". In: *Journal of cardiovascular electrophysiology* 15.6, pp. 667–673.

Morita, H., D. P. Zipes, and J. Wu (2009). "Brugada syndrome: insights of ST elevation, arrhythmogenicity, and risk stratification from experimental observations". In: *Heart Rhythm* 6.11, S34–S43.

Nademanee, K., G. Veerakul, P. Chandanamattha, L. Chaothawee, A. Ariyachaipanich, K. Jirasirirojanakorn, K. Likittanasombat, K. Bhuripanyo, and T. Ngarmukos (2011). "Prevention of Ventricular Fibrillation Episodes in Brugada Syndrome by Catheter Ablation Over the Anterior Right Ventricular Outflow Tract Epicardium: Clinical Perspective". In: *Circulation* 123.12, pp. 1270–1279.

Nademanee, K., G. Veerakul, S. Nimmannit, V. Chaowakul, K. Bhuripanyo, K. Likittanasombat, K. Tunsanga, S. Kuasirikul, P. Malasit, S. Tansupasawadikul, et al.

(1997). “Arrhythmogenic marker for the sudden unexplained death syndrome in Thai men”. In: *Circulation* 96.8, pp. 2595–2600.

Nakazawa, K., T. Sakurai, A. Takagi, R. Kishi, K. Osada, T. Nanke, F. Miyake, N. Matsumoto, and S. Kobayashi (2003). “Autonomic imbalance as a property of symptomatic Brugada syndrome”. In: *Circulation journal* 67.6, pp. 511–514.

Nerbonne, J. M. and R. S. Kass (2005). “Molecular physiology of cardiac repolarization”. In: *Physiological reviews* 85.4, pp. 1205–1253.

Nishizaki, M., N. Yamawake, H. Sakurada, and M. Hiraoka (2013). “ECG interpretation in Brugada syndrome”. In: *Journal of Arrhythmia* 29.2, pp. 56–64.

Okamura, H., T. Kamakura, H. Morita, K. Tokioka, I. Nakajima, M. Wada, K. Ishibashi, K. Miyamoto, T. Noda, T. Aiba, et al. (2015). “Risk stratification in patients with Brugada syndrome without previous cardiac arrest”. In: *Circulation Journal* 79.2, pp. 310–317.

Paul, M., M. Meyborg, P. Boknik, U. Gergs, W. Schmitz, G. Breithardt, T. Wichter, and J. Neumann (2011). “Autonomic dysfunction in patients with Brugada syndrome: further biochemical evidence of altered signaling pathways”. In: *Pacing and Clinical Electrophysiology* 34.9, pp. 1147–1153.

Pierre, B., D. Babuty, P. Poret, C. Giraudeau, O. Marie, P. Cosnay, and L. Fauchier (2007). “Abnormal nocturnal heart rate variability and QT dynamics in patients with Brugada syndrome”. In: *Pacing and clinical electrophysiology* 30.s1, S188–S191.

Priori, S. G., C. Blomström-Lundqvist, A. Mazzanti, N. Blom, M. Borggrefe, J. Camm, P. Elliott, D. Fitzsimons, R. Hatala, G. Hindricks, et al. (2015). “Task Force for the Management of Patients with Ventricular Arrhythmias and the Prevention of Sudden Cardiac Death of the European Society of Cardiology (ESC). 2015 ESC guidelines for the management of patients with ventricular arrhythmias and the prevention of sudden cardiac death: the Task Force for the Management of Patients with Ventricular Arrhythmias and the Prevention of Sudden Cardiac Death of the European Society of Cardiology (ESC) endorsed by: Association for European Paediatric and Congenital Cardiology (AEPC)”. In: *Europace* 17, pp. 1601–1687.

Priori, S. G., C. Napolitano, M. Gasparini, C. Pappone, P. Della Bella, U. Giordano, R. Bloise, C. Giustetto, R. De Nardis, M. Grillo, et al. (2002). “Natural history of Brugada syndrome”. In: *Circulation* 105.11, pp. 1342–1347.

Priori, S. G., M. Gasparini, C. Napolitano, P. Della Bella, A. G. Ottonelli, B. Sassone, U. Giordano, C. Pappone, G. Mascioli, G. Rossetti, et al. (2012). “Risk stratification in Brugada syndrome: results of the PRELUDE (PRogrammed ELectrical stimUlation preDictive valuE) registry”. In: *Journal of the American College of Cardiology* 59.1, pp. 37–45.

Priori, S. G., A. A. Wilde, M. Horie, Y. Cho, E. R. Behr, C. Berul, N. Blom, J. Brugada, C.-E. Chiang, H. Huikuri, et al. (2013). “Executive summary: HRS/EHRA/APHRS

expert consensus statement on the diagnosis and management of patients with inherited primary arrhythmia syndromes". In: *Europace* 15.10, pp. 1389–1406.

Probst, V., I. Denjoy, P. G. Meregalli, J.-C. Amirault, F. Sacher, J. Mansourati, D. Babuty, E. Villain, J. Victor, J.-J. Schott, et al. (2007). "Clinical aspects and prognosis of Brugada syndrome in children". In: *Circulation* 115.15, pp. 2042–2048.

Probst, V., C. Veltmann, L. Eckardt, P. Meregalli, F. Gaita, H. Tan, D. Babuty, F. Sacher, C. Giustetto, E. Schulze-Bahr, et al. (2010). "Long-term prognosis of patients diagnosed with Brugada syndrome results from the FINGER Brugada Syndrome Registry". In: *Circulation* 121.5, pp. 635–643.

Rosso, R., A. Glick, M. Glikson, A. Wagshal, M. Swissa, S. Rosenhek, I. Shetboun, V. Khalamizer, T. Fuchs, M. Boulos, et al. (2008). "Outcome after implantation of cardioverter defibrillator in patients with Brugada syndrome: a multicenter Israeli study (ISRABRU)". In: *The Israel Medical Association journal* 10.6, pp. 435–439.

Sarkozy, A., T. Boussy, G. Kourgiannides, G.-B. Chierchia, S. Richter, T. De Potter, P. Geelen, F. Wellens, M. Dingena Spreeuwenberg, and P. Brugada (2007). "Long-term follow-up of primary prophylactic implantable cardioverter-defibrillator therapy in Brugada syndrome". In: *European heart journal* 28.3, pp. 334–344.

Schweizer, P. A., R. Becker, H. A. Katus, and D. Thomas (99). "Successful acute and long-term management of electrical storm in Brugada syndrome using orciprenaline and quinine/quinidine". In: *Clinical research in cardiology* 7.467–470.

Sieira, J., G. Dendramis, and P. Brugada (2016). "Pathogenesis and management of Brugada syndrome". In: *Nature Reviews Cardiology* 13.12, pp. 744–756.

Sieira, J., G. Ciconte, G. Conte, G.-B. Chierchia, C. de Asmundis, G. Baltogiannis, G. Di Giovanni, Y. Saitoh, G. Irfan, R. C. Arroyo, et al. (2015a). "Asymptomatic Brugada syndrome: clinical characterization and long term prognosis". In: *Circulation: Arrhythmia and Electrophysiology* 8.5, pp. 1144–1150.

Sieira, J., G. Conte, G. Ciconte, C. De Asmundis, G.-B. Chierchia, G. Baltogiannis, G. Di Giovanni, Y. Saitoh, G. Irfan, R. Casado-Arroyo, et al. (2015b). "Prognostic value of programmed electrical stimulation in Brugada syndrome: 20 years experience". In: *Circulation: Arrhythmia and Electrophysiology* 8.4, pp. 777–784.

Smith, J. J. (1990). *Circulatory response to the upright posture*. 6. CRC Press.

Subramanian, M., M. A. Prabhu, M. S. Harikrishnan, S. S. Shekhar, P. G. Pai, and K. Natarajan (2017). "The Utility of Exercise Testing in Risk Stratification of Asymptomatic Patients with type 1 Brugada Pattern". In: *Journal of Cardiovascular Electrophysiology* 28, pp. 677–683.

Thomas, G. D. (2011). "Neural control of the circulation". In: *Advances in physiology education* 35.1, pp. 28–32.

Tokuyama, T., Y. Nakano, A. Awazu, Y. Uchimura-Makita, M. Fujiwra, Y. Watanabe, A. Sairaku, K. Kajihara, C. Motoda, N. Oda, et al. (2014). "Deterioration of the

circadian variation of heart rate variability in Brugada syndrome may contribute to the pathogenesis of ventricular fibrillation". In: *Journal of cardiology* 64.2, pp. 133–138.

Vatta, M., R. Dumaine, G. Varghese, T. A. Richard, W. Shimizu, N. Aihara, K. Nademanee, R. Brugada, J. Brugada, G. Veerakul, et al. (2002). "Genetic and biophysical basis of sudden unexplained nocturnal death syndrome (SUNDS), a disease allelic to Brugada syndrome". In: *Human molecular genetics* 11.3, pp. 337–345.

Whitaker, R. H. (2014). "Anatomy of the heart". In: *Medicine* 42.8, pp. 406–408.

Wichter, T., P. Matheja, L. Eckardt, P. Kies, K. Schäfers, E. Schulze-Bahr, W. Haverkamp, M. Borggrefe, O. Schober, G. Breithardt, et al. (2002). "Cardiac autonomic dysfunction in Brugada syndrome". In: *Circulation* 105.6, pp. 702–706.

Wolpert, C., C. Echternach, C. Veltmann, C. Antzelevitch, G. P. Thomas, S. Spehl, F. Streitner, J. Kuschyk, R. Schimpf, K. K. Haase, et al. (2005). "Intravenous drug challenge using flecainide and ajmaline in patients with Brugada syndrome". In: *Heart Rhythm* 2.3, pp. 254–260.

Yan, G.-X. and C. Antzelevitch (1999). "Cellular basis for the Brugada syndrome and other mechanisms of arrhythmogenesis associated with ST-segment elevation". In: *Circulation* 100.15, pp. 1660–1666.

Zipes, D. P., A. J. Camm, M. Borggrefe, A. E. Buxton, B. Chaitman, M. Fromer, G. Gregoratos, G. Klein, A. J. Moss, R. J. Myerburg, et al. (2006). "ACC/AHA/ESC 2006 guidelines for management of patients with ventricular arrhythmias and the prevention of sudden cardiac death: a report of the American College of Cardiology/American Heart Association Task Force and the European Society of Cardiology Committee for Practice Guidelines (Writing Committee to Develop guidelines for management of patients with ventricular arrhythmias and the prevention of sudden cardiac death) developed in collaboration with the European Heart Rhythm Association and the Heart Rhythm Society". In: *Europace* 8.9, pp. 746–837.

CHAPTER 3

Univariate analysis of the autonomic function in Brugada syndrome: signal-processing feature extraction

The previous chapter introduced the problem of risk stratification and, thus, clinical management in patients suffering from Brugada syndrome (BS). Despite the increasing evidence that BS prognosis significantly depends on autonomic imbalance, it is still unclear which autonomic tests and indicators yield the highest predictive values. Indeed, previous works assessing the autonomic function of BS patients through heart rate variability (HRV) analysis have lead to contradictory results. Therefore, in this chapter, classic HRV markers are evaluated in the clinical series previously described, in order to compare the outcomes with reported studies.

Moreover, there are still limited data on the role of standard autonomic maneuvers in this population, and the temporal evolution and non-linear dynamics of cardiovascular signals in the context of BS have yet to be exploited. Therefore, in order to find new biomarkers capable of identifying BS patients at high risk of major cardiac events, this chapter also estimates and compares the time-varying HRV, heart rate complexity (HRC) and baroreflex sensitivity (BRS) of the symptomatic and asymptomatic groups of patients composing our clinical databases.

The subsequent sections introduce the extraction of cardiovascular series as a preprocessing stage, followed by a concise explanation of the methods applied to capture the autonomic function of BS patients. Finally, along with a description of the clinical data used, the results obtained for each substudy are presented and discussed.

3.1. Data preprocessing

From the standard 12-lead ECG recordings, RR-interval and R-peak amplitude series were extracted by using a noise-robust wavelet-based algorithm for QRS complex detection and

subsequent R-wave peak location (Dumont et al., 2010). Based on a Pan & Tompkins detector (Pan et al., 1985), the algorithm includes a high-pass filter that attenuates low-frequency components (P and T waves) and retains high-frequency information (mainly the QRS complex). Then, the detector converts the filtered signal through a derivative, a squaring function and a temporal averaging, and an adaptive threshold applied to the transformed signal identifies a time window in which the maximum amplitude on the raw ECG signal corresponds to the R-wave peak location.

The systolic blood pressure associated to each heartbeat was also detected from blood pressure (BP) signals, as the maxima above a manually adjusted threshold. Figure 3.1 displays a representative example of five consecutive beats where the systolic pressures and R-wave peaks were detected.

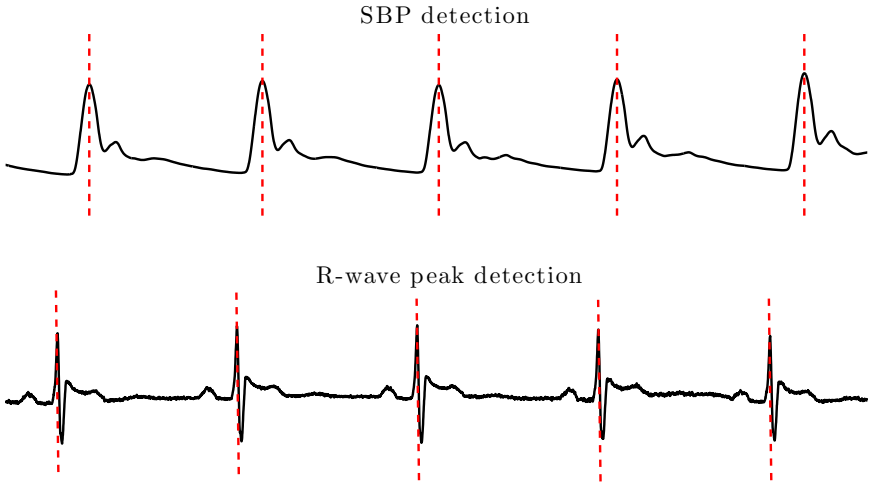

Figure 3.1– Representative SBP and R-wave peak detections from BP and ECG signals, where the latter displays a Brugada-like saddleback pattern.

Systolic blood pressure (SBP) and ECG-derived respiration (EDR) series were extracted from the systolic pressure and R-wave peak amplitudes of each heartbeat; whereas the RR (or RR-interval) series was obtained from the time difference between consecutive R-wave peak locations. Manual corrections to the extracted series were performed when necessary and, for frequency analysis, in order to obtain uniformly sampled data at a rate of 4 Hz, a cubic splines interpolation was applied.

3.2. Feature extraction

In order to evaluate the autonomic function of BS patients, several methods capturing the heart rate variability (HRV), heart rate complexity (HRC) and baroreflex sensitivity (BRS), described in the following subsections, were applied to the previously extracted series.

3.2.1. Heart rate variability

Heart rate variability (HRV) analysis is widely employed in clinical practice to characterize the autonomic nervous system function. Although HRV is mainly assessed in long-term stationary conditions, other approaches accounting for the time-varying autonomic response to transitory changes have been proposed.

3.2.1.1. Stationary conditions

On stationary conditions, according to the Task Force on HRV (European Society of Cardiology et al., 1996), the following time-domain variables were computed: mean and standard deviation of RR series ($\overline{RR}$ and $SDNN$), $NN50$ as the number of pairs of adjacent RR intervals differing by more than 50 ms and $pNN50$ as the proportion of $NN50$ divided by the total number of intervals. Additionally, $MIRR$ was calculated as the interquartile range of the RR sequence, $SDANN$ as the standard deviation of the entire 5-min RR means, $SDNN5min$ as the mean of the 5-min RR standard deviations, and $rMSSD$ as the root mean square of the successive difference between adjacent RR intervals.

Classical spectral HRV parameters were estimated for each patient by an autoregressive model based on the Burg method (Burg, 1975) and the Broersen's combined information criterion (Broersen, 2000) to optimize model orders. Total power (TP) was calculated as the sum of the four spectral bands: ultra-low frequency (ULF: $0 - 0.003$ Hz), very-low frequency (VLF: $0.003 - 0.04$ Hz), low frequency (LF: $0.04 - 0.15$ Hz) and high frequency (HF: $0.15 - 0.4$ Hz). The HF component reflects the parasympathetic activity, whereas the LF component is modulated by both sympathetic and parasympathetic autonomic contributions (Malliani et al., 1994; Ori et al., 1992). They were calculated as the average of 5-min intervals and normalized by subtracting the VLF component from the TP in order to reduce the effect of noise artifacts:

$$LF_{nu} = \frac{LF}{TP - VLF} \tag{3.1}$$

$$HF_{nu} = \frac{HF}{TP - VLF} \tag{3.2}$$

Moreover, the global sympathovagal balance was estimated through the $\frac{LF}{HF}$ ratio.

3.2.1.2. Non-stationary conditions

Given that signals during ANS stimulations, such as exercise or HUT testing, are typically non-stationary, spectral characteristics associated with HRV were analyzed using a time-frequency (TF) approach. In order to remove the very low frequency component, RR series were high-pass filtered at 0.03 Hz with a 4^{th} order Butterworth filter applied in both forward and backward directions so as to remove phase distortion. Then, a smoothed pseudo Wigner-Ville distribution (SPWVD) transform from the Time-Frequency toolbox (Auger et al., 1996) was employed since it has proved its usefulness for the analysis of cardiovascular signals (Orini et al., 2010).

The Wigner Ville distribution is a quadratic time-frequency method defined as the Fourier transform of the instantaneous autocorrelation function (Hlawatsch et al., 1992). However, since it is affected by significant interference terms, the SPWVD introduces a smoothing kernel function $\Psi(\tau, \upsilon)$, defined in Costa et al (Costa et al., 1995), that attenuates interferences while maintaining a suitable time-frequency resolution. Being $A_{RR}(\tau, \upsilon)$ the Ambiguity Function of the RR series, $x_{RR}(t)$, the SPWVD is defined as:

$$A_{RR}(\tau, \upsilon) = \int_{-\infty}^{\infty} x_{RR}\left(t + \frac{\tau}{2}\right) x_{RR}^{*}\left(t - \frac{\tau}{2}\right) e^{-j2\pi\upsilon t} dt \tag{3.3}$$

$$\psi(\tau, \upsilon) = exp\left\{-\pi\left[\left(\frac{\upsilon}{\upsilon_o}\right)^2 + \left(\frac{\tau}{\tau_o}\right)^2\right]^{2\lambda}\right\} \tag{3.4}$$

$$C_{RR}(t, f) = \int\int \psi(\tau, \upsilon) A_{RR}(\tau, \upsilon) e^{j2\pi(t\upsilon - \tau f)} d\upsilon d\tau \tag{3.5}$$

Kernel parameters were adjusted to $\upsilon_0 = 0.06$ and $\tau_0 = 0.03$, obtaining temporal and spectral resolutions of 16.7 seconds and 0.033 Hz, respectively. Among all the analyzed combinations, this one lead to the most efficient interference terms cancellation for the lowest TF filtering.

HRV was measured as the total power in LF and HF bands (noted as LFb and HFb), obtained from the SPWVD:

$$LF(t) = \int_{LFb} C_{RR}(t, f) df \tag{3.6}$$

$$HF(t) = \int_{HFb} C_{RR}(t, f) df \tag{3.7}$$

Assuming that sympathetic activity always lies within the standard LF band, this band was fixed between 0.04 and 0.15 Hz for the whole stress test. However, the total power in the HF band captures parasympathetic activity, closely related to respiratory sinus arrhythmia (RSA). Since respiratory frequency during ANS stimulation, especially during exertion, may not be restricted to the classic HF band ($0.15 - 0.4$ Hz) and can increase up to 0.7 Hz, HRV analysis within the standard frequency band would lead to unreliable measures of the parasympathetic activity. In order to overcome this limitation, a time-varying HF band, based on an estimation of the respiration activity captured by the ECG-Derived respiration (EDR) series was defined (Bailón et al., 2007).

The applied EDR method estimates respiratory information from the amplitude modulation of R-wave peaks (Moody et al., 1986). The estimated respiration signal was then band-pass filtered by a 4^{th} order Butterworth filter between 0.15 and 0.7 Hz, applied in both forward and backward directions to remove frequencies out of the respiratory range. The same SPWVD transform used

for RR series was then applied to EDR filtered signals to estimate the instantaneous respiratory frequency.

The simplest estimation method consists in finding the frequency presenting the largest peak in the spectrum at each time instant $\hat{f}(t)$. However, in order to avoid spurious peak detections, for each time instant t_k, the search interval was limited to frequencies between 2δ Hz, centered around a reference frequency $f_r(t_k) : [f_r(t_k) - \delta, f_r(t_k) + \delta]$. This reference frequency was defined as the exponential average of previous estimates:

$$f_r(t_k) = \beta f_r(t_{k-1}) + (1 - \beta)\hat{f}(t_{k-1}), \tag{3.8}$$

where β is the forgetting factor. As in (Bailón et al., 2006), a value of β=0.7 was used, based on real respiratory patterns during exercise testing, and δ=0.01, since respiratory frequency variations are not supposed to be faster than 0.01 Hz per 0.25 s. Moreover, to reduce the risk of spurious frequency detections in the initialization of $f_r(t)$, the first instantaneous respiratory frequency $f_r(t_0)$ was selected within the standard HF band ($0.15 - 0.4$ Hz). Once the estimated respiratory frequency series $f_r(t)$ was obtained, the time-varying HF band for HRV analysis was defined as $HFb(t) = [f_r(t) - 0.125, f_r(t) + 0.125]$ Hz, with t covering the whole test.

Unlike classical HRV parameters, SPWVD leads to time-frequency HRV estimators that are indeed time series that vary during the application of autonomic maneuvers. These markers, accounting for the sympathetic and parasympathetic influences of the ANS on heart rate, were normalized by the total power (TP), defined as the sum of both spectral bands ($TP(t) = LF(t) + HF(t)$), leading to the time series $LF_{nu}(t)$ and $HF_{nu}(t)$:

$$LF_{nu}(t) = \frac{LF(t)}{TP(t)} \cdot 100 \tag{3.9}$$

$$HF_{nu}(t) = \frac{HF(t)}{TP(t)} \cdot 100 \tag{3.10}$$

From this definition of normalization, it should be noted that $LF_{nu} = 100 - HF_{nu}$ and, thus, statistical results for both time series are identical. $\frac{LF}{HF}(t)$ was also calculated from dividing $LF(t)$ by $HF(t)$, so as to obtain the time-varying global sympathovagal balance.

3.2.2. Heart rate complexity

Non-linear HRV markers have been developed to characterize HR dynamics that may not be captured by classical approaches. Since RR series in healthy subjects have been found to fluctuate following a complex non-uniform pattern associated with a 1/f-like distribution (inverse power law), heart rate complexity (HRC) was assessed by power-law scaling analysis, along with another widely used measure of HRC, known as sample entropy.

3.2.2.1. Power-law scaling analysis

The scaling exponent β measures the power-law behavior as the slope of the regression line calculated by the least-squares method on the linear portion of power spectral density (PSD) against frequency plots on a bi-logarithmic scale. Several studies on power-law scaling analysis have employed the frequency band $[0.0001 - 0.01]$ Hz to analyze long-term fluctuations when evaluating SCD and myocardial infarction (Huikuri et al., 1998; Tapanainen et al., 2002). However, for short-term recordings, this technique has also been applied using the $[0.003 - 0.1]$ Hz band (Lombardi et al., 2000).

PSD was estimated using the Burg method and the Broersen's combined information criterion to optimize the autoregressive model orders. Since the analysis was performed in short segments of the RR series during exercise testing, the scaling exponent β was extracted from the frequency band $[0.003 - 0.1]$ Hz; -2.5 to -1 on a logarithmic scale.

3.2.2.2. Sample entropy

Heart rate complexity, or irregularity, may also be quantified by the sample entropy ($SampEn$) method. As a refined version of the traditionally used Approximate Entropy (Richman JS, 2000), it is defined as the negative natural logarithm of the conditional probability that two sequences of m consecutive data points, which are similar to each other with a tolerance r, will remain similar when one more consecutive point is included.

Thus, from a given time series of L points, $x = \{x(1), x(2), \cdots, x(L)\}$, based on the embedded dimension m and tolerance r, $SampEn$ is calculated as follows:

1. $L - m + 1$ new time series of size m are constructed as:

$$X^m(i) = \{x(i), x(i+1), \cdots, x(i+m-1)\}, \text{ where } i = 1, \cdots, L - m + 1 \tag{3.11}$$

2. Then, the distance between each couple of time series, including itself, is computed as:

$$d[X^m(i), X^m(j)] = \mathbf{max}[|x(i+k) - x(j+k)|], \text{ where } 0 \leq k \leq m - 1 \tag{3.12}$$

3. For each vector $X^m(i)$, the number of template matchings is calculated as:

$$N^m(i) = \mathbf{card}(d[X^m(i), X^m(j)]) \leq r \tag{3.13}$$

4. Being $C_r^m(i) = N^m(i)/(L - m + 1)$ the probability that any vector $X^m(j)$ matches $X^m(i)$, the average of C_r^m over i is:

$$\phi^m(r) = \frac{1}{L - m + 1} \sum_{i=1}^{L-m+1} C_m^r(i) \tag{3.14}$$

5. By increasing the size of time series to $m + 1$ and repeating the previous step to obtain $\phi^{m+1}(r)$, the theoretical value of $SampEn$ is defined as:

$$SampEn(m, r) = \lim_{L \to \infty} [\ln(\phi^m(r) - \phi^{m+1}(r))] \tag{3.15}$$

Thus, for a finite value of L, $SampEn$ is estimated as:

$$SampEn(m, r, L) = \ln(\phi^m(r) - \phi^{m+1}(r)) \tag{3.16}$$

Large values of $SampEn$ indicate high irregularity and great complexity, whereas smaller values refer to a more regular and predictable signal, commonly associated with disease (Javorka et al., 2008; Khandoker AH, 2009; Tuzcu et al., 2006). Based on (Lake et al., 2002), the embedding dimension was chosen as $m = 3$ and the tolerance distance as $r = 0.2 \cdot SD$, in order to study the HRC of BS patients overnight.

3.2.3. Baroreflex sensitivity

Several methods have been proposed to non-invasively estimate spontaneous baroreflex sensitivity (BRS) from variations in SBP and RR series. Since they are difficult to compare and often lead to conflicting results, previous works have already analyzed different BRS estimates in health and disease (Bernardi et al., 2010; Laude et al., 2004). In this work, eight previously described BRS approaches, summarized in Table 3.1, were computed and compared in a BS context, during HUT testing.

3.2.3.1. Temporal BRS estimates

First, BRS was estimated by the sequence method for positive ($BRS^{+/+}$) and negative ($BRS^{-/-}$) sequences. This approach considers three or more consecutive beats in which increasing/decreasing SBP values are followed by progressive lengthening/shortening in RR series (Di Rienzo et al., 1985). Those slopes of the regression lines relating positive/negative changes in both signals with a fitting coefficient higher than 0.8 are then averaged to obtain, respectively, $BRS^{+/+}$ and $BRS^{-/-}$.

Then, $BRS - SD$ (Bernardi et al., 2010) was computed as the standard deviation of detrended RR series (σ_{RR}), divided by the standard deviation of detrended SBP series (σ_{SBP}).

$$BRS - SD = \frac{\sigma_{RR}}{\sigma_{SBP}} \tag{3.17}$$

3.2.3.2. Spectral BRS estimates

Regarding spectral methods, $BRS - LF$, $BRS - HF$ and $BRS - LHF$ were calculated as the square root of the ratio of the autoregressive powers of RR (P_{RR}) and SBP (P_{SBP}) series in the LF ($0.04 - 0.15$ Hz), HF ($0.15 - 0.40$ Hz) and simultaneously in both frequency bands LHF ($0.04 - 0.40$ Hz) (Pagani et al., 1988), when coherence between both series was greater than a threshold γ. Figure 3.2 illustrates the application of this threshold to the coherence function in order to determine the spectral bands used to calculate $BRS - LF$, $BRS - HF$ and $BRS - LHF$ estimates.

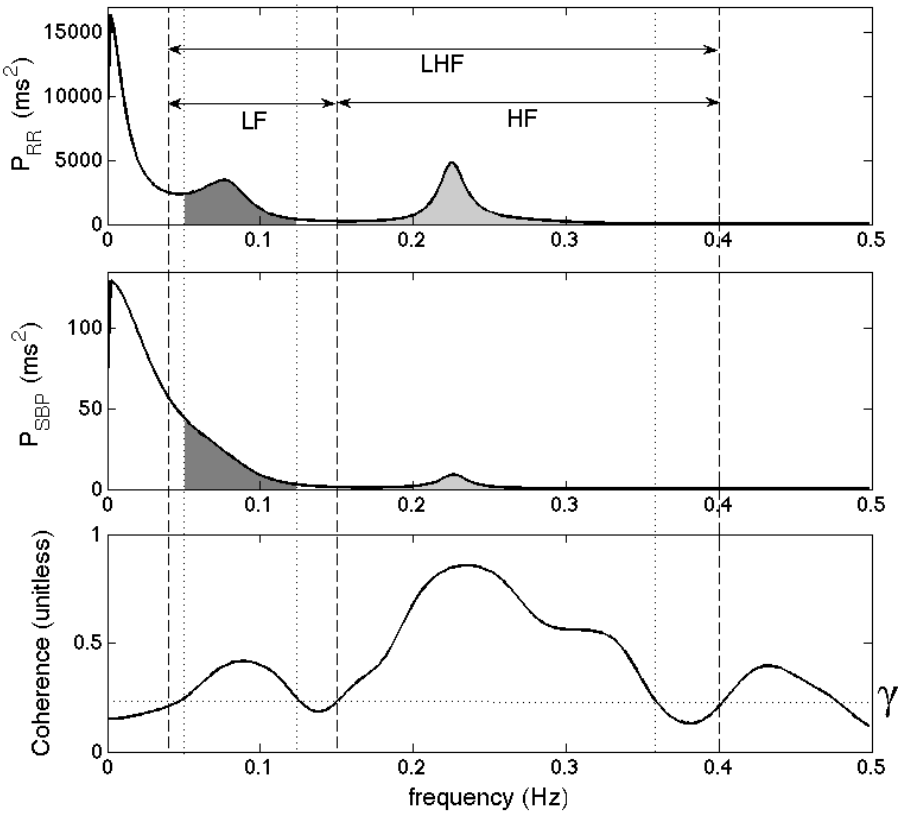

Figure 3.2– Schematic representation of BRS estimation, based on the spectral power of bands LF, HF and LHF; at frequencies where the coherence between SBP and RR signals is greater than a threshold γ.

$$BRS - X = \sqrt{\frac{P_{RR}}{P_{SBP}}\Big|_X}, \text{ where } X \in \{LF, HF, LHF\} \tag{3.18}$$

Spectral power was obtained as the average of applying the Burg method with optimized orders based on the Broersen's combined information criterion on 5-min intervals. Coherence was estimated from a Welch periodogram with a 50% overlap and Hanning windowing, and the threshold γ was based on the approach defined in (Gallet et al., 2011):

$$\gamma = 1 - \alpha^{\frac{1}{\hat{K}-1}} \tag{3.19}$$

$$\hat{K} = \frac{K}{1 + 2(\frac{K-1}{K})\rho_w^2} \tag{3.20}$$

where $\alpha = 0.05$ refers to the significance level, $\rho_w = 0.17$ is the overlap coefficient for the Hanning-window 50% overlap and K accounts for the number of analyzed segments, which depends on signal length.

3.2.3.3. Transfer-function BRS estimates

Finally, $BRS{-}TF_{TH}$ was extracted from the averaged transfer function magnitude ($|TF_{SBP,RR}|$) within the LF range (Robbe et al., 1987), at frequencies of maximum coherence upon the threshold γ defined in (Gallet et al., 2011). However, since the coherence criterion has been refused to guarantee accurate BRS measurements when the baroreflex becomes strongly depressed, $BRS-TF_{LF}$ was also obtained from the average of $|TF_{SBP,RR}|$ over the whole LF band, without considering coherence values (Pinna et al., 2002). In both cases, the transfer function was estimated from a Welch periodogram with 50% overlap and Hanning windowing. Figure 3.3 represents the spectral bands used to calculate BRS estimates based on the transfer function of SBP and RR series.

$$BRS - TF_X = \frac{1}{N_X} \sum_X |TF_{RR,SBP}|, \text{ where } X \in \{LF, TH\} \tag{3.21}$$

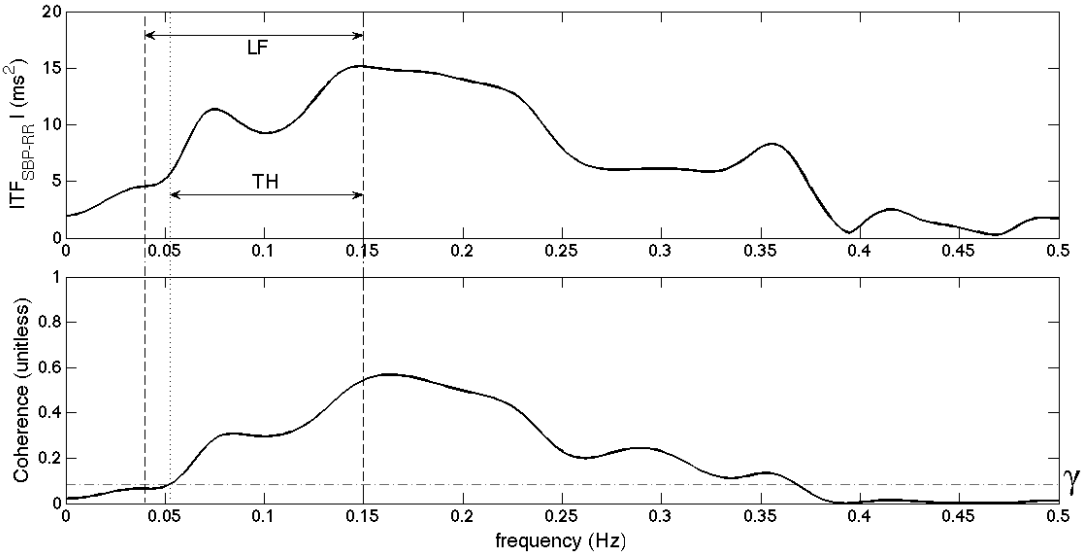

Figure 3.3– Schematic representation of BRS estimation, based on the averaged transfer function magnitude of SBP and RR series, at bands LF and TH.

3.3. Inter-patient analysis

Methods described in the previous section were applied to different clinical datasets, in order to characterize and compare the autonomic function of symptomatic and asymptomatic BS patients under different conditions.

Table 3.2 summarizes the analyzed markers, data sources and number of patients of each substudy. First, the HRV and HRC of 87 patients included in the Holter database were analyzed overnight. HRV was also assessed during exercise in 105 patients composing both Holter and Cardionics databases. Then, HRC during exercise was evaluated in the 69 BS patients coming

Table 3.1– Brief description of the analyzed BRS estimates.

BRS estimate	**Description**
$BRS^{+/+}$	Averaged slopes of the regression lines relating positive changes in both RR and SBP series for sequences of 3 or more consecutive beats
$BRS^{-/-}$	Averaged slopes of the regression lines relating negative changes in both RR and SBP series for sequences of 3 or more consecutive beats
$BRS-SD$	Ratio of the standard deviation of RR and SBP series
$BRS-LF$	Square root of the ratio of the spectral powers of RR and SBP series at the LF band, at frequencies where coherence $> \gamma$
$BRS-HF$	Square root of the ratio of the spectral powers of RR and SBP series at the HF band, at frequencies where coherence $> \gamma$
$BRS-LHF$	Square root of the ratio of the spectral powers of RR and SBP series at both LF and HF bands (LHF band), at frequencies where coherence $> \gamma$
$BRS-TF_{TH}$	Averaged transfer function magnitude at the LF band, at frequencies where coherence $> \gamma$
$BRS-TF_{LF}$	Averaged transfer function magnitude at the LF band

from the Holter database, in order to include resting phases, before and after the test, to the analysis. The HRV during HUT testing of 65 patients from the Holter database was likewise characterized. Finally, since the Task Force database included both BP and ECG signals of 32 BS patients, a study on their BRS was conducted.

The following subsections describe the methodology and clinical data used for each substudy, as well as the main results obtained.

3.3.1. Heart rate variability and complexity at night

Previous studies assessing the autonomic function through HRV analysis along 24-hour ECG recordings have led to contradictory results (Behar et al., 2016; Hermida et al., 2003; Kostopoulou et al., 2010; Krittayaphong et al., 2003; Nakazawa et al., 2003; Pierre et al., 2007; Tokuyama et al., 2014). Although linear temporal and spectral HRV parameters

TABLE 3.2– Analyzed indices, sample of patients included in the study and source database for each autonomic analysis.

Autonomic analysis	**Indices**	**Sample**	**Source database**
Night analysis	HRV	87	Holter
	HRC	87	Holter
Exercise testing	HRV	105	Holter + Cardionics
	HRC	69	Holter
HUT testing	HRV	65	Holter
	BRS	32	Task Force

are unable to capture the complexity of HR regulation, indices accounting for the non-linear dynamics of RR series, such as *SampEn*, could unmask autonomic differences in BS patients at different levels of risk. Therefore, in this section, the HRV and HRC, as well as their circadian fluctuations, of 23 symptomatic and 64 asymptomatic BS patients are assessed and compared overnight.

3.3.1.1. Clinical data description

Patients' age ranged from 19 to 79 years old (45.63 ± 13.03 years old) and 71.26% were males. Twenty-three patients had the following documented symptoms: syncope (60.87%), cardiac arrest (34.78%), dizziness (13.04%) and, less frequently, palpitations (4.35%) and nocturnal convulsions (4.35%). The remaining 64 patients were considered as asymptomatic.

Cardioverter defibrillator implantations (ICD) had been performed in 15 of 64 (23.44%) asymptomatic patients, based on a positive EPS (Electrophysiological Study) test, whereas all symptomatic patients were ICD carriers. Genetic testing in search of *SCN5A* mutations was completed in 71 patients (21 were symptomatic) and is pending in 6 asymptomatic and 1 symptomatic subjects. The test was not performed in 9 patients (1 symptomatic), since no mutations had been identified in their families. Among 27 patients in whom the *SCN5A* mutation was found, 10 were symptomatic. Table 3.3 summarizes patients' clinical characteristics.

3.3.1.2. Methods

Heart rate variability was measured by means of the classic temporal and spectral indices described in Section 3.2.1.1 for stationary conditions, and complexity of RR series was evaluated through the *SampEn* method described in Section 3.2.2.2.

Comparisons between symptomatic and asymptomatic patients overnight (midnight to 6 a.m.), as well as for each interval of one hour, were evaluated by Mann-Whitney U non-parametric tests. Moreover, fluctuations in HRV and HRC at night were calculated as in (BEHAR et al., 2016), using a coefficient of variation δ = (maximum − minimum value)/maximum value.

Table 3.3– Clinical characteristics of asymptomatic and symptomatic study groups at night.

	Asymptomatic (n=64)	**Symptomatic** (n=23)	*p*-**value**
Age, *years old*	45.50 ± 13.08	46.00 ± 13.16	0.996
Male sex, *n(%)*	43 (67.19%)	19 (82.61%)	0.163
ICD implantation, *n (%)*	15 (23.44%)	23 (100%)	< 0.001
Presence of SCN5A mutation, *n (%)*	17 (34.00%)	10 (47.62%)	0.284

Values are mean ± standard deviation or number of observations (%).
All between-groups differences, apart from ICD implantation, are statistically non-significant.

Logistic regression is a statistical method that finds the best fitting model to describe the relationship between a dichotomous outcome (here the presence/absence of symptoms) and a set of independent variables $X_1, \cdots, X_k$. It generates the coefficients $b_o, b_1, \cdots, b_k$ (and its standard errors and significance levels) that maximize the likelihood of observing the sample values in order to predict a logit transformation of the probability of suffering symptoms from the following formula:

$$logit(p) = \ln \frac{p}{1-p} = b_0 + b_1 X_1 + \cdots + b_k X_k \tag{3.22}$$

Therefore, binary logistic regression models were applied to each variable differing significantly between groups in order to predict the probability of experiencing symptoms related to those HRV and HRC measures.

3.3.1.3. Results

When the whole night was taken into account, similar results with no significant differences between study groups were found. However, the variation coefficient of $SDANN$, $\delta SDANN$, was significantly higher in symptomatic patients between 1 a.m. and 5 a.m. ($p < 0.005$).

Regarding HRV and HRC differences analyzed for each interval of one hour, some relevant tendencies, represented by some exemplifying indices in Figure 3.4, were observed. Table 3.4 summarizes the mean ± standard deviation values for symptomatic and asymptomatic patients, and the associated *p*-values for each significant case.

Based on the results, symptomatic patients showed a decreased heart rate complexity. During nighttime, they displayed reduced values of $SampEn$ with respect to asymptomatic subjects, which turned to be significant between 1 a.m. - 2 a.m. and 4 a.m. - 5 a.m. Similarly, a decreased HRV was also captured in symptomatic BS patients, which was statistically significant between 5 a.m. - 6 a.m., according to $SDNN$, $MIRR$ and $SDANN$. Significant differences were also captured by $MIRR$ between midnight - 1 a.m. and by $SDANN$ between 2 a.m. - 3 a.m.

TABLE 3.4– Mean ± standard deviation, for asymptomatic and symptomatic patients, and associated p-values in significant variables.

	Asymptomatic (n=64)	**Symptomatic** (n=23)	p-**value**
SampEn			
1 a.m. - 2 a.m.	1.19 ± 0.25	1.04 ± 0.36	0.045
4 a.m. - 5 a.m.	1.12 ± 0.26	0.95 ± 0.37	0.017
SDNN			
5 a.m. - 6 a. m.	97.04 ± 36.93	79.48 ± 33.65	0.029
MIRR			
Midnight - 1 a.m.	88.95 ± 59.16	64.48 ± 29.10	0.032
5 a.m. - 6 a.m.	113.86 ± 62.46	85.74 ± 49.64	0.014
SDANN			
2 a.m. - 3 a.m.	38.77 ± 23.81	26.83 ± 16.16	0.027
5 a.m. - 6 a.m.	46.65 ± 24.59	35.16 ± 22.90	0.025
$\delta SDANN$ **(1 a.m. - 5 a.m.)**	0.56 ± 0.14	0.67 ± 0.10	< 0.005

Figure 3.4 represents the circadian variation of HRV and HRC at night for both groups of patients, by showing the evolution of the mean at each hour for the most significant autonomic markers: *MIRR* and *SampEn*. Likewise, the main tendency of these markers is represented by fitted regression lines for each group of patients. The graphs show a similar evolution along the night in terms of regression line slopes between both groups, but symptomatic patients display lower mean HRV and HRC values.

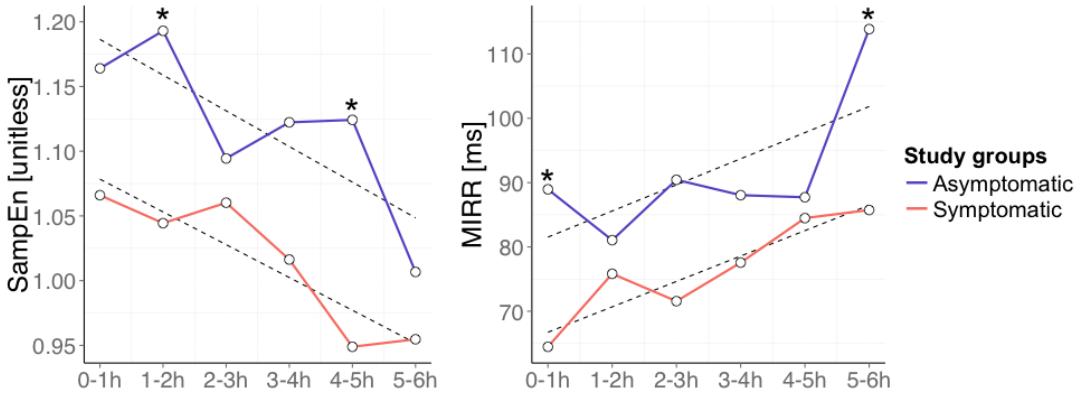

FIGURE 3.4– Mean *SampEn* and mean *MIRR* for symptomatic and asymptomatic BS patients at each hour overnight (*p <0.05). Dotted black lines are fitted linear regression lines that represent the main tendencies of each variable along the night, for both study groups.

Finally, Table 3.5 summarizes the odds ratios (OR), 95% confidence intervals (CI) and p-values associated with each univariate model.

Table 3.5– Odds ratios, 95% confidence intervals and p-values from univariate analysis of significant autonomic markers.

	OR	**95% CI**	p**-value**
SampEn			
1 a.m. - 2 a.m.	0.171	0.032 - 0.913	0.039*
4 a.m. - 5 a.m.	0.129	0.023 - 0.714	0.019*
SDNN			
5 a.m. - 6 a. m.	0.984	0.969 - 1.000	0.053
MIRR			
Midnight - 1 a.m.	0.983	0.967 - 1.000	0.047*
5 a.m. - 6 a.m.	0.989	0.978 - 1.000	0.060
SDANN			
2 a.m. - 3 a.m.	0.969	0.941 - 0.998	0.037*
5 a.m. - 6 a.m.	0.978	0.956 - 1.001	0.059
$\delta SDANN$ **(1 a.m. - 5 a.m.)**	1039.321	11.293 - 95650.848	0.003*

*$p < 0.05$ when comparing symptomatic and asymptomatic study groups.

MIRR between midnight - 1 a.m. turned to be an independent predictor for the occurrence of symptoms in univariate analysis with a 1.7% decreased risk per one point increase. Between 2 a.m. - 3 a.m., *SDANN* displayed a decreased risk of the 3.1%. $\delta SDANN$ between 1 a.m. - 5 a.m. was also a significant predictor of symptoms, as well as *SampEn* between 1 a.m. - 2 a.m. and between 4 a.m. - 5 a.m. showed a decreased risk of the 82.9% and 87.1%, respectively, per one point of *SampEn* increase.

3.3.2. Heart rate variability during exercise testing

The autonomic function can be better characterized by stimulating the ANS in a controlled and repeatable fashion, through the application of standardized maneuvers such as exercise testing. Indeed, previous works have reported the potential of exercise to predict cardiac events in BS (Masrur et al., 2015; Subramanian et al., 2017). However, cardiovascular signals during exertion are typically non-stationary, and the temporal progression of the autonomic response to exercise and recovery has never been analyzed in the context of BS. Therefore, in this section, the inter-patient temporal evolution of HRV in response to exercise testing is characterized by a time-frequency approach, and the results are compared according to the symptomatic status of 105 BS patients.

3.3.2.1. Clinical data description

Participants' age ranged from 19 to 74 years old (45.17 ± 13.62 years old) and 76.2% were males. Twenty-four patients presented documented symptoms of ventricular origin: syncope (50%), cardiac arrest (41.7%), dizziness (12.5%) and, less frequently, palpitations and nocturnal

convulsions (4.2%). ICDs had been implanted in 18 of 81 (22.2%) asymptomatic patients, based on a positive EPS test, whereas all symptomatic patients had ICDs implanted. Among 76 patients (19 were symptomatic) in whom genetic analysis was performed, an *SCN5A* mutation was found in 27 (35.5%). Table 3.6 summarizes patients' clinical characteristics.

TABLE 3.6– Symptomatic and asymptomatic patients' clinical characteristics for HRV analysis during exercise testing.

	Symptomatic (n=24)	**Asymptomatic (n=81)**	*p*-**value**
Age, *years old*	46.25 ± 15.23	44.85 ± 13.20	0.852
Male sex, *n (%)*	60 (74.1%)	20 (83.3%)	0.352
ICD implantation, *n (%)*	24 (100%)	18 (22.2%)	< 0.001
Presence of *SCN5A* mutation, *n (%)*	6 (31.6%)	21 (36.8%)	0.680

Values are mean ± standard deviation or number of observations (%).
All between-groups differences, apart from ICD implantation, are statistically non-significant.

3.3.2.2. Methods

HRV time series were extracted from the time-frequency analysis described in Section 3.2.1.2, based on the smoothed pseudo Wigner-Ville distribution (SPWVD) of RR series that adapts frequency bands to respiratory information resulting from EDR signals. These HRV time series were averaged in temporal non-overlapped windows of 1 minute for each patient, leading to $\overline{LF^i}$, $\overline{LF^i_{nu}}$, $\overline{HF^i}$, $\overline{HF^i_{nu}}$ and $\overline{LF/HF^i}$, which stand for each time series intra-patient mean for the following time periods: $i \in \{WU1, WU2, EX1, EX2, EX3, PE, AR1, AR2, AR3, PR1, PR2, PR3\}$. Since each test differed in the incremental exercise phase duration and the shortest case in our clinical series lasted less than 5 minutes, only the first 3 minutes of incremental exertion ($EX1$, $EX2$ and $EX3$), as well as the last minute before peak effort (PE), were assessed. In addition, the entire warm-up ($WU1$ and $WU2$) and active ($AR1$, $AR2$ and $AR3$) and passive recovery ($PR1$, $PR2$ and $PR3$) phases were compared between symptomatic and asymptomatic patients. Fig 3.5 displays the analyzed periods for different phases of the exercise test, indicating the peak effort instant.

Finally, HRV features extracted during exercise and recovery were compared between symptomatic and asymptomatic groups, by Mann-Whitney U non-parametric tests. In order to compare the last minute of exertion and recovery, all patients had to be synchronized with respect to the peak effort instant.

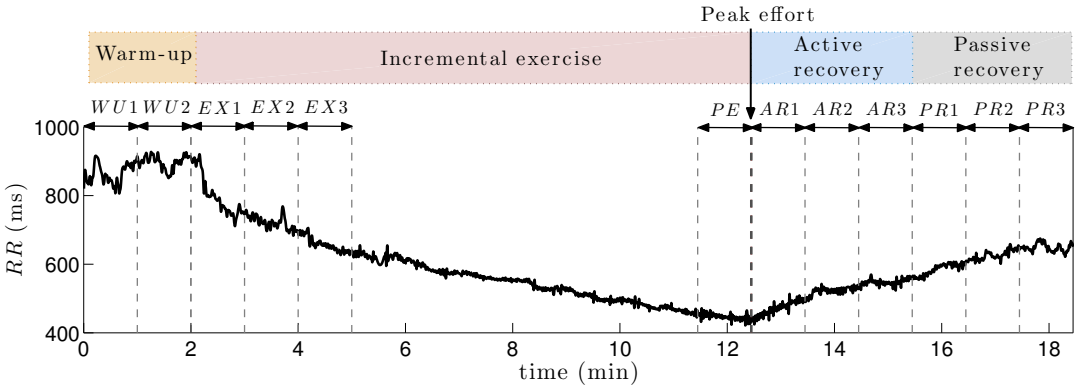

Figure 3.5– Exercise testing was divided in four phases: warm-up, incremental exercise, active recovery and passive recovery. HRV time series estimated from the RR series were averaged in the following 1-min windows: both minutes of warm-up ($WU1$ and $WU2$), first 3 minutes of incremental exercise ($EX1$, $EX2$, $EX3$), last minute of exercise before peak effort (PE), 3 minutes of active recovery ($AR1$, $AR2$, $AR3$) and 3 minutes of passive recovery ($PR1$, $PR2$, $PR3$).

3.3.2.3. Results

The upper panel of Fig 3.6 displays an example of EDR series. Below, the SPWVD spectral power of respiration is shown, along with its estimated instantaneous respiratory frequency $f_r(t)$, which is represented with a dashed red line. Note that, in this example, as the patient approaches the peak effort (dashed vertical line), respiratory frequency exceeds the standard HF band upper limit of 0.4 Hz.

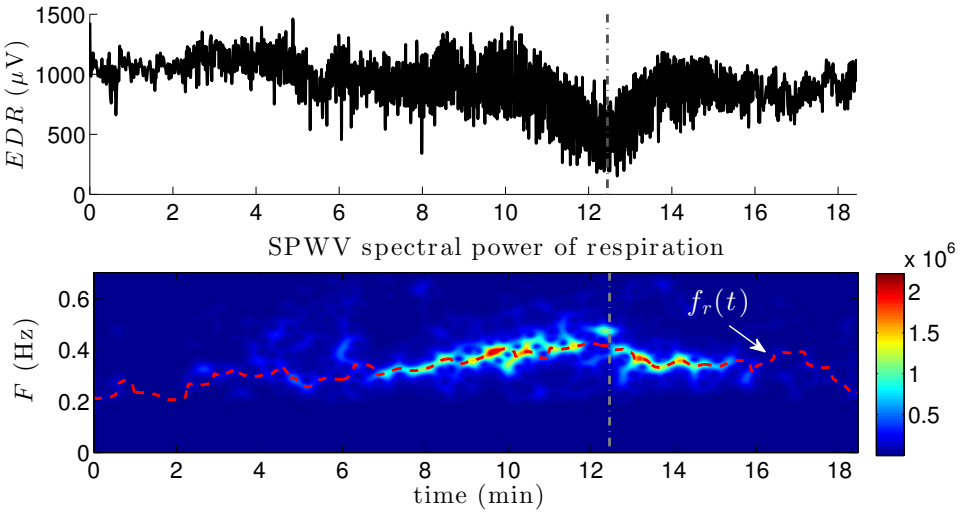

Figure 3.6– Top: example of EDR series, calculated from the patient's R-wave peak amplitudes. Bottom: SPWVD spectral power associated, along with the instantaneous respiratory frequency $f_r(t)$ estimated from a corrected version of the frequencies presenting the maximum spectral powers at each time instant (dashed red line). Vertical dashed lines indicate the peak effort instant, before recovery.

Based on patients' respiratory information, the time-varying patient-specific HF bands were computed. Following the previous example, Fig 3.7 displays the RR series and its associated SPWVD spectral power for the same patient, where the LF and respiration-centered HF bands are represented in dashed white lines (second panel). The third panel shows the time series $LF(t)$ and $HF(t)$ extracted from TF analysis, then normalized by the total power defined as the sum of LF and HF bands at each time instant. Finally, the last panel displays the obtained $HF_{nu}(t)$ series, where the 1-min window to calculate the mean value of HF_{nu} during the first minute of active recovery ($\overline{HF_{nu}^{AR1}}$) is specified.

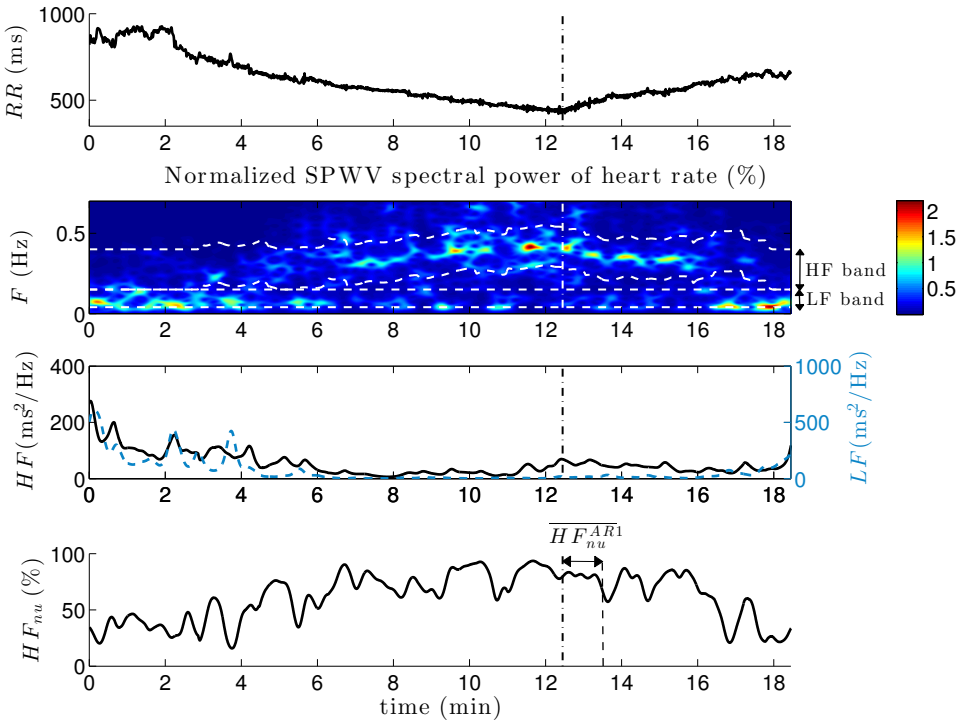

FIGURE 3.7– From the RR series, the normalized SPWVD spectral power is calculated. The second panel indicates LF and HF bands in dashed white lines. In the third panel, the total power in LF (blue dashed line) and HF (black solid line) bands at each time instant are represented. Then, an example of normalized time series (HF_{nu}) accounts for the parasympathetic contribution along the exercise test. A vertical dashed line in all panels refers to the peak effort instant. In the last panel, the time period used to calculate $\overline{HF_{nu}^{AR1}}$ is indicated.

In this example, it should be noted the non-negligible power centered in the HF band as a result of respiration. Moreover, since HF exceeds the standard band, it becomes clear that the use of classic spectral limits would have lead to unreliable measures of the vagal tone.

Regarding inter-group comparison, during the second minute of incremental exercise, statistically significant differences were found in mean normalized HF ($\overline{HF_{nu}^{EX2}}$, $p = 0.041$) and thus in $\overline{LF_{nu}^{EX2}}$. Symptomatic patients showed an increased $\overline{HF_{nu}}$, and a reduced $\overline{LF_{nu}}$, in this time period with respect to asymptomatic patients. However, no significant differences were found between groups after exertion, during recovery.

3.3.3. Heart rate complexity during exercise testing

Since methods based on frequency-domain approaches are unable to capture the complex, non-linear effects of HR regulation, the HRC during exercise testing on a clinical series of 69 BS patients was evaluated through the power-law scaling exponent (β), which has proved its usefulness in detecting decreased complexity in patients with cardiovascular disorders and SCD events (Gomis et al., 2006; Huikuri et al., 1998, 2000; Lombardi et al., 2001; Maestri et al., 2007; Tapanainen et al., 2002). In order to assess HRC during exercise and recovery, but also in baseline conditions, only those patients composing the Holter database were included in the study.

3.3.3.1. Clinical data description

Patients' age ranged from 19 to 73 years old (45.06 ± 12.79 years old) and 78.3% were males. Sixteen patients had the following documented symptoms: syncope (56.25%), cardiac arrest (25%), dizziness (18.75%) and, less frequently, palpitations (12.50%) and nocturnal convulsions (6.25%). ICD implantation had been performed in 15 of 53 (28.3%) asymptomatic patients, based on a positive EPS test, whereas all symptomatic patients were ICD carriers. Among 54 patients (13 were symptomatic) in whom genetic screening was performed, an *SCN5A* mutation was found in 19 (35.2%), from whom 5 were symptomatic. Table 3.7 summarizes participants' baseline characteristics.

Table 3.7– Symptomatic and asymptomatic patients' clinical characteristics for HRC analysis during exercise testing.

	Symptomatic (n=16)	**Asymptomatic (n=53)**	*p*-**value**
Age, *years old*	45.88 ± 15.31	44.81 ± 12.09	0.837
Male sex, *n (%)*	13 (81.3%)	41 (77.4%)	0.743
ICD implantation, *n (%)*	16 (100%)	15 (28.3%)	<0.001
Presence of *SCN5A* mutation, *n (%)*	5 (38.5%)	14 (34.2%)	0.656

Values are mean ± standard deviation or number of observations (%).
All between-groups differences, apart from ICD implantation, are statistically non-significant.

3.3.3.2. Methods

Heart rate complexity was quantified by means of the β slope resulting from power-law scaling analysis, described in Section 3.2.2.1. Comparisons between symptomatic and asymptomatic patients during different phases of the test were evaluated by Mann–Whitney U non-parametric tests. Then, binary logistic regression models were applied to variables that significantly differed

between groups in order to predict the probability of experiencing symptoms, as a function of HRC measures.

3.3.3.3. Results

Table 3.8 summarizes, for each phase of the test, the p-values obtained when comparing β slopes between groups of patients, as well as the R-squared (R^2) values indicating the quality of fit between PSD and fitted models. In general, linear models reached an acceptable goodness of fit, where $R^2 > 0.86$. The lowest fitting qualities were found for exercise and after recovery phases, which were then analyzed in smaller segments with higher R^2, always greater than 0.92.

TABLE 3.8– P-values and R^2 obtained when comparing symptomatic and asymptomatic patients along the exercise test.

	p-value	R^2
Resting	0.320	0.91
Exercise	0.418	0.86
Warm-up	0.135	0.92
Incremental exercise	0.065	0.94
After exercise	0.015*	0.94
Recovery	0.023*	0.95
Active recovery	0.118	0.96
Passive recovery	0.025*	0.96
Rest post-recovery	0.022*	0.89

*$p < 0.05$, Mann-Whitney U test.

Figure 3.8 displays representative examples of β slope extraction presenting good qualities of fit, for a symptomatic and an asymptomatic patient.

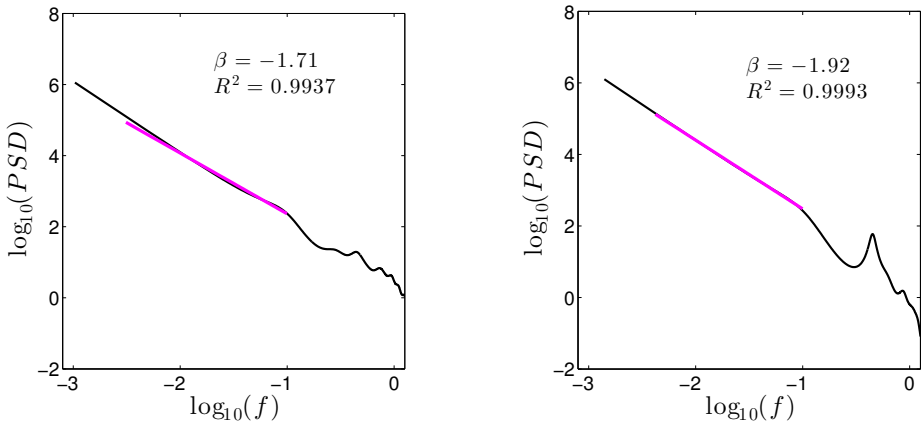

FIGURE 3.8– Representative examples of linear fits for β extraction after exercise in a symptomatic (left) and in an asymptomatic (right) BS patient.

Table 3.9 summarizes the mean ± standard deviation values for symptomatic and asymptomatic patients, and the associated p-values obtained in significant cases. Symptomatic patients showed a statistically significant reduction in β, in comparison to asymptomatic subjects, after exertion ($p = 0.015$); during recovery ($p = 0.023$), and more specifically during the passive recovery phase ($p = 0.025$), and at rest post-recovery ($p = 0.022$). Figure 3.9 reflects a significantly decreased complexity in symptomatic patients for both recovery and post-recovery phases, with respect to asymptomatic subjects.

Table 3.9– Mean ± standard deviation, for symptomatic and asymptomatic patients, and associated p-values in significant variables.

	Symptomatic (n=16)	**Asymptomatic (n=53)**	p**-value**
β**, recovery**	-1.866 ± 0.258	-1.685 ± 0.356	0.023
β**, passive recovery**	-1.773 ± 0.292	-1.655 ± 0.288	0.025
β**, rest post-recovery**	-1.853 ± 0.207	-1.651 ± 0.334	0.022
β**, after exercise**	-1.706 ± 0.335	-1.468 ± 0.423	0.015

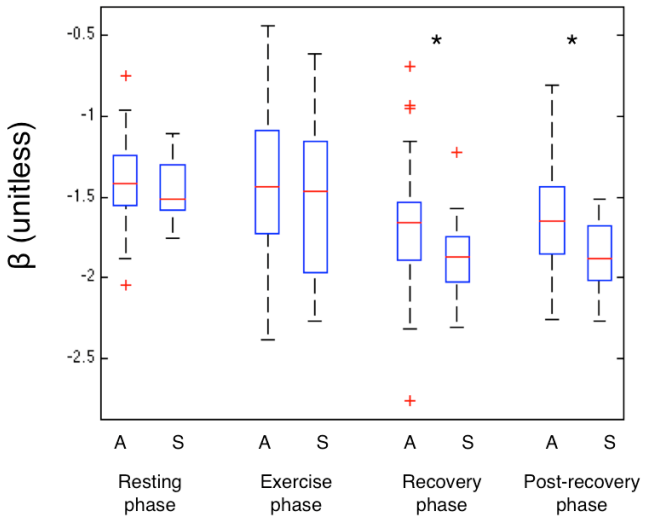

Figure 3.9– Group average results for β during resting, exercise, recovery and post-recovery phases; for symptomatic and asymptomatic BS patients (*p <0.05).

Table 3.10 includes the odds ratio (OR), 95% confidence intervals (CI) and p-values associated with each univariate model. During the rest post-recovery phase, β turned to be an independent predictor in univariate analysis with a 9.7% (p=0.030) decreased risk per one point increase. After exercise, β was also a significant predictor of symptoms, decreasing risk by a 18.9% per each point increase (p=0.049).

TABLE 3.10– Odds ratios, 95% confidence intervals and p-values associated with significant HRC indicators in univariate analysis.

	Odds Ratio	**95% CI**	p**-value**
β**, recovery**	0.180	0.028 - 1.146	0.069
β**, passive recovery**	0.230	0.029 - 1.812	0.163
β**, rest post-recovery**	0.097	0.012 - 0.803	0.030*
β**, after exercise**	0.189	0.036 - 0.992	0.049*

*$p < 0.05$, Mann-Whitney U test.

3.3.4. Heart rate variability during head-up tilt testing

As for exercise testing, given the non-stationarity of signals acquired during head-up tilt (HUT) testing, the autonomic function of 65 BS patients was analyzed by a time-frequency approach.

3.3.4.1. Clinical data description

Participants' age ranged from 19 to 79 years old (46.77 ± 12.57 years old) and 80% were males. Twenty patients had the following documented symptoms: syncope (55%), cardiac arrest (35%), dizziness (15%), palpitations (10%) and nocturnal convulsions (5%). The remaining 45 patients were considered as asymptomatic.

Cardioverter defibrillator implantations (ICD) had been performed in 12 of 45 (26.67%) asymptomatic patients, based on a positive EPS test, whereas all symptomatic patients were ICD carriers. Genetic testing in search of *SCN5A* mutations was completed in 51 patients (18 were symptomatic) and among 17 patients in whom the *SCN5A* mutation was found, 7 were symptomatic. Table 3.11 summarizes patients' clinical characteristics.

TABLE 3.11– Clinical characteristics of symptomatic and asymptomatic study groups for HRV analysis during HUT testing.

	Symptomatic (n=20)	**Asymptomatic** (n=45)	p**-value**
Age, *years old*	46.15 ± 13.95	47.04 ± 12.06	0.706
Male sex, *n(%)*	18 (90%)	34 (75.6%)	0.186
ICD implantation, *n (%)*	20 (100%)	12 (26.7%)	< 0.001
Presence of SCN5A mutation, *n (%)*	7 (38.9%)	10 (30.3%)	0.444

Values are mean ± standard deviation or number of observations (%).
All between-groups differences, apart from ICD implantation, are statistically non-significant.

3.3.4.2. Methods

HRV time series from each patient were estimated by means of the time-frequency analysis described in Section 3.2.1.2, based on the SPWVD that centers HF-frequency bands to the respiratory frequency estimated from EDR signals. These HRV time series were averaged for the whole baseline period (B), in supine rest before tilting. After subtracting these reference values from each time series, they were averaged in temporal non-overlapped windows of 1 minute, leading to $\overline{\Delta LF^i_{nu}}$, $\overline{\Delta HF^i_{nu}}$ and $\overline{\Delta LF/HF^i}$, which stand for the time series intra-patient mean for the following time periods: $i \in \{T1, T2, \cdots, T45, S1, S2, \cdots, S10\}$. T refers to the tilting phase, while S accounts for the supine rest after tilting period. Fig 3.10 illustrates those phases composing the HUT test, as well as some of the analyzed 1-min segments.

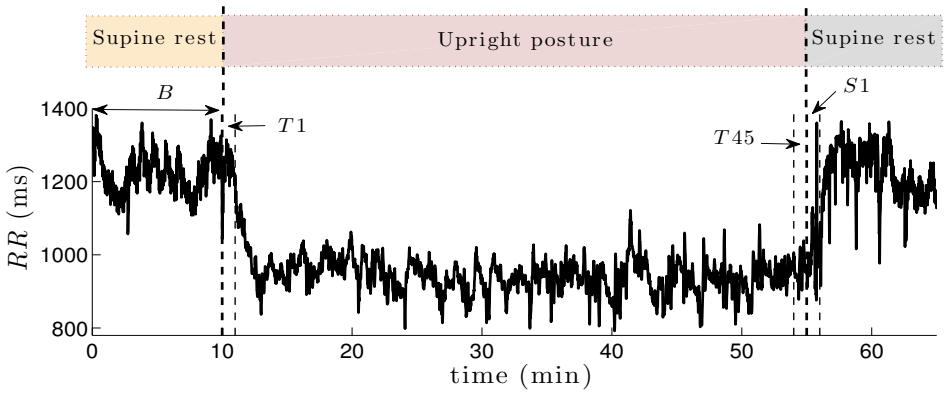

Figure 3.10– HUT testing was divided in three phases: baseline supine rest, upright posture and supine rest after tilting. After subtracting the mean of the baseline phase (B), HRV time series estimated from the RR series were averaged in 1-min windows. $T1$ and $T45$ refer to the first and last minutes of tilting, and $S1$ to the first minute in supine position after tilting.

The extracted HRV features were compared between symptomatic and asymptomatic groups, by Mann-Whitney U non-parametric tests.

3.3.4.3. Results

Figure 3.11 represents the mean $\overline{\Delta HF_{nu}}$ and the mean $\overline{\Delta LF/HF}$ for both groups of patients, highlighting those 1-min segments where differences between symptomatic and asymptomatic patients were significant. It should be noted that, since the baseline value was subtracted for each patient, time series are represented in relative units (r.u.).

Table 3.12 summarizes the mean ± standard deviation values for symptomatic and asymptomatic patients, as well as the obtained p-values for each significant case. As aforementioned, since statistical results for both $\overline{\Delta LF_{nu}}$ and $\overline{\Delta HF_{nu}}$ are identical, the former time series' results have not been included in the table.

During tilting, $\overline{\Delta HF_{nu}}$ decreased with respect to baseline for both groups. However, symptomatic patients presented higher $\overline{\Delta HF_{nu}}$ values. Although this difference was statistically

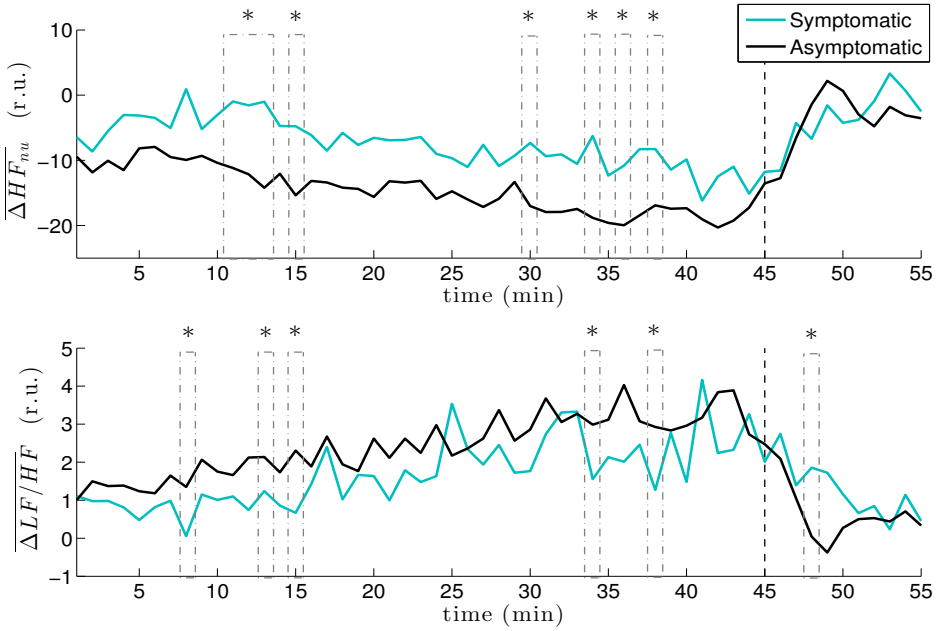

FIGURE 3.11– Mean $\overline{\Delta HF_{nu}}$ (upper panel) and mean $\overline{\Delta LF/HF}$ (lower panel) for both symptomatic (blue) and asymptomatic (black) groups of patients, expressed in relative units (r.u.), with respect to baseline mean. Dashed vertical lines indicate the time instant where the patient changes from upright posture to supine rest, after 45 minutes of tilting. Pointed boxes delimit those 1-min segments where significant differences between groups ($^*p < 0.05$) were found.

significant at different time periods, the largest segment was found before the 15^{th} minute in upright posture ($\overline{\Delta HF_{nu}^{T11}}$: $p = 0.030$; $\overline{\Delta HF_{nu}^{T12}}$: $p = 0.031$; $\overline{\Delta HF_{nu}^{T13}}$: $p = 0.010$; $\overline{\Delta HF_{nu}^{T15}}$: $p = 0.022$). After tilting, $\overline{HF_{nu}}$ was similarly restored to baseline values for both symptomatic and asymptomatic patients.

Conversely, $\overline{\Delta LF/HF}$ increased with respect to baseline in both groups during tilting, being asymptomatic patients those presenting the highest values. Statistically significant differences between groups in $\overline{\Delta LF/HF}$ were found in similar time periods than for $\overline{\Delta HF_{nu}}$, including the segment before the 15^{th} minute in upright posture ($\overline{\Delta LF/HF^{T13}}$: $p = 0.034$; $\overline{\Delta LF/HF^{T15}}$: $p = 0.014$). Moreover, after tilting, asymptomatic patients reached baseline $\overline{LF/HF}$ values more rapidly, leading to significant differences between groups during the third minute in post-tilt supine rest ($\overline{\Delta LF/HF^{S3}}$: $p = 0.047$).

3.3.5. Baroreflex sensitivity during head-up tilt testing

In this section, the autonomic function of 32 BS patients is analyzed by estimating their baroreflex sensitivity (BRS) during a standardized head-up tilt (HUT) test. However, since there is no gold standard to non-invasively estimate BRS, eight previously described methods are applied, in order to quantify their level of agreement and compare their robustness. Then, the obtained results are compared between symptomatic and asymptomatic groups.

Table 3.12– Mean ± standard deviation, for symptomatic and asymptomatic patients, and associated p-values in significant 1-min segments.

	Symptomatic (n=20)	**Asymptomatic (n=45)**	p**-value**
$\overline{\Delta HF_{nu}^{T11}}$	-0.96± 17.8210	-11.19 ± 18.34	0.030
$\overline{\Delta HF_{nu}^{T12}}$	-1.57 ± 19.63	-12.15 ± 16.99	0.031
$\overline{\Delta HF_{nu}^{T13}}$	-1.02 ± 21.09	-14.21 ± 16.79	0.010
$\overline{\Delta HF_{nu}^{T15}}$	-4.78 ± 18.66	-15.37 ± 18.81	0.022
$\overline{\Delta HF_{nu}^{T30}}$	-7.32 ± 19.24	-17.01 ± 16.34	0.040
$\overline{\Delta HF_{nu}^{T34}}$	-6.26 ± 22.24	-18.82 ± 16.54	0.012
$\overline{\Delta HF_{nu}^{T36}}$	-10.81 ± 19.78	-19.96 ± 14.68	0.037
$\overline{\Delta HF_{nu}^{T38}}$	-8.26 ± 17.80	-16.90 ± 19.02	0.026
$\overline{\Delta LF/HF^{T8}}$	0.06 ± 1.69	1.35 ± 2.21	0.026
$\overline{\Delta LF/HF^{T13}}$	1.24 ± 4.38	2.14 ± 2.84	0.034
$\overline{\Delta LF/HF^{T15}}$	0.67 ± 2.00	2.30 ± 2.97	0.014
$\overline{\Delta LF/HF^{T34}}$	1.55 ± 3.16	2.99 ± 2.97	0.039
$\overline{\Delta LF/HF^{T38}}$	1.27 ± 2.67	2.93 ± 3.86	0.046
$\overline{\Delta LF/HF^{S3}}$	1.85 ± 3.39	0.04 ± 1.39	0.047

3.3.5.1. Clinical data description

Patients' age ranged from 20 to 79 years old (52.21 ± 14.78 years old) and 25 (78.1%) were males. Nine patients had the following documented symptoms: 4 syncopes, 3 cardiac arrests and 2 nocturnal convulsions. ICD implantation had been performed in 2 of 23 (8.7%) asymptomatic patients, based on a positive EPS test, whereas all symptomatic patients were ICD carriers. Among 31 patients (9 were symptomatic) in whom genetic screening was performed, an *SCN5A* mutation was found in 10 (32.3%), from whom 2 were symptomatic. Table 3.13 summarizes participants' baseline characteristics.

TABLE 3.13– Symptomatic and asymptomatic patients' clinical characteristics for BRS analysis during HUT testing.

	Symptomatic (n=9)	**Asymptomatic (n=23)**	***p*-value**
Age, *years old*	54.44 ± 14.46	51.35 ± 15.13	0.983
Male sex, *n (%)*	9 (100%)	16 (69.6%)	0.070
ICD implantation, *n (%)*	9 (100%)	2 (8.7%)	<0.001
Presence of *SCN5A* mutation, *n (%)*	2 (22.2%)	8 (36.4%)	0.468

Values are mean ± standard deviation or number of observations (%).
All between-groups differences, apart from ICD implantation, are statistically non-significant.

3.3.5.2. Methods

Baroreflex sensitivity was evaluated and compared by means of eight different BRS estimates described in Section 3.2.3. Since the analyzed methods require stationary data, four 10-min segments from each recording were analyzed, leading to 128 BRS estimates for each method: i) in supine position before the test, ii) in upright posture after 10 minutes of tilting, iii) in standing position after 20 minutes and iv) in supine position after tilting.

The level of agreement between each method and the remaining approaches was calculated by the intraclass correlation coefficient (ICC). Results were considered low when $0 < r < 0.5$, medium when $0.5 < r < 0.7$ and high when $r > 0.7$.

Then, assuming an age-associated reduction in BRS, which has been previously reported (LAITINEN et al., 1998), Pearson's correlation coefficients (PCC) and associated p-values were calculated between BRS estimates in resting conditions and patients' age. The closer to -1 the PCC, the more confident the negative linear correlation between age and the BRS measure was considered.

Finally, comparisons between symptomatic and asymptomatic patients for the different phases of the HUT test were performed by Mann-Whitney U non-parametric tests.

3.3.5.3. Results

Figure 3.12 represents the mean and 95% confidence interval (CI) of BRS estimates, calculated on each 10-min segment of the HUT test for the whole population.

Considering the general tendency along the four segments under study, estimates typically decreased at the beginning of tilting, progressively incremented for the second standing phase and remained increasing after the test, without reaching baseline values. All methods captured a reduction in BRS after 10 minutes of tilting with respect to baseline, as well as an increase after the HUT test. However, temporal approaches ($BRS^{+/+}$, $BRS^{-/-}$ and $BRS - SD$) still captured a reduction in BRS in the second segment of tilting, as well as $BRS^{+/+}$ detected a

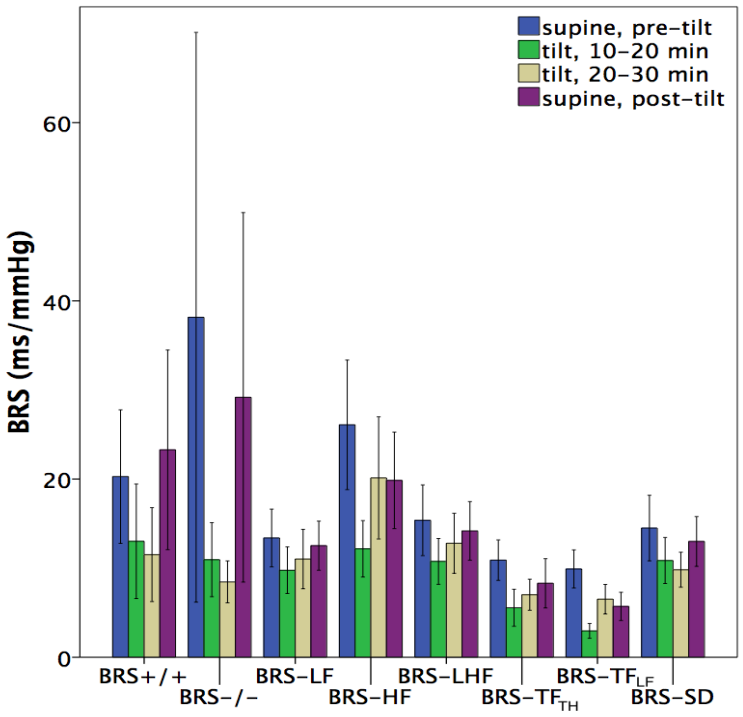

Figure 3.12– Mean and 95% CI of BRS estimates, for each method and phase of the HUT test.

higher BRS recovery after the test with respect to baseline. Moreover, a strong variability in the results coming from the sequence method could be noted from the error bars.

Since some segments did not meet the required properties to apply the analyzed methods, some BRS estimates could not be calculated. Table 3.14 shows, for each method, the number of missed 10-min segments, among the 128 available. The sequence method provided the highest number of missed values, whereas $BRS-SD$ and $BRS-TF_{LF}$ gave results in all cases. The resting methods using coherence as a parameter of quality lead to two or more missed values.

Table 3.14– Missed BRS estimates, among 128 segments.

BRS estimate	**Missings**
$BRS^{+/+}$	40
$BRS^{-/-}$	43
BRS-LF	9
BRS-HF	3
BRS-LHF	2
$BRS\text{-}TF_{TH}$	25
$BRS\text{-}TF_{LF}$	0
BRS-SD	0

Table 3.15 presents results from the ICC analysis for all BRS estimates and for different phases of the HUT test.

TABLE 3.15– Mean ± standard deviation of ICC for each method.

BRS estimate	**Supine**	**Standing**	**Whole test**
$BRS^{+/+}$	0.37 ± 0.10	0.54 ± 0.18	0.45 ± 0.17
$BRS^{-/-}$	0.38 ± 0.15	0.46 ± 0.29	0.42 ± 0.23
BRS-LF	0.73 ± 0.24	0.69 ± 0.20	0.71 ± 0.22
BRS-HF	0.68 ± 0.17	0.44 ± 0.30	0.56 ± 0.27
BRS-LHF	0.76 ± 0.22	0.75 ± 0.17	0.75 ± 0.20
$BRS\text{-}TF_{TH}$	0.69 ± 0.28	0.70 ± 0.26	0.69 ± 0.27
$BRS\text{-}TF_{LF}$	0.59 ± 0.29	0.53 ± 0.30	0.56 ± 0.29
BRS-SD	0.72 ± 0.24	0.67 ± 0.25	0.70 ± 0.24

In supine position, estimations using the sequence method showed the lowest agreement, whereas $BRS-LF$, $BRS-LHF$ and $BRS-SD$ were in high accordance with the other methods. In standing position, $BRS^{-/-}$ and $BRS-HF$ were in low agreement, while $BRS-LHF$ and $BRS-TF$ were highly consistent with the other measures. When analyzing supine and standing positions conjointly, both results coming from the sequence method showed low accordance, whereas $BRS-LF$, $BRS-LHF$ and $BRS-SD$ were in high agreement.

Table 3.16 shows that the lowest correlation between age and BRS came from sequence analysis ($BRS^{+/+}$), whereas $BRS-LF$ was the method showing the greatest correlation ($p = 0.002$).

TABLE 3.16– Pearson's correlation coefficients (PCC) and associated p-values for each method, when comparing age and BRS.

BRS estimate	**PCC**	***p*-value**
$BRS^{+/+}$	-0.015	0.953
$BRS^{-/-}$	-0.406	0.085
BRS-LF	-0.520	0.002*
BRS-HF	-0.325	0.074
BRS-LHF	-0.505	0.003*
$BRS\text{-}TF_{TH}$	-0.490	0.005*
$BRS\text{-}TF_{LF}$	-0.505	0.003*
BRS-SD	-0.344	0.054

*$p < 0.05$

Finally, comparisons between groups for the different phases of the HUT test showed no significant differences in BRS related to symptomatic status (Table 3.17).

Table 3.17– P-values when comparing the BRS of symptomatic and asymptomatic BS patients.

	Supine, pre-tilt	**Tilt, 10-20 min**	**Tilt, 20-30 min**	**Supine, post-tilt**
$BRS^{+/+}$	0.152	0.720	0.495	0.301
$BRS^{-/-}$	0.898	0.354	0.194	0.425
BRS-LF	0.681	0.753	0.842	0.722
BRS-HF	0.842	0.642	0.520	0.363
BRS-LHF	0.967	0.520	0.774	0.509
$BRS\text{-}TF_{TH}$	0.912	0.953	0.983	0.687
$BRS\text{-}TF_{LF}$	0.621	0.321	0.805	0.711
BRS-SD	0.902	0.386	0.742	0.934

3.3.6. Discussion

In the previous sections, the autonomic function of BS patients was characterized and compared between symptomatic and asymptomatic groups through several HRV, HRC and BRS markers computed at night and during exercise and HUT tests.

In a first study where the HRV and HRC were assessed in 87 BS patients at night, according to time-domain HRV results, symptomatic subjects showed lower $MIRR$, $SDNN$ and $SDANN$ values, particularly during the last hour (5 a.m. - 6 a.m.). Thus, patients with higher risk for cardiac events seem to show a decreased HRV overnight, following the tendency reported in previous publications (Hermida et al., 2003; Krittayaphong et al., 2003; Pierre et al., 2007; Tokuyama et al., 2014), and emphasizing differences during the last hour of sleep.

Regarding circadian fluctuations, based on $\delta SDANN$ results, significantly greater variations during nighttime were observed in symptomatic patients, which concurs with a previous study where the night was analyzed between midnight and 4 a.m. As suggested by (Behar et al., 2016), these results confirm an increased sinus node response to ANS in patients having experienced symptoms, caused by wider fluctuations in autonomic tone, or by a greater sinus node autonomic receptors sensitivity. Thus, the risk of cardiac events might be incremented by these greater variations in sinus node response to ANS.

From HRC analysis, statistically significant differences were observed between 2 a.m. - 3 a.m. and 4 a.m. - 5 a.m in *SampEn*. Symptomatic patients showed more regularity in RR series, probably related to a worse cardiac health condition since a reduced complexity in HR has been associated with disease (Javorka et al., 2008; Khandoker AH, 2009; Tuzcu et al., 2006). The ANS is controlled by complex interactions resulting from feedback loops of non-linear systems that permit the organism to adapt to particular physiological conditions, such as metabolic variations, stress or disease. Thus, according to previous studies, a reduction in the complexity of biological control systems reflects a decreased organism's adaptability, generally associated with age and disease (Goldberger et al., 2002; Magrans et al., 2010; Rabinovich et al., 1998; Smith et al., 2005).

The non-linear HR regulation was also compared in 69 BS subjects who took part in a standardized exercise test. The results showed a significant reduction in β after exertion, during recovery and rest post-recovery in symptomatic patients, with respect to the asymptomatic group. Thus, as in the previous study overnight, subjects at higher risk showed a lower complexity in HR dynamics. Particularly, HRC decreased significantly in symptomatic patients after exertion and recovery, when parasympathetic activity is predominant.

These findings provide further evidence for the role of autonomic imbalance in the pathophysiology of BS. Although no significant differences between symptomatic and asymptomatic groups in HRV markers characterizing the HF component that would directly relate the loss of cardiac variability and complexity with an increase in the vagal tone were found, results highlight the relevance of night analysis and exercise testing in order to unmask significant autonomic changes that may not be captured at daytime, during a regular ECG examination. Indeed, this altered autonomic cardiac system dynamics when vagal tone is predominant concurs with previous studies reporting an increase in Brugada-like ECG changes induced during vagal stimulation (Ikeda et al., 2005), as well as with the fact that most life-threatening cardiac arrhythmias in BS occur at rest and during sleep, when parasympathetic activity is predominant (Kies et al., 2004; Matsuo et al., 1999).

Moreover, the temporal evolution of the autonomic response to a standardized exercise test was also analyzed in a group of 105 BS patients. Statistically significant differences between symptomatic and asymptomatic groups were observed during the second minute of incremental exercise in the mean normalized HF ($\overline{HF_{nu}}$), and thus in the mean normalized LF ($\overline{LF_{nu}}$), suggesting that symptomatic patients showed an increased vagal tone, as well as a reduction in the sympathetic activity in this phase, with respect to asymptomatic patients.

Similarly, according to the time-varying autonomic response to a standardized HUT test assessed in 65 BS patients, an increased parasympathetic tone ($\overline{HF_{nu}}$) and a reduced sympathovagal balance ($\overline{LF/HF}$) were observed in symptomatic patients during tilting. Some significant differences were captured by both autonomic markers around the 35^{th} minute of tilting and, by the sympathovagal balance, during the third minute in supine rest after tilting. Nevertheless, since the largest and most significant segment was found before the 15^{th} minute in upright posture, the results suggest the potential of employing time-reduced HUT testing for risk stratification. Indeed, a previous work already reported the potential of 15-min HUT tests for early syncope detection (Khodor et al., 2016).

Furthermore, the results confirm previous findings where symptomatic BS patients showed higher vagal (Behar et al., 2016; Nakazawa et al., 2003; Tokuyama et al., 2014) and reduced sympathetic (Nakazawa et al., 2003) tones with respect to asymptomatic patients, supporting the idea that decreased sympathetic activity and increased vagal responses could be related to a worse prognosis in Brugada syndrome.

Finally, interactions between blood pressure and heart rate were captured by the analysis of the baroreflex function. Since there is no gold standard to non-invasively estimate BRS, eight different methods were analyzed and compared in 32 BS patients who underwent a standardized

HUT test, in order to quantify the level of agreement and robustness between such measures.

Among the studied methods, those derived from sequence analysis showed a lower robustness when capturing baroreflex function. Although they allow for taking into account the asymmetry of baroreceptor response by calculating distinct estimates for increasing and decreasing arterial pressure values, they can fail to provide results in many recordings when the needed requirements are not met. In contrast to the general tendency, $BRS^{+/+}$ captured a continued decrease in BRS along the HUT test, as well as an increase after the trial, greater than baseline values. In addition, a large variability was found in this measure with respect to the rest of estimates. Results obtained from sequence method were in low agreement with the other techniques and, among all BRS estimates, they presented the lowest correlation with patients' age. On the other hand, $BRS - LF$ was a reliable measure of BRS in this clinical series. Although it also failed to provide some results, $BRS - LF$ was in accordance with expected tendencies. It also showed a high level of agreement with the rest of measures.

Regarding differences between symptomatic and asymptomatic patients, as in a previous study where (Mizumaki et al., 2005) assessed the baroreflex function of BS patients through the invasive phenylephrine method, no significant differences in BRS were observed along the HUT test. Although cardiovascular diseases often coexist with disabilities in baroreflex mechanisms, no association between BRS values and symptomatic status in BS was identified.

3.4. Conclusion

In this chapter, several HRV, HRC and BRS markers were compared between symptomatic and asymptomatic groups, under different autonomic conditions.

At night, symptomatic patients showed lower HRV and HRC, but no signifficant differences in sympathetic and parasympathetic tones were noted. Moreover, greater fluctuations in the sinus node response to the ANS was observed in the symptomatic group.

During exercise testing, symptomatic patients showed an increased vagal function and a reduced sympathetic activity, with respect to asymptomatic BS patients, under conditions of incremental exercise. Moreover, lower HRC values were noted in symptomatic patients under conditions of recovery and rest after recovery.

Regarding the autonomic response to HUT testing, symptomatic patients presented an increased parasympathetic tone and a reduced sympathovagal balance with respect to asymptomatic patients during tilting, and particularly before the 15^{th} minute of the test. After tilting, sympathovagal balance was more rapidly restored to baseline values in asymptomatic patients.

Although comparisons are based on a relatively small population of BS patients and, thus, conclusions on predictors of symptoms cannot be inferred, results indicate important trends in HRV and HRC of clinical relevance with a potential impact on the identification of BS patients at high risk. Nevertheless, since univariate analyses are unable to capture the multifactorial nature of the disease, they result in moderately significant differences between symptomatic and asymptomatic groups. Therefore, in the next chapter, a multivariate approach following a

step-based machine learning method is proposed, exploiting the features extracted in this chapter, in order to improve classification performance.

References

Auger, F., P. Flandrin, P. Gonçalvès, and O. Lemoine (1996). *Time-Frequency Toolbox*. CNRS France, Rice University.

Bailón, R., P. Laguna, L. Mainardi, and L. Sornmo (2007). "Analysis of heart rate variability using time-varying frequency bands based on respiratory frequency". In: *Engineering in Medicine and Biology Society, 2007. EMBS 2007. 29th Annual International Conference of the IEEE*, pp. 6674–6677.

Bailón, R., L. Sornmo, and P. Laguna (2006). "A robust method for ECG-based estimation of the respiratory frequency during stress testing". In: *IEEE transactions on biomedical engineering* 53.7, pp. 1273–1285.

Behar, N., B. Petit, V. Probst, F. Sacher, G. Kervio, J. Mansourati, P. Bru, A. Hernandez, and P. Mabo (2016). "Heart rate variability and repolarization characteristics in symptomatic and asymptomatic Brugada syndrome". In: *Europace*, euw224.

Bernardi, L., G. De Barbieri, M. Rosengård-Bärlund, V.-P. Mäkinen, C. Porta, and P.-H. Groop (2010). "New method to measure and improve consistency of baroreflex sensitivity values". In: *Clinical Autonomic Research* 20.6, pp. 353–361.

Broersen, P. M. T. (2000). "Finite sample criteria for autoregressive order selection". In: *IEEE Transactions on Signal Processing* 48.12, pp. 3550–3558.

Burg, J. P. (1975). "Maximum Entropy Spectral Analysis". PhD thesis. Stanford, CA 94305: Stanford University.

Costa, A. H. and G. Boudreau-Bartels (1995). "Design of time-frequency representations using a multiform, tiltable exponential kernel". In: *IEEE Transactions on Signal Processing* 43.10, pp. 2283–2301.

Di Rienzo, M., G. Bertinieri, G. Mancia, and A. Pedotti (1985). "A new method for evaluating the baroreflex role by a joint pattern analysis of pulse interval and systolic blood pressure series". In: *Medical and Biological Engineering and Computing* 23, pp. 313–314.

Dumont, J., A. I. Hernandez, and G. Carrault (2010). "Improving ECG beats delineation with an evolutionary optimization process". In: *IEEE Transactions on Biomedical Engineering* 57.3, pp. 607–615.

European Society of Cardiology, T. F. of the et al. (1996). "Heart rate variability standards of measurement, physiological interpretation, and clinical use". In: *European Heart Journal* 17.354–381.

Gallet, C. and C. Julien (2011). "The significance threshold for coherence when using the Welch's periodogram method: effect of overlapping segments". In: *Biomedical Signal Processing and Control* 6.4, pp. 405–409.

Goldberger, A. L., C.-K. Peng, and L. A. Lipsitz (2002). "What is physiologic complexity and how does it change with aging and disease?" In: *Neurobiology of aging* 23.1, pp. 23–26.

Gomis, P., P. Caminal, M. Vallverdu, S. Warren, and G. Wagner (2006). "Non-linear dynamic analysis of the cardiac rhythm during transient myocardial ischemia". In: *Biomedizinische Technik* 51.4, pp. 178–181.

Hermida, J.-S., A. Leenhardt, B. Cauchemez, I. Denjoy, G. Jarry, F. Mizon, P. Milliez, J.-L. Rey, P. Beaufils, and P. Coumel (2003). "Decreased nocturnal standard deviation of averaged NN intervals". In: *European heart journal* 24.22, pp. 2061–2069.

Hlawatsch, F. and G. F. Boudreaux-Bartels (1992). "Linear and quadratic time-frequency signal representations". In: *IEEE signal processing magazine* 9.2, pp. 21–67.

Huikuri, H. V., T. H. Mäkikallio, K. J. Airaksinen, T. Seppänen, P. Puukka, I. J. Räihä, and L. B. Sourander (1998). "Power-law relationship of heart rate variability as a predictor of mortality in the elderly". In: *Circulation* 97.20, pp. 2031–2036.

Huikuri, H. V., T. H. Mäkikallio, C.-K. Peng, A. L. Goldberger, U. Hintze, M. Møller, et al. (2000). "Fractal correlation properties of RR interval dynamics and mortality in patients with depressed left ventricular function after an acute myocardial infarction". In: *Circulation* 101.1, pp. 47–53.

Ikeda, T., M. Takami, K. Sugi, Y. Mizusawa, H. Sakurada, and H. Yoshino (2005). "Noninvasive Risk Stratification of Subjects with a Brugada-Type Electrocardiogram and No History of Cardiac Arrest". In: *Annals of Noninvasive Electrocardiology* 10.4, pp. 396–403.

Javorka, M., Z. Trunkvalterova, I. Tonhajzerova, J. Javorkova, K. Javorka, and M. Baumert (2008). "Short-term heart rate complexity is reduced in patients with type 1 diabetes mellitus". In: *Clinical Neurophysiology* 119.5, pp. 1071–1081.

Khandoker AH Jelinek HF, P. M. (2009). "Identifying diabetic patients with cardiac autonomic neuropathy by heart rate complexity analysis". In: *BioMedical Engineering OnLine* 8.1, p. 3.

Khodor, N., G. Carrault, D. Matelot, H. Amoud, M. Khalil, N. T. du Boullay, F. Carre, and A. Hernández (2016). "Early syncope detection during head up tilt test by analyzing interactions between cardio-vascular signals". In: *Digital Signal Processing* 49, pp. 86–94.

Kies, P., T. Wichter, M. Schäfers, M. Paul, K. P. Schäfers, L. Eckardt, L. Stegger, E. Schulze-Bahr, O. Rimoldi, G. Breithardt, et al. (2004). "Abnormal myocardial presynaptic norepinephrine recycling in patients with Brugada syndrome". In: *Circulation* 110.19, pp. 3017–3022.

Kostopoulou, A., M. Koutelou, G. Theodorakis, A. Theodorakos, E. Livanis, T. Maounis, A. Chaidaroglou, D. Degiannis, V. Voudris, D. Kremastinos, et al. (2010). "Disorders of the autonomic nervous system in patients with Brugada syndrome: a pilot study". In: *Journal of cardiovascular electrophysiology* 21.7, pp. 773–780.

Krittayaphong, R., G. Veerakul, K. Nademanee, and C. Kangkagate (2003). "Heart rate variability in patients with Brugada syndrome in Thailand". In: *European Heart Journal* 24.19, pp. 1771–1778.

Laitinen, T., J. Hartikainen, E. Vanninen, L. Niskanen, G. Geelen, and E. Länsimies (1998). "Age and gender dependency of baroreflex sensitivity in healthy subjects". In: *Journal of Applied Physiology* 84.2, pp. 576–583.

Lake, D., J. Richman, M. Griffin, and J. Moorman (2002). "Sample entropy analysis of neonatal heart rate variability". In: *American Journal of Physiology - Regulatory, Integrative and Comparative Physiology* 283.3, R789–R797.

Laude, D., J.-L. Elghozi, A. Girard, E. Bellard, M. Bouhaddi, P. Castiglioni, C. Cerutti, A. Cividjian, M. Di Rienzo, J.-O. Fortrat, et al. (2004). "Comparison of various techniques used to estimate spontaneous baroreflex sensitivity (the EuroBaVar study)". In: *American Journal of Physiology-Regulatory, Integrative and Comparative Physiology* 286.1, R226–R231.

Lombardi, F., T. H. Mäkikallio, R. J. Myerburg, and H. V. Huikuri (2001). "Sudden cardiac death: role of heart rate variability to identify patients at risk". In: *Cardiovascular research* 50.2, pp. 210–217.

Lombardi, F., A. Porta, M. Marzegalli, S. Favale, M. Santini, A. Vincenti, A. De Rosa, et al. (2000). "Heart rate variability patterns before ventricular tachycardia onset in patients with an implantable cardioverter defibrillator". In: *The American journal of cardiology* 86.9, pp. 959–963.

Maestri, R., G. D. Pinna, A. Accardo, P. Allegrini, R. Balocchi, G. D'addio, M. Ferrario, D. Menicucci, A. Porta, R. Sassi, et al. (2007). "Nonlinear indices of heart rate variability in chronic heart failure patients: redundancy and comparative clinical value". In: *Journal of cardiovascular electrophysiology* 18.4, pp. 425–433.

Magrans, R., P. Gomis, P. Caminal, and G. Wagner (2010). "Multifractal and nonlinear assessment of autonomous nervous system response during transient myocardial ischaemia". In: *Physiological measurement* 31.4, pp. 565–580.

Malliani, A., F. Lombardi, and M. Pagani (Jan. 1994). "Power spectrum analysis of heart rate variability: a tool to explore neural regulatory mechanisms." In: *British Heart Journal* 71.1, pp. 1–2.

Masrur, S., S. Memon, and P. D. Thompson (2015). "Brugada syndrome, exercise, and exercise testing". In: *Clinical cardiology* 38.5, pp. 323–326.

Matsuo, K., T. Kurita, M. Inagaki, M. Kakishita, N. Aihara, W. Shimizu, A. Taguchi, K. Suyama, S. Kamakura, and K. Shimomura (1999). "The circadian pattern of the development of ventricular fibrillation in patients with Brugada syndrome". In: *European heart journal* 20.6, pp. 465–470.

Mizumaki, K., A. Fujiki, K. Nishida, M. Sakabe, T. Tsuneda, M. Sugao, J. Iwamoto, and H. Inoue (2005). "Baroreceptor Reflex in Brugada Syndrome: Different ECG Responses Between Patients With and Without Ventricular Fibrillation (ECG/Body Surface Potential

Mapping/Holter 2 (A), The 69th Annual Scientific Meeting of the Japanese Circulation Society)". In: *Circulation journal: official journal of the Japanese Circulation Society* 69, p. 150.

Moody, G. B., R. G. Mark, M. A. Bump, J. S. Weinstein, A. D. Berman, J. E. Mietus, and A. L. Goldberger (1986). "Clinical validation of the ECG-derived respiration (EDR) technique". In: *Computers in Cardiology*. Vol. 13, pp. 507–510.

Nakazawa, K., T. Sakurai, A. Takagi, R. Kishi, K. Osada, T. Nanke, F. Miyake, N. Matsumoto, and S. Kobayashi (2003). "Autonomic imbalance as a property of symptomatic Brugada syndrome". In: *Circulation journal* 67.6, pp. 511–514.

Ori, Z., G. Monir, J. Weiss, X. Sayhouni, and D. Singer (1992). "Heart rate variability. Frequency domain analysis." In: *Cardiology clinics* 10.3, pp. 499–537.

Orini, M., L. T. Mainardi, E. Gil, P. Laguna, and R. Bailón (2010). "Dynamic assessment of spontaneous baroreflex sensitivity by means of time-frequency analysis using either RR or pulse interval variability". In: *2010 Annual International Conference of the IEEE Engineering in Medicine and Biology*, pp. 1630–1633.

Pagani, M., V. Somers, R. Furlan, S. Dell'Orto, J. Conway, G. Baselli, S. Cerutti, P. Sleight, and A. Malliani (1988). "Changes in autonomic regulation induced by physical training in mild hypertension." In: *Hypertension* 12.6, pp. 600–610.

Pan, J. and W. J. Tompkins (1985). "A real-time QRS detection algorithm". In: *IEEE transactions on biomedical engineering* 3, pp. 230–236.

Pierre, B., D. Babuty, P. Poret, C. Giraudeau, O. Marie, P. Cosnay, and L. Fauchier (2007). "Abnormal nocturnal heart rate variability and QT dynamics in patients with Brugada syndrome". In: *Pacing and clinical electrophysiology* 30.s1, S188–S191.

Pinna, G. and R. Maestri (2002). "New criteria for estimating baroreflex sensitivity using the transfer function method". In: *Medical and Biological Engineering and Computing* 40.1, pp. 79–84.

Rabinovich, M. and H. Abarbanel (1998). "The role of chaos in neural systems". In: *Neuroscience* 87.1, pp. 5–14.

Richman JS, M. J. (2000). "Physiological time-series analysis using approximate entropy and sample entropy". In: *American Journal of Physiology - Heart and Circulatory Physiology* 278.6, H2039–H2049.

Robbe, H., L. Mulder, H. Rüddel, W. A. Langewitz, J. Veldman, and G. Mulder (1987). "Assessment of baroreceptor reflex sensitivity by means of spectral analysis." In: *Hypertension* 10.5, pp. 538–543.

Smith, R. G., L. Betancourt, and Y. Sun (2005). "Molecular endocrinology and physiology of the aging central nervous system". In: *Endocrine reviews* 26.2, pp. 203–250.

Subramanian, M., M. A. Prabhu, M. S. Harikrishnan, S. S. Shekhar, P. G. Pai, and K. Natarajan (2017). "The Utility of Exercise Testing in Risk Stratification of Asymptomatic Patients with type 1 Brugada Pattern". In: *Journal of Cardiovascular Electrophysiology* 28, pp. 677–683.

Tapanainen, J. M., P. E. B. Thomsen, L. Køber, C. Torp-Pedersen, T. H. Mäkikallio, A.-M. Still, K. S. Lindgren, and H. V. Huikuri (2002). "Fractal analysis of heart rate variability and mortality after an acute myocardial infarction". In: *The American journal of cardiology* 90.4, pp. 347–352.

Tokuyama, T., Y. Nakano, A. Awazu, Y. Uchimura-Makita, M. Fujiwra, Y. Watanabe, A. Sairaku, K. Kajihara, C. Motoda, N. Oda, et al. (2014). "Deterioration of the circadian variation of heart rate variability in Brugada syndrome may contribute to the pathogenesis of ventricular fibrillation". In: *Journal of cardiology* 64.2, pp. 133–138.

Tuzcu, V., S. Nas, T. Borklu, and A. Ugur (2006). "Decrease in the heart rate complexity prior to the onset of atrial fibrillation". In: *Europace* 8.6, pp. 398–402.

CHAPTER 4

Multivariate analysis: machine learning approach to identify Brugada patients at high risk

In the previous chapter, significant differences in the HRV and HRC of symptomatic and asymptomatic BS patients were noted. However, the multifactorial etiology of BS requires complex approaches capable of capturing multiple mechanisms underlying the disease. Therefore, this chapter proposes a multivariate method based on a step-based machine learning approach, designed to optimally combine the previously extracted autonomic features in order to improve classification of BS patients, based on their symptomatic status. Although previous works have already proposed predictive models combining several indicators to assess risk in BS (Delise et al., 2014, 2011; Kawazoe et al., 2016; Okamura et al., 2015), multivariate approaches based on the autonomic function of these patients have yet to be exploited.

Moreover, since the selection of those autonomic indicators best explaining the syndrome can be challenging, especially when the number of sources exceeds the amount of observations in a biomedical context where intra- and inter-patient variabilities are significant, a robust approach based on a two-step feature selection process including a filter and a wrapper method is implemented. The proposed methodology is first optimized and evaluated on the most extensive clinical dataset available, acquired during exercise in 105 BS patients. Then, in order to validate the model on independent datasets and compare outcomes for classifiers designed from features extracted during different autonomic tests, a reduced clinical database acquired overnight, and during exercise and HUT testing in 44 patients is analyzed.

4.1. Global classification methodology

Figure 4.1 illustrates the global methodology proposed in order to differentiate symptomatic and asymptomatic BS patients. This methodology is based on a general machine learning

approach built from the following four main steps:

A. **Feature extraction.** Although this step can be adapted to any method extracting autonomic information from cardiovascular signals described in Chapter 3, Figure 4.1A represents HRV features extraction from time-frequency analysis. In this case, the standard 12-lead ECG signals acquired during ANS stimulation are analyzed to detect each QRS complex and extract the RR and EDR series of each patient. A time-frequency (TF) method based on the smoothed pseudo Wigner-Ville distribution (SPWVD) of RR series that adapts frequency bands to respiratory information resulting from EDR signals is applied to estimate the evolution of different spectral HRV markers. The output of this step is matrix R_M^N, which contains the calculated raw HRV features, with M markers for the N patients available on the whole database.

B. **Feature conditioning.** In order to handle the impact of markers measured at different scales, all features of R_M^N are standardized, leading to matrix F_M^N. Then, in order to reduce the effect of imbalanced classes, synthetic symptomatic patients are generated and included in the analysis by a class balancing approach, resulting in matrix $F_M^{N_b}$, with N_b observations.

C. **Feature selection**. After balancing all standardized features, $F_M^{N_b}$ is divided in a training subset F_M^{Ntr} (Ntr, 75% randomly selected patients) and the remaining testing subset F_M^{Nte}. Then, a two-step feature selection process including a filter and a wrapper method is applied in order to capture the most relevant features. In Figure 4.1C, $F_{M_f}^{Ntr}$ and $F_{M_w}^{Ntr}$ indicate the standardized training subsets kept after applying filter (M_f) and wrapper (M_w) methods, respectively. Based on the M_w selected features after training, a new standardized testing subset $F_{M_w}^{Nte}$ is defined.

D. **Classification.** In the final step, a linear discriminant analysis (LDA) classifier is applied to both the training and testing subsets, to distinguish symptomatic vs. asymptomatic patients. After training the classifier with $F_{M_w}^{Ntr}$, its performance is finally evaluated and quantified based on $F_{M_w}^{Nte}$.

Apart from feature extraction which was already explained in the previous chapter, a more detailed description of each step is presented in the following sections.

4.1.1. Feature conditioning

All markers obtained from the feature extraction step are considered as candidates for the construction of a model classifying symptomatic and asymptomatic BS patients. However, in order to equalize the contribution of all features to multivariate analysis, each raw marker j for each patient i is standardized as follows:

$$F_j^i = \frac{R_j^i - \mu_j}{\sigma_j}, \tag{4.1}$$

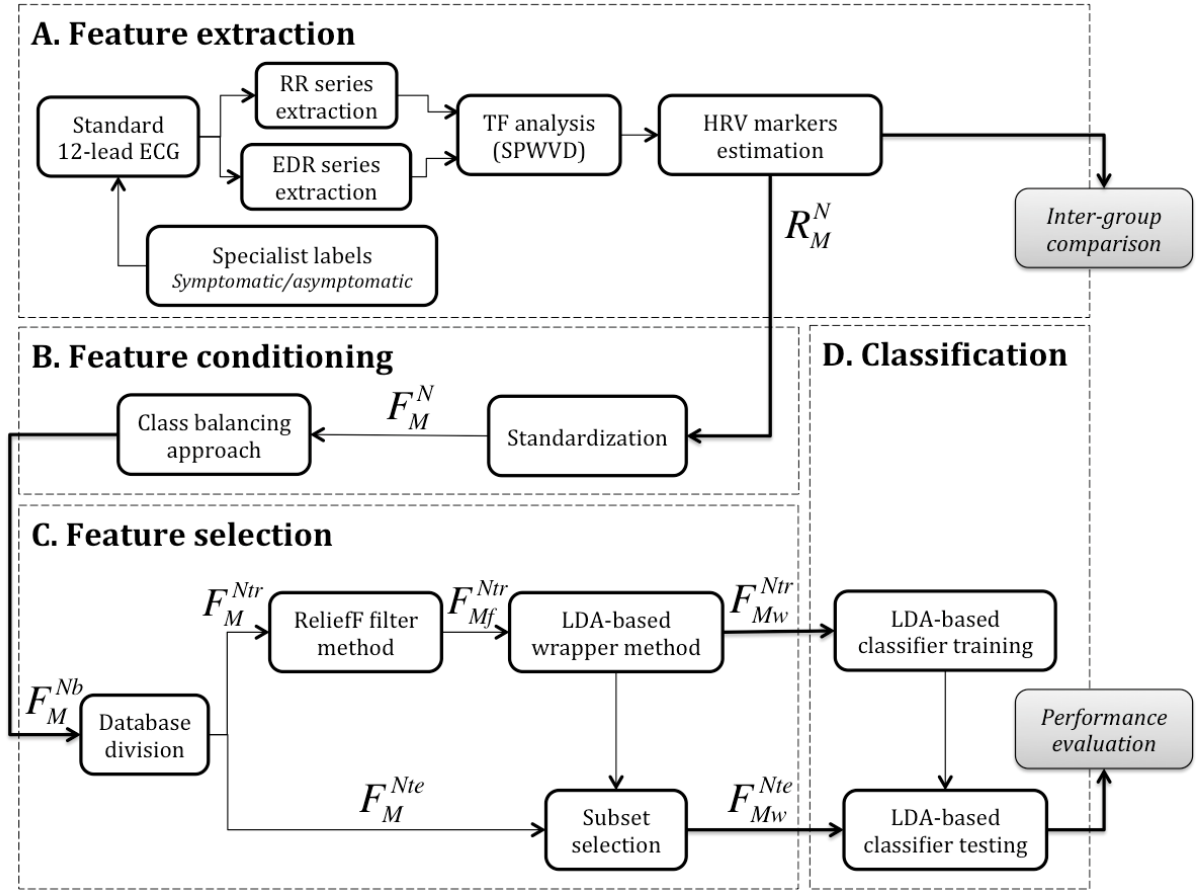

FIGURE 4.1– Data processing is composed of four major steps. A) In this example, feature extraction is focused on the estimation of a matrix of time-frequency HRV markers (R_M^N, with N patients and M different HRV features), using a time-varying frequency band that depends on the estimated instantaneous respiratory rate. B) Feature conditioning consists on standardizing and balancing R_M^N, leading to matrixes F_M^N and $F_M^{N_b}$, respectively, where N_b refers to the number of observations after class balancing. C) Feature selection, which starts by randomly defining patient subsets for training, (N_{tr}, 75% of patients) and testing (N_{te}, the rest of patients), followed by the estimation of a minimal feature dimension $M_w < M$, that maximizes classification performance, using filtering and wrapper methods. D) The final step is dedicated to classification and performance evaluation.

where μ_j is the mean and σ_j the standard deviation of a specific feature $j = 1, \cdots, M$, taking into account the data from all patients $i = 1, \cdots, N$. The new standardized dataset is defined in matrix F_M^N.

Then, to attenuate the impact of imbalanced classes, synthetic symptomatic samples are generated by applying the ADASYN approach (HE et al., 2008), defined as follows:

1. Being F_M^N the input dataset with N samples $\{\mathbf{x}_i, y_i\}$, $i = 1, \cdots, N$, where $\mathbf{x}_i$ is an instance in the M dimensional feature space X and $y_i \in Y = \{1, -1\}$ is the class identity label associated with $\mathbf{x}_i$; N_s and N_a refer to the number of minority (symptomatic) and majority (asymptomatic) class examples or observations. Therefore, $Ns \leq N_a$ and $N_s + N_a = N$.

2. The number of synthetic data samples to generate for the minority class is obtained from:

$$G = (N_a - N_s) \cdot \zeta, \tag{4.2}$$

where $\zeta \in [0, 1]$ specifies the balance level after synthetic data generation. To obtain a fully balanced data set, this parameter is fixed to $\zeta = 1$.

3. For each example $\mathbf{x}_i \in minorityclass$, k nearest neighbors (k-NN) are identified, based on the Euclidean distance in the M dimensional space, and the ratio r_i is calculated as:

$$r_i = \Delta_i / K \quad i = 1, \cdots, N_s \tag{4.3}$$

where Δ_i is the number of examples in the k-NN of $\mathbf{x}_i$ that belong to the majority class; therefore, $r_i \in [0, 1]$.

4. Then, r_i is normalized according to $\hat{r_i} = r_i / \sum_{i=1}^{N_s} r_i$, and the number of synthetic data samples to generate for each minority example $\mathbf{x}_i$ is obtained from:

$$g_i = \hat{r_i} \cdot G \tag{4.4}$$

5. Finally, for each minority class example $\mathbf{x}_i$, each synthetic sample, among the g_i to generate, is obtained from the random selection of one minority class example $\mathbf{x}_{zi}$ from the k-NN for data $\mathbf{x}_i$. Then, the synthetic sample is generated as:

$$\mathbf{s}_i = \mathbf{x}_i + (\mathbf{x}_{zi} - \mathbf{x}_i) \cdot \lambda \tag{4.5}$$

where $(\mathbf{x}_{zi} - \mathbf{x}_i)$ is the difference vector in the M dimensional space, and λ is a random number $\lambda \in [0, 1]$.

Since this method randomly chooses examples from the minority class to generate new samples, the algorithm is applied 50 times and the mean from all realizations is kept as the final balanced dataset $F_M^{N_b}$, where N_b refers to the total amount of observations after class balancing. Figure 4.2 illustrates the feature conditioning process.

4.1.2. Feature selection

To reduce the number of attributes included in the model so as to decrease its computational cost, a two-step feature selection approach is applied to identify the most relevant features in distinguishing between symptomatic and asymptomatic patients. As previously mentioned, Figure 4.1 specifies the methodology followed for feature extraction and posterior feature selection, only applied to a randomly selected sample of 75% of the feature database (F_M^{Ntr}: training subset). The remaining 25% (F_M^{Nte}: testing subset) is then used for model validation.

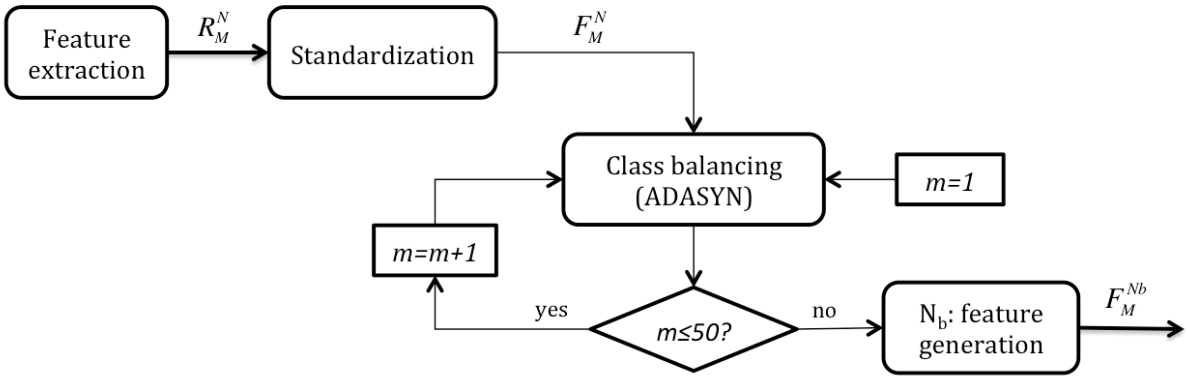

FIGURE 4.2– The raw feature dataset extracted from the previous step R_M^N is standardized, leading to F_M^N. Then, a class balancing method is repeated 50 times, so the final value for the balanced dataset $F_M^{N_b}$ is obtained as the mean from all realizations.

4.1.2.1. ReliefF filter method

The first step in the feature selection process is a simple filter method based on the ReliefF algorithm (ROBNIK-ŠIKONJA et al., 2003). Since this approach ignores the effects of attributes on classification, it can rapidly remove some irrelevant and redundant features.

The algorithm estimates feature weights W according to their capability of distinguishing between data from different classes, here symptomatic and asymptomatic patients. First, it randomly selects n data samples or observations. For each data sample x_i, it searches for k nearest neighbors from the same class (known as nearest hits) and for other k from the other class (known as nearest misses), and averages the contribution of all k nearest hits/misses, here noted as x_i^H and x_i^M. The weight allocated to each attribute results from:

$$W = \sum_{i=1}^{n} \frac{x_i - x_i^M}{n} - \sum_{i=1}^{n} \frac{x_i - x_i^H}{n} \tag{4.6}$$

where the first term refers to the mean difference between the feature value of all analyzed data samples and the nearest misses contributions, and the second term is the mean difference between the same feature values and the nearest hits contributions.

The best feature should present the same value for samples of the same class and differentiate between instances from different classes. Therefore, the algorithm assigns a relevance weight ranged from -1 to 1 to each feature, with large positive weights allocated to significant attributes. However, it should be noted that, since this method is based on a k-NN approach, feature weights usually depend on k. For small values of k, the estimates can be unreliable for noisy data; while for k values comparable with the number of observations, the algorithm can fail to find significant attributes. Thus, ReliefF is computed for $k = 10, \cdots, 19$ and W is obtained as the average of all the obtained weights.

Moreover, since extracted feature values are supposed to significantly vary over patients, a bootstrap technique is applied (GUYON et al., 2003). The algorithm is run 50 times on different

randomly chosen subsets including 60% of the training dataset F_M^{Ntr}, here represented as $F_M^{Ntr_i}$. Then, the relevance of each feature is obtained as the median of the 50 realizations analyzed. Figure 4.3 displays the methodology followed to select M_f as the 75% most relevant attributes that are kept for further analysis.

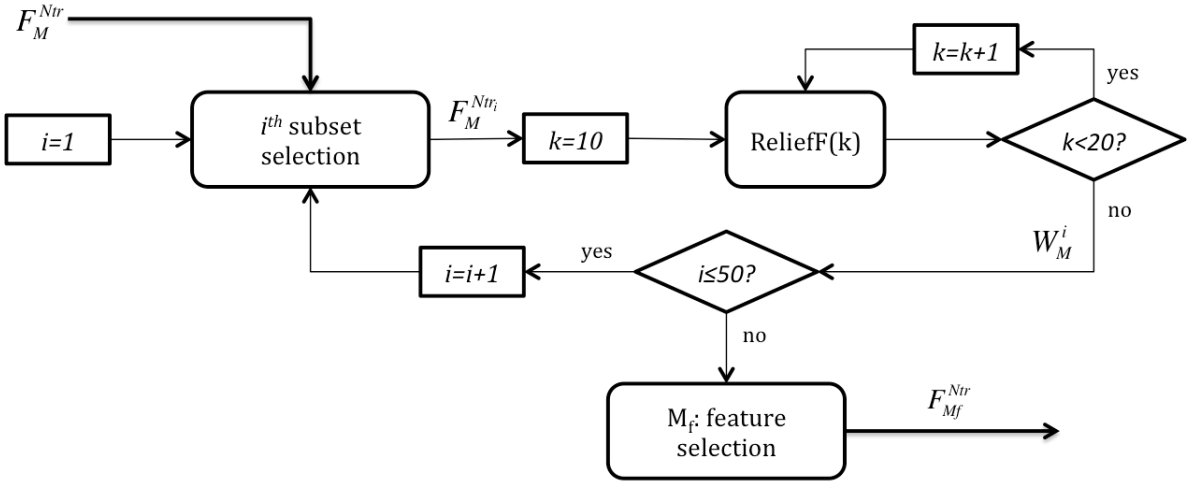

FIGURE 4.3– In this step, the complete training dataset F_M^{Ntr} is employed. For each iteration i, a random subset composed of 60% of the training data is defined. The weight of all features W_M^i in this subset is computed as the averaged weight along $k = 10, \cdots, 19$. This process is repeated 50 times and the final weight of each feature is obtained as the median from all realizations. Finally, the M_f most relevant features are selected and $F_{M_f}^{Ntr}$ is kept as input for the wrapper feature selection step.

4.1.2.2. LDA-based wrapper method

For final feature selection, a second step is applied on the reduced subset of attributes resulting from the previous stage. It consists in a wrapper algorithm based on a Linear Discriminant Analysis (LDA) classifier as a black box, implemented using the floating search method. Since this approach is based on classification performance, the final subset is only optimized for this particular classifier (KOHAVI et al., 1997).

The floating method combines the application of both sequential forward and backward selection strategies (PUDIL et al., 1994). The former, is a *bottom-up* search process that, after the inclusion of a new feature (forward step), it performs a series of successive conditional exclusions (backward steps) as long as the resulting subset improves the previously evaluated solution. Conversely, the backward selection strategy is a *top-down* search process that begins with the elimination of a feature (backward step) and re-selects previously removed features (forward steps) while they improve classification performance. Since in the *top-down* search discarded features cannot be re-selected, as well as in the *bottom-up* search selected features cannot be later discarded, the combination of both strategies overcomes limitations encountered when these methods are applied separately.

Linear discriminant analysis (LDA) is a simple and robust classification method which searches for the linear combination of features best separating two classes (KUNCHEVA, 2004), here symptomatic and asymptomatic patients. Being x_i, where $i = 1, 2, \cdots, d$, the input features, the LDA model is defined as:

$$Z = \beta_1 x_1 + \beta_2 x_2 + \cdots + \beta_d x_d \tag{4.7}$$

where β_i, hereafter β, are the linear model coefficients to be estimated based on the maximization of the score function $S(\beta)$:

$$S(\beta) = \frac{\beta^T \mu_s - \beta^T \mu_a}{\beta^T C \beta} \tag{4.8}$$

Being μ_s and μ_a the mean vectors, C_s and C_a the covariance matrices, as well as n_s and n_a the number of samples in each class, the coefficients are identified by the following equations:

$$\beta = C^{-1}(\mu_s - \mu_a) \tag{4.9}$$

$$C = \frac{n_a C_a + n_s C_s}{n_s + n_a} \tag{4.10}$$

Figure 4.4 represents the wrapper feature selection process in more detail. As in the previous step, it is repeated 50 times on different randomly chosen subsets of training data $F_{M_f}^{Ntr_i}$. Those features appearing more than L times, among the 50 realizations, are kept for the final subset $F_{M_w}^{Ntr}$. The value of L is optimized, based on performance metrics, so as to find the best selection of features M_w leading to the finest classifier distinguishing between symptomatic and asymptomatic BS patients.

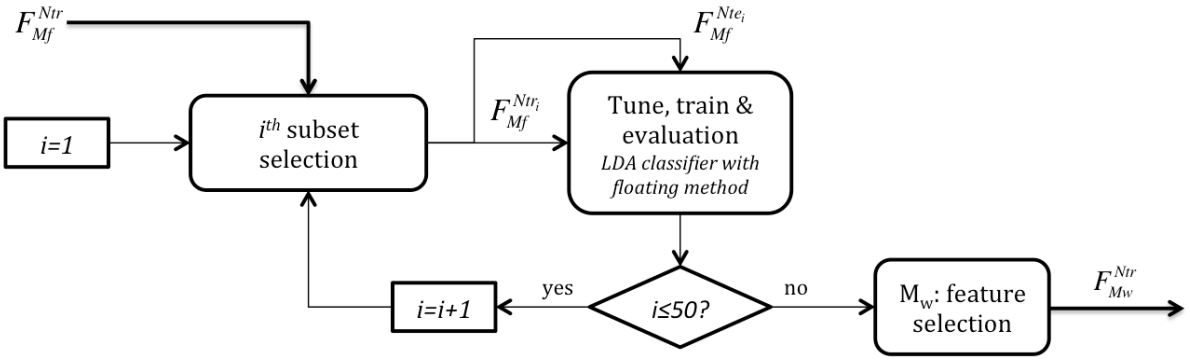

FIGURE 4.4– Starting from the training set obtained from the filter feature selection step $F_{M_f}^{Ntr}$, for each iteration i, a subset with 75% of the data $F_{M_f}^{Ntr_i}$ is chosen to tune and train an LDA-based classifier, then evaluated with the remaining 25% of the random subset $F_{M_f}^{Nte_i}$. The strategy is repeated 50 times and those attributes appearing more than L times among all realizations are kept for the final feature subset $F_{M_w}^{Ntr}$.

4.1.3. LDA-based classifier

After selecting the best set of features, an LDA classifier is implemented using a 5-fold cross-validation approach in order to reduce overfitting. This technique divides the entire training subset $F_{M_w}^{Ntr}$ into 5 blocks where each classifier is firstly trained on 4 portions and then tested on the 5^{th} block. This is performed for the 5 different possible combinations of blocks for training/testing so the outputs of each solution are then averaged.

In addition, to estimate the classifier's mean performance variability when applied to testing data, 5-fold cross-validation is run 10 times on differently divided subsets of training data. Figure 4.5 illustrates the steps followed to train and test the LDA classifier. As specified in previous sections, 75% of the data $F_{M_w}^{Ntr}$ are used for training, and the remaining 25% $F_{M_w}^{Nte}$ for testing.

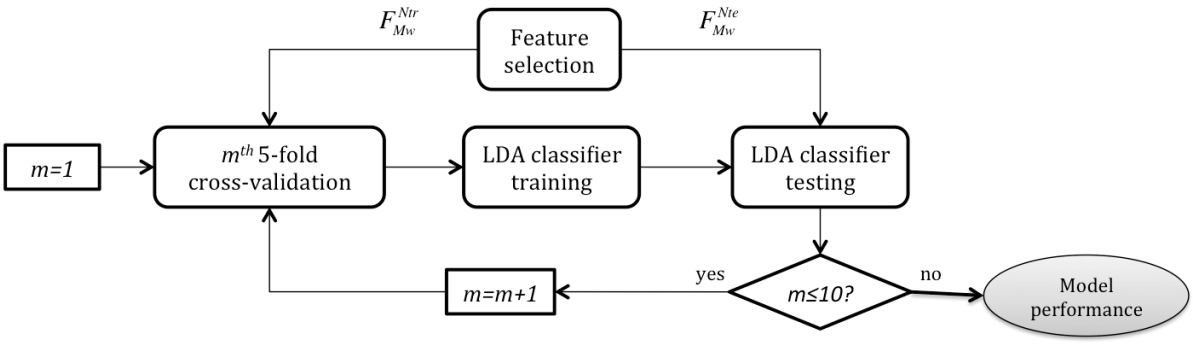

FIGURE 4.5– After feature extraction, conditioning and selection, a 5-fold cross-validation is run 10 times in order to assess the classifier performance, tuned using the training subset $F_{M_w}^{Ntr}$ and evaluated on the testing subset $F_{M_w}^{Nte}$.

Finally, model performance is evaluated, based on the resulting confusion matrix, which specifies the number of true positives (TP), true negatives (TN), false positives (FP) and false negatives (FN), when comparing true and predicted labels if symptomatic patients are considered as positives.

First, the AUC or area under the ROC (Receiver Operating Characteristic) curve is computed to quantify the classifier performance. This measure is also assessed in order to optimize the threshold L that leads to the best performing classifier after wrapper feature selection.

Moreover, classical sensitivity ($Se = TP/(TP + FN)$) and specificity ($Sp = TN/(TN + FP)$) measures, associated with the optimal operating point in the ROC curve, are calculated to quantify the classifier capability of correctly detecting symptomatic and asymptomatic patients, respectively.

4.2. Multivariate classification

The described classification methodology was first applied on features extracted during exercise testing in 105 BS patients. Then, in order to compare the classification performance of predictive models designed with features obtained during different autonomic tests, a reduced clinical database acquired overnight, and during exercise and HUT testing including 44 patients was analyzed.

4.2.1. Classification results during exercise

HRV features extracted from a time-frequency analysis performed during exercise testing in 105 BS patients, were included in the proposed machine learning approach, in order to design a predictive model capable of distinguishing between symptomatic and asymptomatic BS patients.

4.2.1.1. Clinical data description

Table 4.1 summarizes patients' clinical characteristics. Their ages ranged from 19 to 74 years old (45.17 ± 13.62 years old) and 76.2% were males. Twenty-four patients presented documented symptoms of ventricular origin: syncope (50%), cardiac arrest (41.7%), dizziness (12.5%) and, less frequently, palpitations and nocturnal convulsions (4.2%). ICDs had been implanted in 18 of 81 (22.2%) asymptomatic patients, based on a positive EPS (Electrophysiological Study) test, whereas all symptomatic patients had ICDs implanted. Among 76 patients (19 were symptomatic) in whom genetic analysis was performed, an SCN5A mutation was found in 27 (35.5%).

TABLE 4.1– Symptomatic and asymptomatic patients' clinical characteristics for classification based on HRV features extracted during exercise testing.

	Symptomatic (n=24)	**Asymptomatic (n=81)**	***p*-value**
Age, *years old*	46.25 ± 15.23	44.85 ± 13.20	0.852
Male sex, *n (%)*	60 (74.1%)	20 (83.3%)	0.352
ICD implantation, *n (%)*	24 (100%)	18 (22.2%)	< 0.001
Presence of *SCN5A* mutation, *n (%)*	6 (31.6%)	21 (36.8%)	0.680

Values are mean ± standard deviation or number of observations (%).
All between-groups differences, apart from ICD implantation, are statistically non-significant.

4.2.1.2. Feature extraction

Estimated features from time-frequency analysis (Section 3.3.2.) included the following averaged non-overlapped windows of 1 minute: $\overline{LF^i}$, $\overline{LF^i_{nu}}$, $\overline{HF^i}$, $\overline{HF^i_{nu}}$ and $\overline{LF/HF^i}$, where $i \in \{WU1, WU2, EX1, EX2, EX3, PE, AR1, AR2, AR3, PR1, PR2, PR3\}$. Since each test differed

in the incremental exercise phase duration and the shortest case in the clinical series lasted less than 5 minutes, only the first 3 minutes of incremental exertion ($EX1$, $EX2$ and $EX3$), as well as the last minute before peak effort (PE), were added to the pool of features. In addition, the entire warm-up ($WU1$ and $WU2$) and active ($AR1$, $AR2$ and $AR3$) and passive recovery ($PR1$, $PR2$ and $PR3$) phases were included. Thus, from each HRV time series, 12 intra-patient 1-min means composed the matrix R_M^N, containing $M = 60$ HRV markers for the $N = 105$ patients.

4.2.1.3. Classification results

After standardization, in order to attenuate the effect of imbalanced classes, 55 synthetic symptomatic samples were generated and included in the analysis leading to $N_b = 160$ observations before feature selection, composed of 79 symptomatic and 81 asymptomatic samples. At this point, data were divided in the training (75%) and testing (25%) subsets, including $Ntr = 119$ (59 symptomatic and 60 asymptomatic) and $Nte = 41$ (20 symptomatic and 21 asymptomatic) observations, respectively.

Then, a two-step feature selection process was applied to the training subset. After filter selection, the 15, or 25%, least relevant HRV features were removed from the analysis. Then, a wrapper method based on an LDA classifier, using both forward search and backward elimination, was applied on the feature subset obtained from the filter step, containing $Mf = 45$ features.

Since the algorithm was run 50 times, the number of times each feature was kept along realizations was calculated. The final subset contained those features appearing more than a specific number of times L, optimized based on the performance metric AUC. Figure 4.6 displays the mean and standard deviation of AUC associated with each value of L.

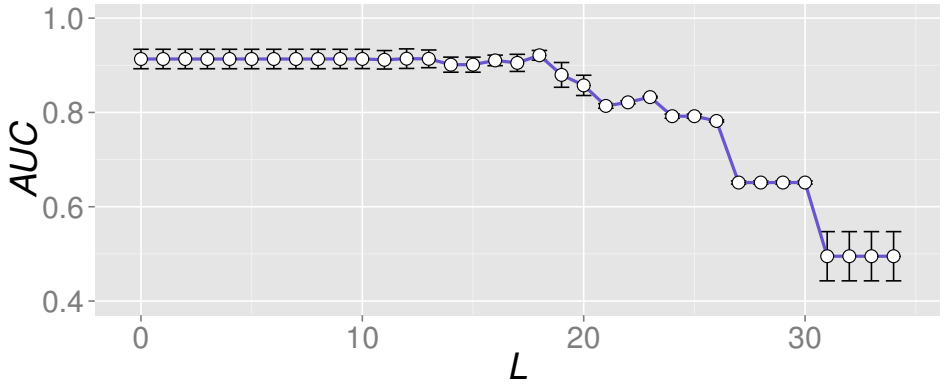

FIGURE 4.6– Mean and standard deviation of AUC for each value of L.

Based on these results, the final classifier placed the threshold at $L = 18$, where a maximum AUC using the minimum number of features was found. When only those parameters appearing more than 18 times were kept, the final subset contained M_w =22 features (listed in Appendix B.1), leading to: $AUC = 0.92 \pm 0.01$, $Se = 0.91 \pm 0.06$ and $Sp = 0.90 \pm 0.05$.

Figure 4.7 displays the mean ROC curves resulting from each 5-fold cross-validation, as well as the global ROC curve and its optimal operating point, for the proposed classifier.

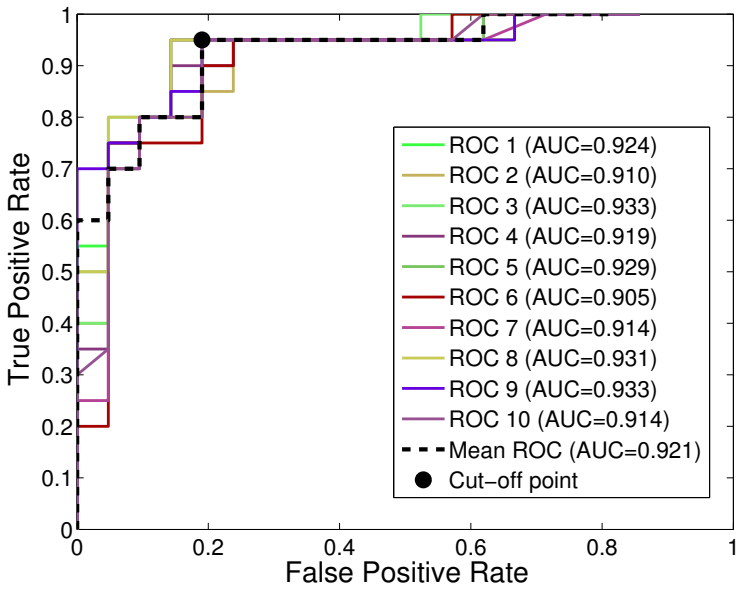

FIGURE 4.7– Mean ROC curves for each cross-validation and global ROC (dashed black line), when features appearing more than 18 times were kept.

4.2.2. Comparison of classification results overnight and during exercise and head-up tilt testing

The same classification strategy was applied to a clinical database including cardiac signals overnight, and during exercise and HUT testing from 44 BS patients. The aim of the study was to validate the model developed in the previous section on independent datasets. Moreover, the predictive values of classifiers designed from features extracted during each autonomic test, as well as from the combination of such tests, were compared; in order to identify those markers and autonomic protocols best distinguishing between symptomatic and asymptomatic groups.

4.2.2.1. Clinical data description

Patients' age ranged from 19 to 73 years old (45.45 ± 12.78 years old) and 38 (86.4%) were males. Eleven patients had the following documented symptoms: syncope (72.7%), cardiac arrest (18.2%) and, less frequently, dizzines, palpitations and nocturnal convulsions (9.1%). ICD implantation had been performed in 10 of 33 (30.3%) asymptomatic patients, based on a positive EPS test, whereas all symptomatic patients were ICD carriers. Among 34 patients (10 were symptomatic) in whom genetic screening was performed, an *SCN5A* mutation was found in 11 (32.4%), from whom 4 were symptomatic. Table 4.2 summarizes participants' baseline characteristics.

TABLE 4.2– Symptomatic and asymptomatic patients' clinical characteristics for classification, based on features extracted overnight, and during exercise and HUT testing.

	Symptomatic (n=11)	**Asymptomatic (n=33)**	*p*-**value**
Age, *years old*	47.09 ± 15.98	44.91 ± 11.77	0.724
Male sex, *n (%)*	9 (81.8%)	29 (87.9%)	0.632
ICD implantation, *n (%)*	11 (100%)	10 (30.3%)	<0.001
Presence of *SCN5A* mutation, *n (%)*	4 (40%)	7 (29.2%)	0.560

Values are mean ± standard deviation or number of observations (%).
All between-groups differences, apart from ICD implantation, are statistically non-significant.

4.2.2.2. Feature extraction

Regarding data extracted during exercise testing, as in the previous section, candidate features were those estimated from the time-frequency analysis described in Section 3.3.2., including the following averaged non-overlapped windows of 1 minute: $\overline{LF^i}$, $\overline{LF^i_{nu}}$, $\overline{HF^i}$, $\overline{HF^i_{nu}}$ and $\overline{LF/HF^i}$, where $i \in \{WU1, WU2, EX1, EX2, EX3, PE, AR1, AR2, AR3, PR1, PR2, PR3\}$. Moreover, HRC information was added to the pool of features by including the β values obtained during exercise and recovery phases (β_{ex}, β_{recov}).

For the design of classifiers based on HUT testing data, candidate features were extracted by means of the time-frequency analysis described in Section 3.3.4. The mean for the whole baseline period (B) was subtracted from each estimated HRV time series, then averaged in temporal non-overlapped windows of 1 minute, leading to the following features: $\overline{\Delta LF^i}$, $\overline{\Delta HF^i}$, $\overline{\Delta LF^i_{nu}}$, $\overline{\Delta HF^i_{nu}}$ and $\overline{\Delta LF/HF^i}$, where $i \in \{T11, T12, T13, T14, T15, S1, S2, S3, S4, S5\}$. For classification purposes, in order to reduce computational cost, only the first 5 minutes after tilting and the time period between 11-15 minutes in upright position were included.

Finally, regarding night analysis, the mean at each hour from midnight to 6 a.m. of the following HRV and HRC parameters were included as candidate features: $\overline{RR}$, $SDNN$, $NN50$, $MIRR$, $SDANN$, $SDNN5min$, $rMSSD$, LF_{nu}, HF_{nu}, LF/HF and $SampEn$.

4.2.2.3. Single-test classification results

In a first phase, three single-test classifiers were built from features extracted during each autonomic test. Regarding the classifier based on exercise testing data, after feature extraction, the input matrix R^N_M contained $M = 62$ markers for the $N = 44$ patients; whereas $M = 50$ features were employed to design the classifier based on HUT testing data, and $M = 66$ candidate features were included in the classifier developed from night information.

For each single-test process, after standardization, in order to attenuate the bias introduced by imbalanced classes, 22 synthetic symptomatic samples were generated, leading to $N_b = 66$

observations before feature selection. Then, data were divided in the training and testing subsets, including $Ntr = 48$ (24 symptomatic and asymptomatic) and $Nte = 18$ (9 symptomatic and asymptomatic) observations, respectively.

As aforementioned, filter selection discarded the 25% least relevant markers and, the final feature subset contained those markers appearing more than a specific number of times L after the application of the wrapper method, optimized based on the maximum AUC value. Figure 4.8 displays the mean and standard deviation of AUC associated with each value of L, for each autonomic test.

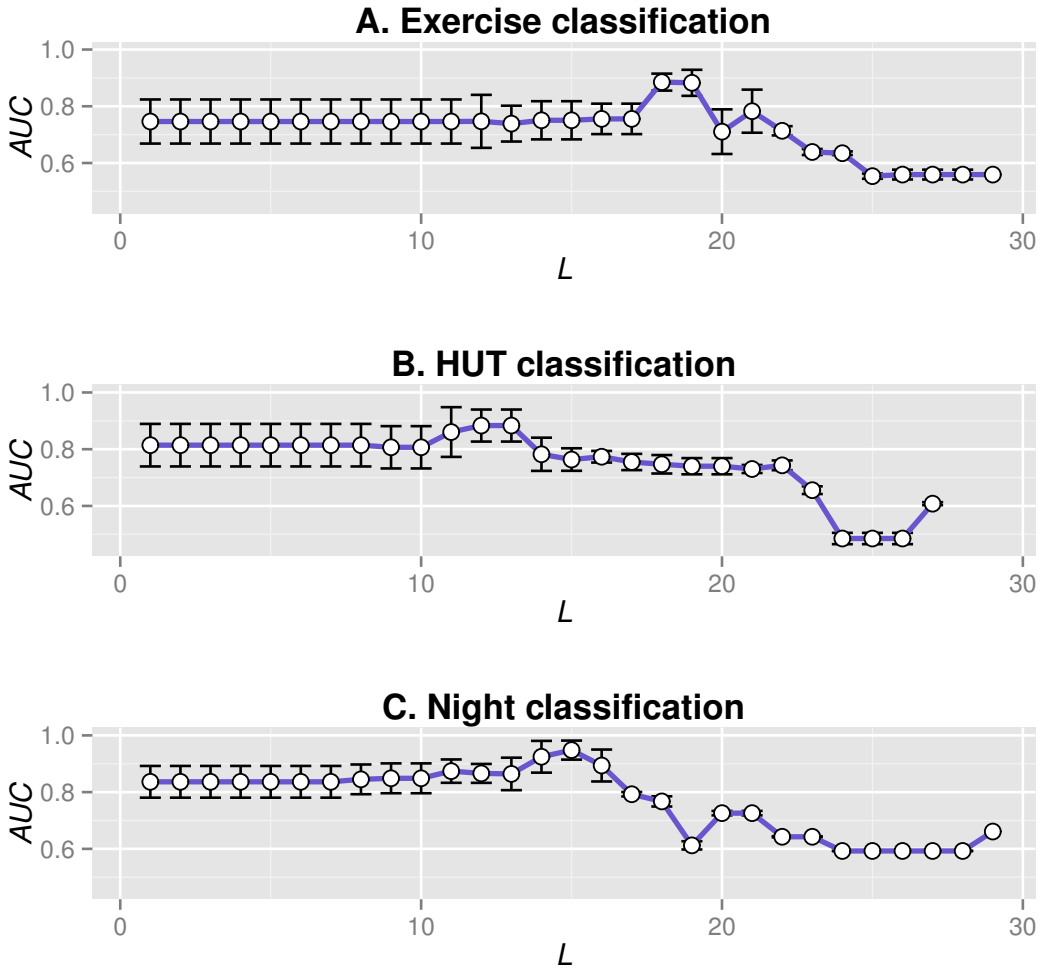

FIGURE 4.8– Mean and standard deviation of AUC values depending on L, for classifiers based on data extracted during A) exercise, B) HUT testing and C) night analysis.

Based on the results, regarding exercise analysis (Figure 4.8A), the final classifier placed the threshold at $L = 18$, being consistent with the previous study where the same optimal L value was selected. When only those parameters appearing more than 18 times after wrapper feature selection were kept, the final subset contained $M_w = 31$ features (listed in Appendix

B.1), leading to an $AUC = 0.89 \pm 0.03$, $Se = 0.88 \pm 0.04$ and $Sp = 0.74 \pm 0.11$. Although this predictive model did not reach the classifier designed in previous section performance ($AUC = 0.92 \pm 0.01$ for $M_w = 22$ features), probably due to a reduced amount of observations for model training, the proposed global classification methodology demonstrated an acceptable generalization capability. Moreover, since an excessive amount of variables when a reduced sample of observations is available may confound classification results, the rebound effect observed in the mean L-dependent AUC became more evident when using a smaller sample of patients.

The optimal AUC for the classifier based on HUT testing data (Figure 4.8B) was found for $L = 12$, leading to a final subset containing M_w= 31 features (listed in Appendix B.2) with a performance of $AUC = 0.88 \pm 0.06$, $Se = 0.74 \pm 0.08$ and $Sp = 0.86 \pm 0.15$. Similar results were observed for both classifiers; HUT classification, though, improved specificity at the expense of worsening sensitivity.

Finally, the optimal AUC regarding night analysis (Figure 4.8C) was found for $L = 15$, leading to the best performance among single-test classifiers ($AUC = 0.95 \pm 0.03$, $Se = 0.94 \pm 0.08$, $Sp = 0.80 \pm 0.12$), with the least amount of features (M_w= 26). The final subset is listed in Appendix B.3.

4.2.2.4. Multiple-test classification results

In order to evaluate if the combination of different autonomic test could outperform the results found for night analysis, classifiers designed from features of different autonomic tests were characterized and compared. Table 4.3 includes the optimal AUC values obtained for each single-test classifier, as well as for each classifier built from the combination of different autonomic tests.

TABLE 4.3– Mean and standard deviation of optimal AUC values, for all single- and mutiple-test classifiers.

Classifier	**Performance (AUC)**
Exercise	0.89 ± 0.03
HUT	0.88 ± 0.06
Night	0.95 ± 0.03
Exercise - HUT	0.91 ± 0.04
Exercise - Night	0.84 ± 0.08
HUT - Night	0.89 ± 0.04
Exercise - HUT - Night	0.92 ± 0.04

Based on the results, the predictive value of exercise testing ($AUC = 0.89 \pm 0.03$) increased by adding information from HUT testing ($AUC = 0.91 \pm 0.04$), and it was even improved by including night information ($AUC = 0.92 \pm 0.04$). However, the best results were found when nighttime was separately analyzed ($AUC = 0.95 \pm 0.03$).

4.3. Discussion

The proposed model was first optimized and evaluated on a clinical database of 105 BS patients, during exercise testing, leading to a mean AUC of 92% only using about one third of the total amount of HRV features included at the first step. Filter feature selection discarded the least relevant and most redundant features, holding the 75% of the initial features subset, to which the LDA-based wrapper algorithm was applied. On the one hand, the results after filtering show that all autonomic markers during the last minutes of incremental exercise and recovery were kept, evidencing the relevance of these test segments in classifying BS patients. On the other hand, although $\overline{HF_{nu}^{EX2}}$ lead to significant results in univariate analysis, ReliefF identified this marker as a redundant feature and only kept $\overline{LF_{nu}^{EX2}}$ for further analysis.

Since classification performance significantly depends on the number of chosen features after wrapper feature selection, the algorithm was optimized to obtain the best AUC using the minimum number of features. Thus, when selecting only those features appearing more than 35% of times after wrapper application, an optimal classifier containing 22 parameters was implemented. Among the final subset of features, only one $\frac{LF}{HF}$ marker was kept, acquired during the second minute of active recovery. The remaining parameters equally belonged to LF and LF_{nu} or HF and HF_{nu} measures. Regarding test phases, only one feature came from the warm-up phase ($\overline{HF_{nu}^{WU1}}$) and other 5 markers were acquired during the passive recovery stage; but most parameters were measured during incremental exercise and active recovery, and more specifically during the last minutes of both phases.

In a second study, in order to determine which autonomic tests and indicators yield the highest predictive values to identify BS patients at high risk of SCD, several classifiers designed from features extracted during different autonomic tests in 44 BS patients were designed and compared. Although exercise and HUT testing together lead to better predictive results than when their markers were analyzed separately, the classifier based on autonomic features obtained during nighttime analysis presented the best performance ($AUC = 95\%$).

Among the 26 final features composing this optimal classifier, only one $SampEn$ marker was kept, acquired between 4 a.m. - 5 a.m. The remaining parameters mostly belonged to temporal HRV measures, although 6 spectral features were also retained. Regarding analyzed hours, parameters were obtained along the whole night; however, the time period including more features was between 4 a.m - 5 a.m.

Thus, findings provide further evidence for the relevant role of night analysis to identify BS patients at high risk, when parasympathetic activity is predominant. The results concur with previous studies reporting that most major cardiac events in BS occur at rest and during sleep (Kies et al., 2004; Matsuo et al., 1999). Moreover, although recent studies have also proposed prediction models for risk stratification in BS patients using non-invasive parameters (Kawazoe et al., 2016), this model outperformed previous approaches, evidencing the interest of analyzing HRV and HRC features overnight to better understand VF risk in this population.

4.4. Conclusion

This chapter proposes a multivariate method based on a step-based machine learning approach, designed to optimally combine the previously extracted autonomic features in order to improve classification of BS patients, based on their symptomatic status.

A predictive model based on a two-step feature selection strategy captured the most discriminant HRV features in order to distinguish between symptomatic and asymptomatic patients. Despite the difficulty in finding differences between these populations, classification results show the potential of autonomic markers extracted at night for the identification of symptoms in Brugada syndrome. Thus, the proposed model is presented as a potential instrument to better identify those asymptomatic BS patients at high risk who may benefit from an ICD implantation. Moreover, it might be used for processing HRV data acquired from the ICD on implanted BS patients, in order to control their risk of VF occurrence during follow-up.

However, since this predictive model does not integrate explicit biological *a priori* knowledge, the next chapter introduces a model-based approach based on computational models integrating physiological information on interactions between the cardiac function, and the circulatory and autonomic systems, in order to provide a step forward towards the understanding of autonomic modulation in BS.

References

Delise, P., G. Allocca, N. Sitta, and P. Di Stefano (2014). "Event rates and risk factors in patients with Brugada syndrome and no prior cardiac arrest: a cumulative analysis of the largest available studies distinguishing ICD-recorded fast ventricular arrhythmias and sudden death". In: *Heart Rhythm* 11.2, pp. 252–258.

Delise, P., G. Allocca, E. Marras, C. Giustetto, F. Gaita, L. Sciarra, L. Calo, A. Proclemer, M. Marziali, L. Rebellato, et al. (2011). "Risk stratification in individuals with the Brugada type 1 ECG pattern without previous cardiac arrest: usefulness of a combined clinical and electrophysiologic approach". In: *European heart journal* 32.2, pp. 169–176.

Guyon, I. and A. Elisseeff (2003). "An introduction to variable and feature selection". In: *Journal of machine learning research* 3, pp. 1157–1182.

He, H., Y. Bai, E. A. Garcia, and S. Li (2008). "ADASYN: Adaptive synthetic sampling approach for imbalanced learning". In: *2008 IEEE International Joint Conference on Neural Networks (IEEE World Congress on Computational Intelligence)*, pp. 1322–1328.

Kawazoe, H., Y. Nakano, H. Ochi, M. Takagi, Y. Hayashi, Y. Uchimura, T. Tokuyama, Y. Watanabe, H. Matsumura, S. Tomomori, et al. (2016). "Risk stratification of ventricular fibrillation in Brugada syndrome using noninvasive scoring methods". In: *Heart Rhythm* 13.10, pp. 1947–1954.

Kies, P., T. Wichter, M. Schäfers, M. Paul, K. P. Schäfers, L. Eckardt, L. Stegger, E. Schulze-Bahr, O. Rimoldi, G. Breithardt, et al. (2004). "Abnormal myocardial presynaptic norepinephrine recycling in patients with Brugada syndrome". In: *Circulation* 110.19, pp. 3017–3022.

Kohavi, R. and G. H. John (1997). "Wrappers for feature subset selection". In: *Artificial intelligence* 97.1, pp. 273–324.

Kuncheva, L. I. (2004). *Combining pattern classifiers: methods and algorithms*. John Wiley & Sons.

Matsuo, K., T. Kurita, M. Inagaki, M. Kakishita, N. Aihara, W. Shimizu, A. Taguchi, K. Suyama, S. Kamakura, and K. Shimomura (1999). "The circadian pattern of the development of ventricular fibrillation in patients with Brugada syndrome". In: *European heart journal* 20.6, pp. 465–470.

Okamura, H., T. Kamakura, H. Morita, K. Tokioka, I. Nakajima, M. Wada, K. Ishibashi, K. Miyamoto, T. Noda, T. Aiba, et al. (2015). "Risk stratification in patients with Brugada syndrome without previous cardiac arrest". In: *Circulation Journal* 79.2, pp. 310–317.

Pudil, P., F. Ferri, J. Novovicova, and J. Kittler (1994). "Floating search methods for feature selection with nonmonotonic criterion functions". In: *Pattern Recognition, 1994. Vol. 2-Conference B: Computer Vision & Image Processing., Proceedings of the 12th IAPR International. Conference on*. Vol. 2, pp. 279–283.

Robnik-Šikonja, M. and I. Kononenko (2003). "Theoretical and empirical analysis of ReliefF and RReliefF". In: *Machine learning* 53.1-2, pp. 23–69.

CHAPTER 5

Cardiovascular response to autonomic nervous system stimulation in Brugada syndrome: model-based feature extraction

The previous chapter proposes a multivariate approach based on a step-based machine learning method so as to identify BS patients at high risk of major cardiac arrhythmias. Although the developed predictive models demonstrated an improved performance with respect to previous works in the field, they are based on generic models assuming strong hypotheses about data statistical properties, and do not integrate explicit biological *a priori* knowledge. Thus, the description of computational models describing interactions between the cardiac function and the circulatory and autonomic nervous systems could be a step forward towards the interpretation of the autonomic function in Brugada syndrome (Coatrieux et al., 2006).

This chapter introduces two system-level model-based approaches to analyze the mechanic, circulatory and autonomic function of BS patients. First, by the introduction of a cardiovascular model and its short-term autonomic regulation in response to HUT testing, followed by a two-step sensitivity analysis, and the development of patient-specific models for both healthy and BS subjects. In a second study, recursive model identifications are applied to estimate the time-varying autonomic response to exercise in symptomatic and asymptomatic patients.

However, these approaches are limited to a univariate analyis of model parameters. Since these markers may provide complementary information with respect to other autonomic indices, such as those studied in Chapter 3, a multivariate analysis including model-based parameters and/or classical autonomic markers may be useful to improve the characterization of BS patients. Therefore, a prospective study in order to evaluate this hypothesis is also presented.

5.1. Autonomic response to head-up tilt testing

In this section, a coupled model integrating the cardiac electrical activity, the cardiovascular system and the baroreceptors reflex control of the autonomic function in response to HUT testing, is implemented. Then, a thorough two-step parameter sensitivity analysis based on a screening method and a global approach is applied to the model to identify the most relevant variables affecting BP and HR in supine and upright postures. Finally, the most relevant parameters found in sensitivity analysis are estimated through an approach based on evolutionary algorithms in 20 subjects (8 controls and 12 BS patients), enabling the assessment of subject-specific cardiovascular conditions.

5.1.1. Global model-based strategy

In order to design model-based subject-specific estimations of the autonomic regulation of cardiovascular dynamics in response to HUT testing, the following three main steps, represented in Figure 5.1 and explained in more detail in the subsequent sections, were applied:

- Construction of the computational model capturing interactions between the cardiovascular system (CVS) and the autonomic nervous system (ANS).
- Selection of the most influential model parameters on outputs, by means of an exhaustive sensitivity analysis.
- Design of subject-specific models by identifying selected parameters, based on experimental and simulated heart rate (HR) and systolic blood pressure (SBP) data.

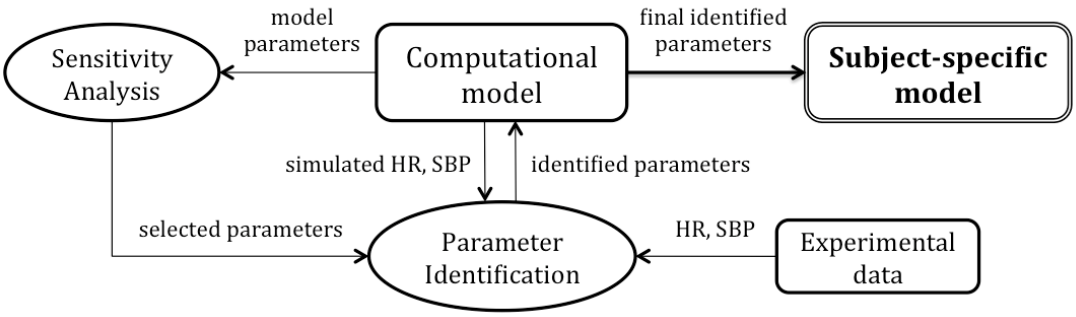

Figure 5.1– Diagram of the global model-based approach. After the construction of a computational model, a sensitivity analysis is applied to select the most relevant parameters identified in the design of subject-specific models based on the experimental data of each patient.

5.1.2. Experimental data description

HUT tests were performed in fasting conditions on 8 controls and 12 BS patients. Controls were healthy subjects without classical cardiovascular risk factors (diabetes, dislypidemia or

hypertension), non-smokers, asymptomatic and not taking cardioactive medication. Five BS patients presented documented symptoms of ventricular origin: cardiac arrest (60%) and syncope (40%). An ICD had been placed in one asymptomatic patient, based on a positive EPS test, whereas all symptomatic patients had ICDs implanted. Three BS patients (2 were symptomatic) presented an SCN5A mutation (25%).

TABLE 5.1– Participants' baseline characteristics.

	Symptomatic (n=5)	**Asymptomatic (n=7)**	**Controls (n=8)**
Age, *years old*	48.0 ± 11.5	51.6 ± 13.2	30.8 ± 5.7
Male sex, *n (%)*	5 (100%)	5 (71.4%)	8 (100%)
ICD implantation, *n (%)*	5 (100%)	1 (14.3%)	-
***SCN5A* mutation,** *n (%)*	2 (40%)	1 (14.3%)	-

Values are mean ± standard deviation or number of observations (%).

Cardiovascular signals from BS patients were obtained from the Task Force database, and the same recording system and protocol were followed to acquire the ECG and BP signals of healthy subjects. SBP and RR series were extracted by means of the same process described in Section 3.1. Then, in order to ease the comparison with model simulations, experimental data were low-pass filtered at 0.04 Hz with a 4^{th} order Butterworth filter applied in both forward and backward directions so as to remove phase distortion. Finally, cardiac signals were only analyzed for 2.5 minutes before and after tilting onset, where the response induced by changing from supine to upright posture is represented.

5.1.3. Computational model

A computational model integrating the cardiovascular system and its short-term autonomic modulation in response to HUT testing was implemented by means of the M2SL simulation library (HERNÁNDEZ et al., 2009). It consists of 4 coupled submodels representing: 1) the cardiac electrical system (CES), 2) the cardiovascular system (CVS), 3) the baroreceptors reflex system (BRS), and 4) the head-up tilt test (HUTT). Figure 5.2 illustrates the submodels composing the closed-loop system, described in more detail in the following subsections.

5.1.3.1. Cardiac electrical system

The cardiac electrical conduction system, represented in Figure 5.3, was based on a simplified discrete model adapted from (HERNÁNDEZ et al., 2002). It is defined as a set of interconnected cellular automata, each one explaining the electrical activation of a group of cardiac cells: the sinoatrial node (SAN), the left atrium (LA), the atrioventricular node (AVN), the upper bundle of His (UBH), the lower bundle of His (LBH), left and right bundle branches (LBB and RBB), and left and right ventricles (LV and RV).

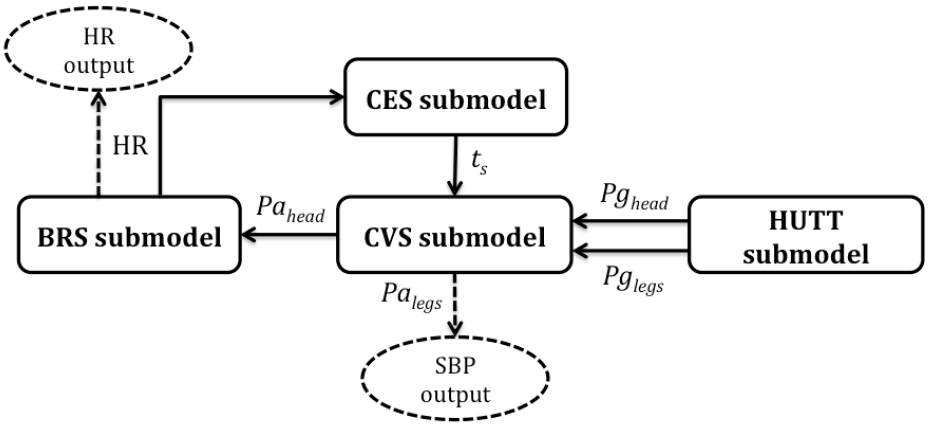

Figure 5.2– Diagram of the integrated model including the cardiac electrical system (CES), the cardiovascular system (CVS), the baroreceptors reflex system (BRS) and the head-up tilt test (HUTT) submodels. Heart rate (HR) and systolic blood pressure (SBP) are the model outputs under study. Pa_{head}: arterial pressure at the head; Pa_{legs}: arterial pressure at the legs; Pg_{head}: pressure due to gravity at the head; Pg_{legs}: pressure due to gravity at the legs; ts: cardiac cycle onset determined by ventricular electrical activation.

Each automaton state periodically changes among the four main electrophysiological activation periods: slow diastolic depolarization (SDD) for nodal cells or *Idle* for myocardial cells, upstroke depolarization period (UDP), absolute refractory period (ARP) and relative refractory period (RRP). When a given cell is activated (at the end of UDP phase), it sends an output activation signal to neighboring cells.

The slope of the SDD phase in SAN, and thus its SDD period, depends on the HR that results from the BRS model; as well as the output electrical activations of LV and RV are connected to the CVS model by triggering the mechanical contractions of each ventricular chamber. Values for most cell parameters were based on (Hernandez Rodriguez, 2000); however, since BS patients present ECG patterns of right bundle branch block, the RBB automata of these patients were adjusted based on their baseline QRS durations, which were generally enlarged with respect to controls. Specifically, to simulate each patient's ventricular depolarization duration, the UDP phase of these automata was manually modified for each case. However, since no spontaneous Brugada-like patterns were identified during the recordings, ECGs were simulated with normal morphologies.

5.1.3.2. Cardiovascular system

In order to represent the hemodynamic effects of postural changes, the cardiovascular model defined in (Ojeda et al., 2015, 2013; Romero-Ugalde et al., 2015; Smith et al., 2004) was adapted. As illustrated in Figure 5.4 and described in previous models of our team (Le Rolle et al., 2008), both pulmonary and systemic circulations were integrated, dividing the latter into three parallel vascular branches: 1) head or higher parts of the body, 2) hydrostatic indifference

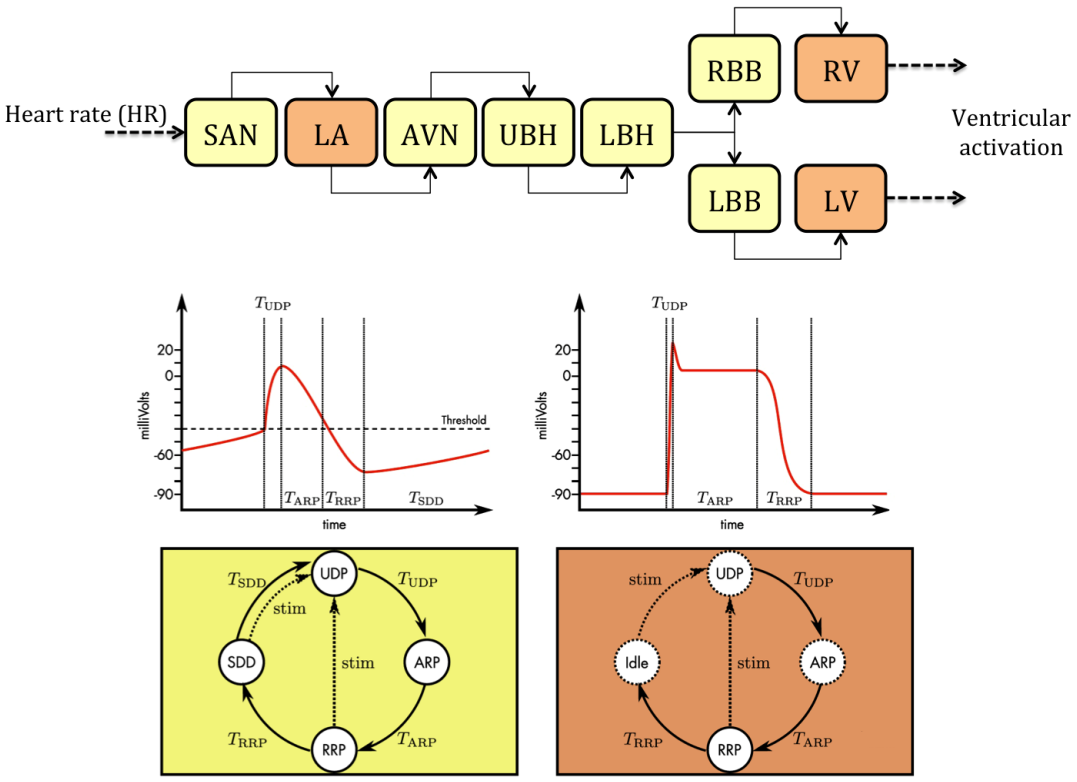

FIGURE 5.3– Diagram of the simplified CES submodel. Top: automata involved on the cardiac electrical system. Yellow boxes represent nodal cell automata and orange boxes, myocardial cells. Bottom: state diagram representing the cycle of a nodal (yellow, left) and a myocardial automaton (orange, right); along with their respective action potential waveforms. Modified from (OJEDA AVELLANEDA, 2013).

point (HIP) or heart level, and 3) legs or lower parts of the body. This subdivision allows to account for differences in heights and, thus, in regulatory mechanisms' impact at each branch, based on its mean distance from the HIP.

For each ventricular chamber, volumes (V) are computed from the integral of their respective net flow ($Q_{in} - Q_{out}$). Blood pressure (P) is then calculated from the pressure-volume relationships associated with systole and diastole: the End Systolic Pressure-Volume Relationship (ESPVR) and the End Diastolic Pressure-Volume Relationship (EDPVR). A periodic function ($e(t)$) drives the transition between the end systolic (P_{es}) and end diastolic (P_{ed}) pressures as follows:

$$P(V,t) = e(t)P_{es}(V) + (1 - e(t))P_{ed}(V)\,, \tag{5.1}$$

$$P_{es}(V) = E_{es} \cdot (V - V_d)\,, \tag{5.2}$$

$$P_{ed}(V) = P_0 \cdot (e^{\lambda(V - V_0)} - 1)\,, \tag{5.3}$$

$$e(t) = A \cdot e^{-B \cdot ((t - t_s) - C)^2}\,. \tag{5.4}$$

In these equations, the end systolic elastance (E_{es}) and the dead volume (V_d), or volume at zero pressure, represent the slope and intercept of the linear relationship between pressure

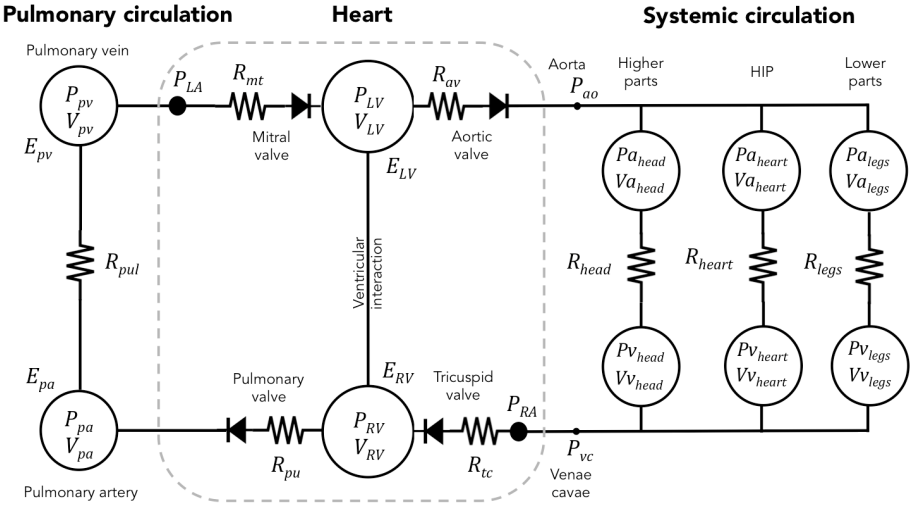

Figure 5.4– Closed-loop model of the cardiovascular system. E: elastance; R: resistance; P: pressure; V: volume; pul: pulmonary; pv: pulmonary vein; pa: pulmonary artery; pu:pulmonary valve; av: aortic valve; ao: aorta; vc: venae cavae; LA: left atrium; LV: left ventricle; RA: right atrium; RV: right ventricle.

and volume during systole. During diastole, this relationship is non-linear and described by a gradient (P_0), curvature (λ) and volume at zero pressure (V_0). The diastolic and systolic dynamics are driven by a Gaussian function (eq. 5.4) described by its amplitude (A), width (B) and center (C). The onset of the cardiac cycle, denoted t_s, is determined by the activation instant of the corresponding chamber in the CES model presented in the previous section.

Atria were not included in the model since they minimally contribute to main cardiac trends. However, in order to account for relevant ventricular interactions, ventricles were coupled through the septum, represented as a flexible common wall between the LV and the RV. The LV free wall volume (V_{LVf}) and the RV free wall volume (V_{RVf}) are defined as:

$$V_{LVf} = V_{LV} - V_{spt}\,, \tag{5.5}$$

$$V_{RVf} = V_{RV} + V_{spt}\,. \tag{5.6}$$

where V_{spt}, V_{LV} and V_{RV} are respectively the septum, LV and RV volumes. Then, the septum volume results from linking the septum pressure (P_{spt}) to the difference between left and right ventricular pressures:

$$P_{spt} = P_{LV} - P_{RV}\,, \tag{5.7}$$

$$P_{spt} = e(t)E_{es,spt} \cdot (V_{spt} - V_{d,spt}) \tag{5.8}$$

$$+(1 - e(t))P_{0,spt}(\exp \lambda(V - V_0) - 1). \tag{5.9}$$

R represents the resistance experienced by blood when passing through blood vessels and valves. Diodes simulate the one-way direction of blood when passing through valves located at

the inlet and exit of ventricles.

Pressures on the peripheral circulation systems are calculated as a linear relationship between their volume and vascular elastance, following eq. 5.2. These pressures are then used to calculate flows between chambers as $Q = \frac{\Delta P}{R}$, where ΔP is the pressure gradient of two chambers and R is the corresponding vascular resistance connecting them.

5.1.3.3. Baroreflex system

Sympathetic and parasympathetic efferent responses to arterial blood pressure regulation were modeled based on (Le Rolle et al., 2008; Ursino et al., 2000). Since arterial baroreceptors are located above the heart level, the input pressure for the BRS model was extracted from the higher systemic compartment. Baroreceptors' dynamics are represented in Figure 5.5 by a first-order transfer function, whose gain and time constant are denoted K_B and T_B.

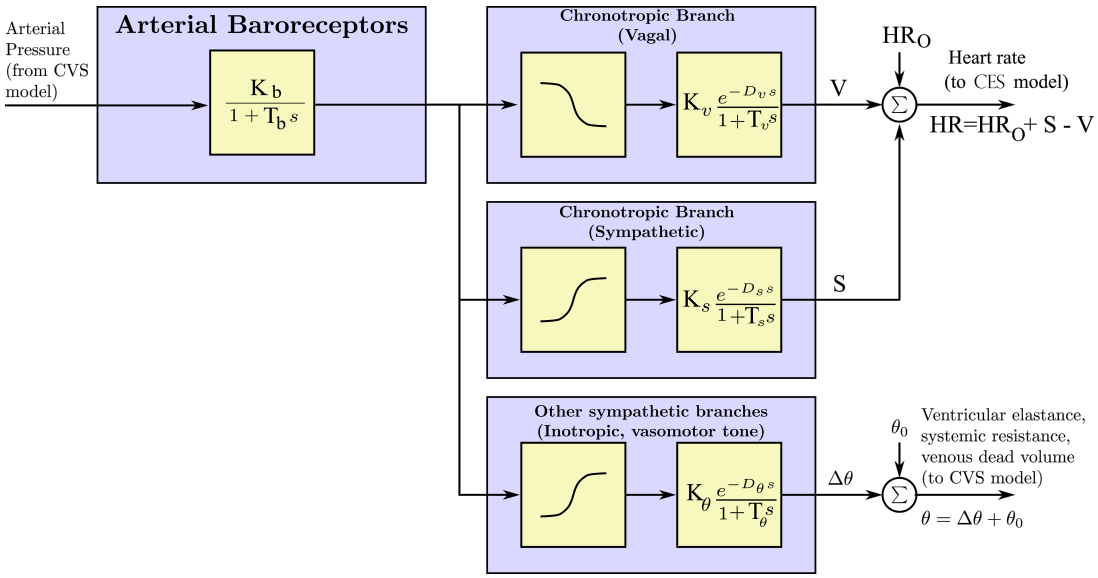

Figure 5.5– Diagram of the BRS model. From the arterial pressure registered at the higher systemic circulation, the baroreflex system regulates heart rate, peripheral resistance, venous volume and heart contractility.

Then, five different efferent pathways control heart rate, peripheric resistance, venous volume and cardiac contractility, and each output is added to the baseline response of each regulated variable.

Chronotropic control is divided in the sympathetic and parasympathetic branches, whereas systemic resistance, venous volume and ventricular elastance are only influenced by the sympathetic system. The same structure, based on a normalization function, a delay and a first-order filter is applied to each efferent pathway. The normalization function is represented by the following sigmoid input-output relationship:

$$F_x(t) = a_x + \frac{b_x}{e^{\lambda_x (P_B(t) - M_x)} + 1} \tag{5.10}$$

where P_B is the arterial baroreceptors' pressure; a_x, b_x, λ_x and M_x are used to adjust the sigmoidal shape; and $x \in \{V, S, R, VV, C\}$ refers to vagal heart rate, sympathetic heart rate, systemic resistance, venous volume and cardiac contractility control, respectively. The same notation was used for the gains (K_x), delays (D_x) and time constants (T_x) describing the first-order transfer functions:

$$\Delta x = K_x \frac{e^{-D_x s}}{1 + T_x s} \tag{5.11}$$

5.1.3.4. Head-up tilt test

Upright posture stimulates blood pressure variations in different body parts. As in (Heldt et al., 2002; Le Rolle et al., 2008), the effect of gravity was implemented at each systemic branch, based on its distance to HIP. Being Pa_k the arterial pressure in supine rest for each systemic branch where $k \in \{head, heart, legs\}$, the arterial pressure at each compartment P_k during tilting is described as:

$$P_k = \begin{cases} Pa_k + Pg_k \cdot sin(\alpha(t)), & t_0 < t < t_{tilt}, \\ Pa_k + Pg_k \cdot sin(\alpha_{max}), & t > t_0 + t_{tilt}. \end{cases} \tag{5.12}$$

Where $\alpha(t)$ is the table angle going from 0 to α_{max}, t_0 is the table inclination onset, t_{tilt} is the time to α_{max} and Pg_k is the pressure due to gravity at each branch, defined as:

$$Pg_k = \rho \cdot g \cdot h_k, \tag{5.13}$$

where ρ is the fluid density, g the gravitational constant and h_k the mean distance between the systemic branch and HIP.

5.1.4. Sensitivity analysis

In order to identify the most influential model parameters on HR and SBP, a two-step sensitivity analysis based on (Hernandez et al., 2011; Le Rolle et al., 2011; Ojeda et al., 2014) was performed. First, by applying the screening method of Morris (Morris, 1991) on parameters coming from the BRS and CVS submodels. A table including the physiological ranges used, based on the litterature (Heldt et al., 2002; Le Rolle et al., 2008; Ursino et al., 2000), is provided in Appendix C. This method not only evaluates non-linearities and interactions between parameters, but it also quantifies each variable's significance with limited computational costs. Hence, it permits excluding unimportant model parameters so as to reduce the dimensionality of subsequent analyses.

Then, to analyze in more detail the source of the variability found in Morris' results, a global sensitivity analysis based on a Sobol approach (Saltelli et al., 2010) was performed. Since the estimation of Sobol's indices requires a significant amount of simulations, only the most relevant parameters after Morris' evaluation were included in the analysis.

5.1.4.1. Screening sensitivity analysis

The sensitivity analysis proposed by Morris consists in the generation of several random trajectories through the parameter space; each trajectory being associated with an estimation of the Elementary Effects EE_{ij} of a parameter x_i on output y_j:

$$EE_{ij} = \left| \frac{y_j(x_1, \cdots, x_i + \Delta, \cdots, x_k) - y_j(x_1, \cdots, x_i, \cdots, x_k)}{\Delta} \right|, \tag{5.14}$$

where $\Delta = \dfrac{p}{2(p-1)}$, p is defined as the number of levels dividing the parameter space Ω and y_j stands for each analyzed model output expressed as a function of k parameters ($y_j = f(x_1, \cdots, x_i, \cdots, x_k)$).

Each trajectory is generated from a value x^*, randomly selected from the p-level grid Ω. Although x^* is not part of the trajectory, it is the base used to generate all the trajectory points, always included in Ω. First, $x^{(1)}$ is obtained increasing one or more components of x^* by Δ. The second trajectory point, $x^{(2)}$, is generated by differing from $x^{(1)}$ in its i^{th} component, being increased or decreased by Δ as follows: $x^{(2)} = x^{(1)} + e_i\Delta$ or $x^{(2)} = x^{(1)} - e_i\Delta$, where i is randomly selected from the set $\{1, 2, \cdots, k\}$. The third sampling point, $x^{(3)}$, is generated by differing from $x^{(2)}$ in only another component i, different from the previously used to generate $x^{(2)}$. It can be either $x^{(3)} = x^{(2)} + e_i\Delta$ or $x^{(3)} = x^{(2)} - e_i\Delta$. And so on, until $x^{(k+1)}$ closes the trajectory. This design produces a trajectory of $(k+1)$ sampling points $\{x^{(1)}, x^{(2)}, \cdots, x^{(k+1)}\}$ where two consecutive points differ in only one component. Figure 5.6 represents an example of trajectory in a space of $k = 3$ parameters.

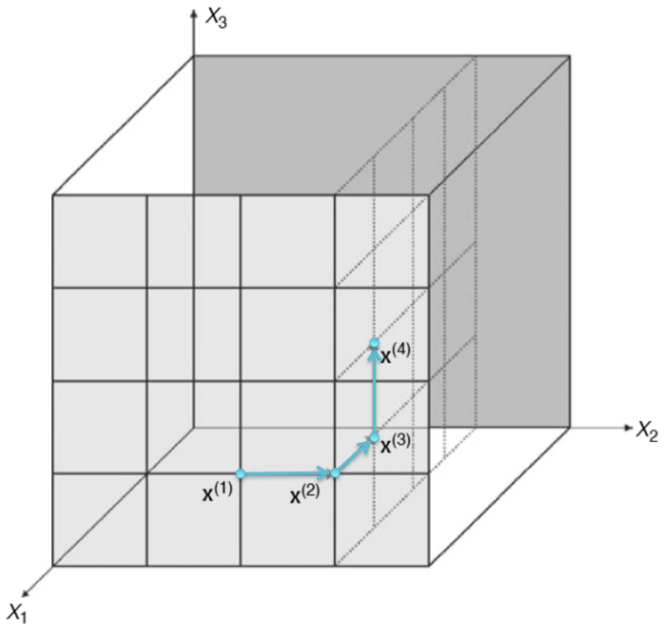

FIGURE 5.6– Exemplifying trajectory in a space of $k = 3$ parameters (SALTELLI et al., 2008).

Globally, trajectories are defined through a matrix $\mathbf{B}^*$ with dimension $(k+1) \times k$, whose rows are composed of the vectors $\mathbf{x}^{(1)}$, $\mathbf{x}^{(2)}$, $\cdots$, $\mathbf{x}^{(k+1)}$ and which is calculated as follows:

$$\mathbf{B}^* = (\mathbf{J}_{k+1,k}\mathbf{x}^* + (\Delta/2)[(2\mathbf{B} - \mathbf{J}_{k+1,k})\mathbf{D}^* + \mathbf{J}_{k+1,k}])\mathbf{P}^* \tag{5.15}$$

$\mathbf{B}$ is a $(k+1) \times k$ matrix formed by 0's and 1's where, for every column $j = 1, \cdots, k$, there are two rows of $\mathbf{B}$ that differ only in the j^{th} entry, as in a strictly lower triangular matrix of 1's. $\mathbf{J}_{k+1,k}$ is a $(k+1) \times k$ matrix of 1's and $\mathbf{x}^*$ are the randomly chosen base values. $\mathbf{D}^*$ is a k-dimensional diagonal matrix in which each element is either +1 or -1 with equal probability, and $\mathbf{P}^*$ refers to a $k \times k$ random permutation matrix in which each row contains one element equal to 1, the rest are 0, and where two columns never have 1's in the same position. $\mathbf{P}^*$ defines the moving order of factors and $\mathbf{D}^*$ determines whether these factors increase or decrease along the trajectory. Finally, $\mathbf{B}^*$ provides the elementary effect of each randomly selected input.

For each combination of parameter x_i and output y_j, the mean μ^*_{ij} and standard deviation σ_{ij} of r elementary effects (EE_{ij}) are calculated. A large value of μ^*_{ij} indicates a significant effect of x_i on y_j, whereas a large σ_{ij} value is related to either non-linear or strongly interacting variables. Thereby, parameters can be classified in negligible (low μ^*_{ij} and σ_{ij}), linear (non-zero $\mu^*_{ij} > \sigma_{ij}$) and non-linear or strongly interacting with other parameters (non-zero $\mu^*_{ij} \leq \sigma_{ij}$), based on their location in the $\mu^* - \sigma$ plane (Figure 5.7A).

Since BP recordings were acquired from the patient's finger positioned next to the legs, the SBP detected at the lower systemic compartment (CVS model), as well as the HR resulting from the BRS submodel were analyzed as model outputs. Thus, elementary effects were evaluated on the mean HR and on the mean SBP, in supine and upright postures as cardiac signals present different behaviors for each postural status: $y \in \{HR_{supine}, SBP_{supine}, HR_{tilt}, SBP_{tilt}\}$.

In order to establish a global rank of importance among parameters, the Euclidean distance in the $\mu^* - \sigma$ plane, D_{ij}, from the origin to each (μ^*_{ij}, σ_{ij}) point was calculated as:

$$D_{ij} = \sqrt{(\mu^*_{ij})^2 + \sigma^2_{ij}}, \tag{5.16}$$

being parameters with high sensitivity or strong interactions those presenting the highest values for D_{ij}. Thus, as illustrated in Figure 5.7B, model parameters were sorted according to their D_{ij} value.

5.1.4.2. Global sensitivity analysis

The variance-based global sensitivity analysis approach first introduced by Sobol (Sobol, 2001) quantifies the uncertainty of output y explained by the variability of each parameter x_i. Sobol defined the *first-order effect*, or *main effect*, as the influence of varying x_i on the output y:

$$S_i = \frac{Var[\mathbb{E}[y|x_i]]}{Var[y]}, \tag{5.17}$$

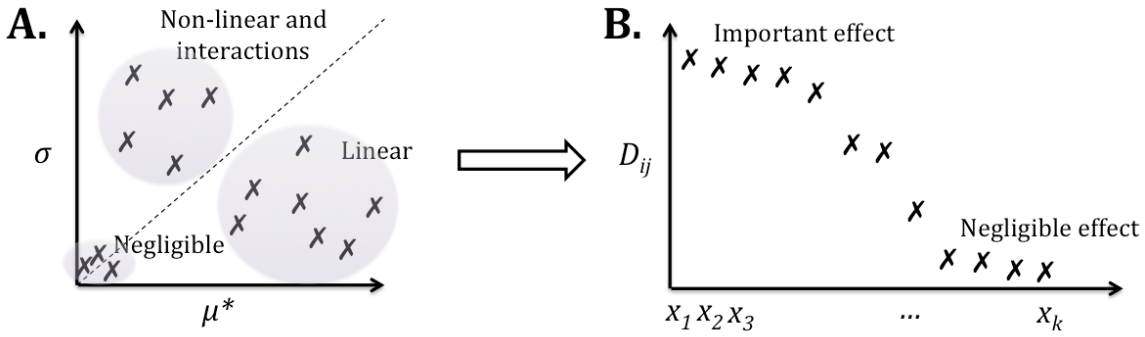

FIGURE 5.7– A) Exemplifying elementary effects results. From the mean and standard deviation of their elementary effects, parameters are classified in having negligible, linear or non-linear effects on model outputs. B) Parameters' relevance quantification, ranked according to D_{ij} indices.

Similarly, higher-order effects are defined as the impact of variations in two or more parameters. Based on variance decomposition, since all effects are strictly positive and the sum of all of them is equal to 1, each effect is within [0,1].

$$\sum_i S_i + \sum_i \sum_{i<j} S_{ij} + \sum_i \sum_{i<j} \sum_{j<l} S_{ijl} + \cdots = 1. \tag{5.18}$$

However, due to the great number of possible combinations introduced by higher-order effects, Saltelli (SALTELLI et al., 2010) proposed a simpler approach, where only the main and total indices are calculated, whereas all higher-order effects are grouped in the *total-order effect*:

$$ST_i = S_i + \sum_{i \neq j} S_{ij} + \sum_{i \neq j \neq l} S_{ijl} + \cdots + S_{123\ldots k} = 1. \tag{5.19}$$

By means of Sobol's main and total indices, the amount of variability explained by each parameter alone (S_i) and by the interaction of such parameter with the others (ST_i) was quantified, on the mean HR and SBP in supine and upright postures. Since these indices are computationally expensive to calculate, 10^6 Monte-Carlo evaluations of quasi-random parameter configurations, designed using a Latin Hypercube Sampling (LHS) approach (MCKAY et al., 1979), were computed.

LHS is a statistical method for generating near-random samples of parameter values from a multidimensional distribution. A square grid is known as a Latin square if, and only if, contains only one sample in each row and each column. Thus, a Latin hypercube is the generalisation of this concept to an arbitrary number of dimensions, whereby each sample is the only one in each axis-aligned hyperplane containing it. By avoiding the probability that all sampling points come from the same local region, this method allows to obtain a stable output with a much smaller number of samples than simple Monte Carlo simulation. However, even with LHS, Monte Carlo analysis requires a great amount of sampling points.

Thus, to reduce the computational cost of estimating variances for the calculation of S_i and ST_i indices, the following strategy, described in (Saltelli et al., 2008), was performed:

1. First, a $N \times 2k$ matrix of quasi-random numbers, based on LHS, where k is the number of parameters, was generated to define the data matrices $\mathbf{A}$ and $\mathbf{B}$, each containing half of the sample. N defines the number of performed simulations.

$$\mathbf{A} = \begin{bmatrix} x_1^{(1)} & x_2^{(1)} & \cdots & x_i^{(1)} & \cdots & x_k^{(1)} \\ x_1^{(2)} & x_2^{(2)} & \cdots & x_i^{(2)} & \cdots & x_k^{(2)} \\ \cdots & \cdots & \cdots & \cdots & \cdots & \cdots \\ x_1^{(N-1)} & x_2^{(N-1)} & \cdots & x_i^{(N-1)} & \cdots & x_k^{(N-1)} \\ x_1^{(N)} & x_2^{(N)} & \cdots & x_i^{(N)} & \cdots & x_k^{(N)} \end{bmatrix} \tag{5.20}$$

$$\mathbf{B} = \begin{bmatrix} x_{k+1}^{(1)} & x_{k+2}^{(1)} & \cdots & x_{k+i}^{(1)} & \cdots & x_{2k}^{(1)} \\ x_{k+1}^{(2)} & x_{k+2}^{(2)} & \cdots & x_{k+i}^{(2)} & \cdots & x_{2k}^{(2)} \\ \cdots & \cdots & \cdots & \cdots & \cdots & \cdots \\ x_{k+1}^{(N-1)} & x_{k+2}^{(N-1)} & \cdots & x_{k+i}^{(N-1)} & \cdots & x_{2k}^{(N-1)} \\ x_{k+1}^{(N)} & x_{k+2}^{(N)} & \cdots & x_{k+i}^{(N)} & \cdots & x_{2k}^{(N)} \end{bmatrix} \tag{5.21}$$

2. Then, a matrix formed by all columns of $\mathbf{B}$ except for the i^{th} column which was taken from $\mathbf{A}$, was defined as $\mathbf{C}_i$:

$$\mathbf{C}_i = \begin{bmatrix} x_{k+1}^{(1)} & x_{k+2}^{(1)} & \cdots & x_i^{(1)} & \cdots & x_{2k}^{(1)} \\ x_{k+1}^{(2)} & x_{k+2}^{(2)} & \cdots & x_i^{(2)} & \cdots & x_{2k}^{(2)} \\ \cdots & \cdots & \cdots & \cdots & \cdots & \cdots \\ x_{k+1}^{(N-1)} & x_{k+2}^{(N-1)} & \cdots & x_i^{(N-1)} & \cdots & x_{2k}^{(N-1)} \\ x_{k+1}^{(N)} & x_{k+2}^{(N)} & \cdots & x_i^{(N)} & \cdots & x_{2k}^{(N)} \end{bmatrix} \tag{5.22}$$

3. Model outputs were then computed for all the input values in matrices $\mathbf{A}$, $\mathbf{B}$ and $\mathbf{C}_i$, obtaining the following three vectors of model outputs of length N:

$$y_A = f(\mathbf{A}) \qquad y_B = f(\mathbf{B}) \qquad y_{C_i} = f(\mathbf{C}_i) \tag{5.23}$$

   The cost of this approach is N model simulations for matrix $\mathbf{A}$, plus N runs for matrix $\mathbf{B}$, plus k times N to estimate the k output vectors coming from matrix $\mathbf{C}_i$. The total cost is, thus, $N(k+2)$, much lower than the N^2 simulations needed in the brute-force method.

4. First-order sensitivity indices are then estimated as follows:

$$S_i = \frac{Var[\mathbb{E}[y|x_i]]}{Var[y]} = \frac{y_A \cdot y_{C_i} - f_0^2}{y_A \cdot y_A - f_0^2} = \frac{(1/N)\sum_{j=1}^{N} y_A^{(j)} y_{C_i}^{(j)} - f_0^2}{(1/N)\sum_{j=1}^{N} (y_A^{(j)})^2 - f_0^2} \tag{5.24}$$

where f_0^2 is calculated as:

$$f_0^2 = \left(\frac{1}{N} \sum_{j=1}^{N} y_A^{(j)} \right)^2 \tag{5.25}$$

5. Finally, total-order indices are estimated as:

$$S_{T_i} = 1 - \frac{Var[\mathbb{E}[y|x_{\ i}]]}{Var[y]} = 1 - \frac{y_B \cdot y_{C_i} - f_0^2}{y_A \cdot y_A - f_0^2} = 1 - \frac{(1/N)\sum_{j=1}^{N} y_B^{(j)} y_{C_i}^{(j)} - f_0^2}{(1/N)\sum_{j=1}^{N} (y_A^{(j)})^2 - f_0^2} \tag{5.26}$$

5.1.5. Parameter identification

Based on sensitivity results, a reduced group of parameters were selected for subject-specific model identification. The optimization process was computed by comparing experimental signals acquired during HUT testing with simulation outputs, through the minimization of the error function ϵ, defined as:

$$\epsilon(\theta) = \sum_{j=1}^{4} \sum_{i=1}^{N_j} \left| \frac{Y_{sim,\theta}^j(i) - Y_{exp}^j(i)}{max(Y_{exp}^j(i))} \right|^2 \tag{5.27}$$

$Y_{exp}^j(i)$ and $Y_{sim,\theta}^j(i)$ are the i^{th} experimental value and the i^{th} model output sample for the simulation of Y^j when using the set of parameters θ, respectively. Moreover, N_j indicates the number of samples for each output being compared and Y^j refers to HR and SBP signals for the whole test and only during the transition of table inclination: $Y \in \{SBP_{total}, SBP_{transition}, HR_{total}, HR_{transition}\}$. Note that identification is based on both HR and SBP signals, and mainly on their transitory periods since they are accounted twice to ensure that errors in this segment are particularly penalized. Transitory periods in SBP and HR signals are specially relevant since they respectively reflect the cardiovascular and autonomic responses to postural change.

As in previous works of our team (Le Rolle et al., 2015, 2011; Ojeda et al., 2014), the best set of parameters for each subject were identified through an approach based on evolutionary algorithms (EA). These stochastic search methods are founded on theories of natural evolution, such as selection, crossover and mutation (Goldberg et al., 1988). Being an individual an optimization solution (a parameter value set), the algorithm started with the initialization of 50 random individuals, each parameter value of the individual being randomly selected from a specified parameter space. By quantifying each individual fitness through the error function ϵ, the population was continuously evolved for 30 generations, following four main steps:

1. Selection of parent individuals for combination, biased towards those having the best errors.

2. According to a probability p_c, combination of parent individuals through crossover to generate new children. Then, with a probability p_m, modification of these individuals by mutations.

3. Fitness assessment in new individuals.

4. Replacement of individuals having the lowest fitness.

5.1.6. Results and discussion

5.1.6.1. Sensitivity analysis

As in (Le Rolle et al., 2011), the screening method of Morris was applied with a grid of $p = 20$ and $r = 5 \cdot k = 310$ elementary effects, performing a total of almost 20,000 simulations. Figure 5.8 represents Morris sensitivity results on the mean SBP and HR signals for supine and tilt phases, only labeling the most relevant parameters in order to improve readability.

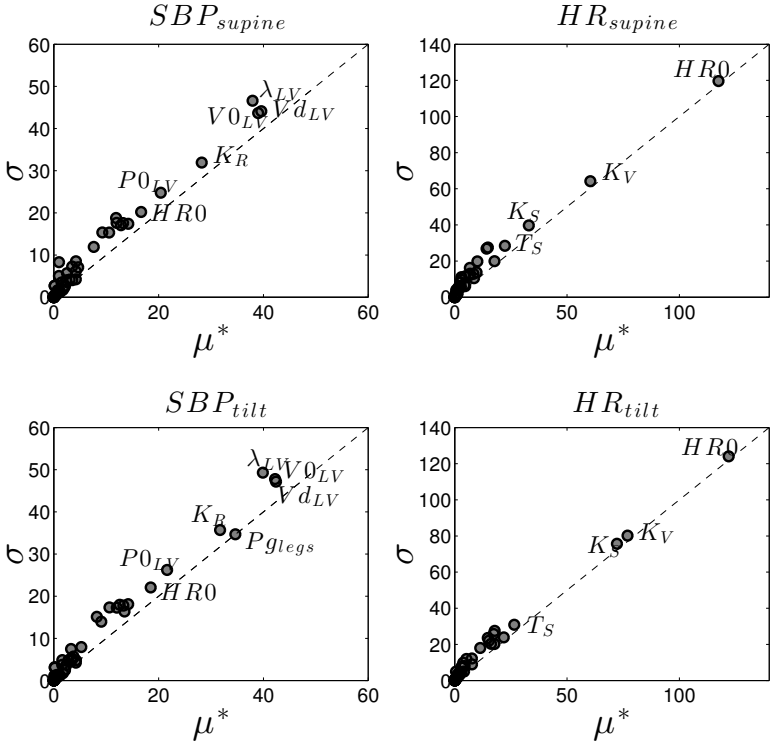

Figure 5.8– Absolute mean (μ^*) and standard deviation (σ) of the elementary effects for the mean SBP and HR, during supine and tilt phases. Only the most significant parameters are labeled: λ_{LV} (LV end-diastolic exponent), Vd_{LV} (LV volume at zero end-systolic pressure), $V0_{LV}$ (LV volume at zero end-diastolic pressure), K_R (gain for peripheral resistance regulation), $P0_{LV}$ (intrinsic LV pressure), $HR0$ (intrinsic heart rate), K_V (gain of the vagal HR regulation), K_S (sympathetic gain), T_S (sympathetic time constant), and Pg_{legs} (pressure due to gravity at the lower systemic compartment).

Overall, the distribution of model parameters in the $\mu^* - \sigma$ space indicates effects on HR and SBP that are either non-linear or caused by the interaction with other parameters. Although some of them are close to the $\mu^* = \sigma$ reference line, Pg_{legs} was the most linearly related parameter to SBP_{tilt}.

Nevertheless, many parameters showed a significant effect on the analyzed outputs. In order to identify those variables having the highest sensitivities or the strongest interactions, Figure 5.9 displays the 15 most influential parameters on each analyzed output based on their D_i index, represented along with their μ_i^* and σ_i values.

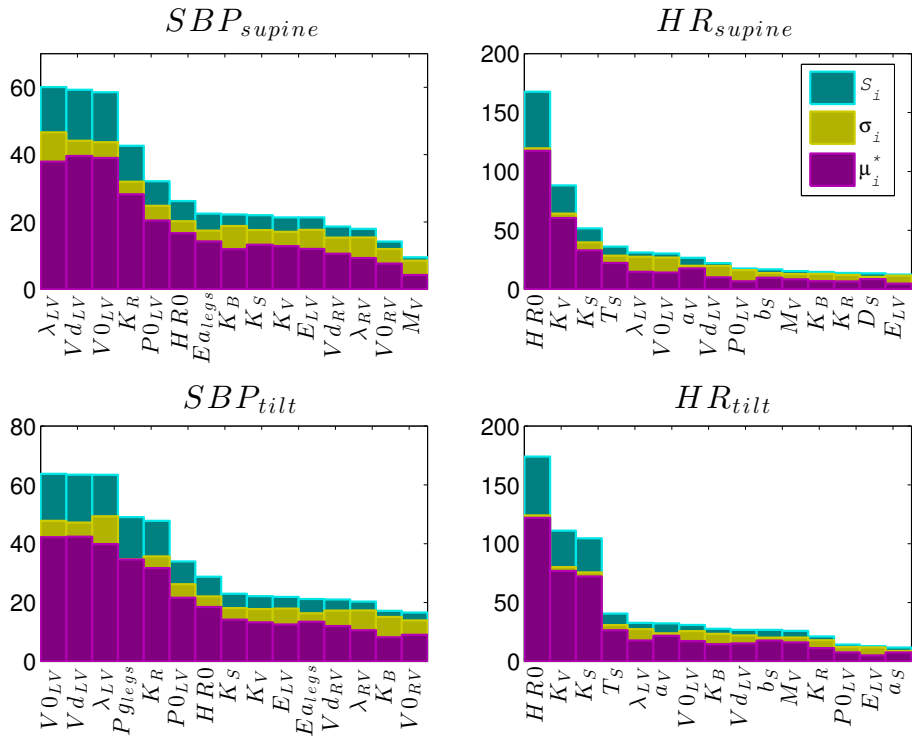

FIGURE 5.9– Most influential parameters on HR and SBP in supine and upright postures, based on the Morris distance D_i (green bars). For each parameter, the absolute mean μ_i^* (purple bars) and the standard deviation σ_i (yellow bars) of the elementary effects are also displayed.

Similar results were obtained for supine and upright postures. Regarding SBP, the main difference concerned Pg_{legs}, being negligible in supine rest but turning into a significant parameter during tilting. Concerning HR, the most influential variables in supine remained the same during tilting. However, K_S gained importance with respect to supine rest, probably due to the sympathetic activation caused by postural change.

As expected, HR was mostly modulated by BRS variables, whereas SBP was more affected by CVS parameters coming from the LV. However, the effect of some RV variables was still considerable. This may be relevant in BS, where patients present ECG patterns of RBBB. Indeed, the model defines that RV parameters can affect LV through the septum wall, as well as through the closed-loop circulation.

Table 5.2 specifies those parameters retained for further analysis. Although they were mainly selected based on Morris' results, M_S was also added in order to evaluate the M_V complementary parameter, since it could be relevant during the sympathetic activation stimulated by postural change. Likewise, K_C was included so as to analyze the effect of HUT testing in heart contractility

regulation and, although RV parameters were not as significant as those coming from the LV, λ_{RV} was also included in the analysis.

Table 5.2– Parameters selected for global sensitivity analysis.

	Parameter description	**Submodel**
λ_{LV}	LV end-diastolic exponent	CVS
Vd_{LV}	LV volume at zero end-systolic pressure	CVS
$V0_{LV}$	LV volume at zero end-diastolic pressure	CVS
K_R	Gain for peripheral resistance regulation	BRS
$P0_{LV}$	intrinsic LV pressure	CVS
$HR0$	Intrinsic heart rate	BRS
$Eart_{legs}$	Arterial elastance under HIP	CVS
K_B	Baroreceptors gain	BRS
K_S	Gain of the sympathetic HR regulation	BRS
K_V	Vagal gain	BRS
E_{LV}	LV elastance	BRS
T_S	Sympathetic time constant	BRS
a_V	Vagal normalization independent term	BRS
b_S	Sympathetic normalization gain	BRS
M_V	Vagal normalization center	BRS
Pg_{legs}	Pressure due to gravity under HIP	CVS
M_S	Sympathetic normalization center	BRS
K_C	Contractility gain	BRS
λ_{RV}	RV end-diastolic exponent	CVS

Regarding global sensitivity analysis, since results were similar to those found in Morris analysis, in order to identify those parameters causing the greatest changes between supine and upright postures, not only the mean HR and SBP in supine rest, but also the Sobol indices on the percentage ratio between supine and upright postures were analyzed: $\%HR, \%SBP$. Figure 5.10 shows the estimated Sobol's main and total indices for the analyzed outputs.

According to the results, SBP showed a significant dependence on λ_{LV}, $V0_{LV}$ and Vd_{LV}, whereas HR was mostly modulated by $HR0$, K_V and K_S. Moreover, these parameters not only presented the highest total effects, but also the greatest main effects, suggesting that a non-negligible part of their effect is due to the parameter variation itself.

Thus, HR was found to be further affected by autonomic parameters than by CVS variables; particularly, by intrinsic HR and baroreflex gains modulating the sympathetic and parasympathetic chronotropic branches, the ANS component responsible for regulating HR. Since BP and HR are closely connected through the baroreflex arc, SBP was also significantly affected by these autonomic variables. However, results seem to indicate that SBP is primarily affected by those parameters modulating diastole in the left ventricle.

Although $HR0$ demonstrated high sensitivities in both Morris and Sobol analyses, in order to reduce computational cost, it was not included in the identification process. In exchange, $HR0$

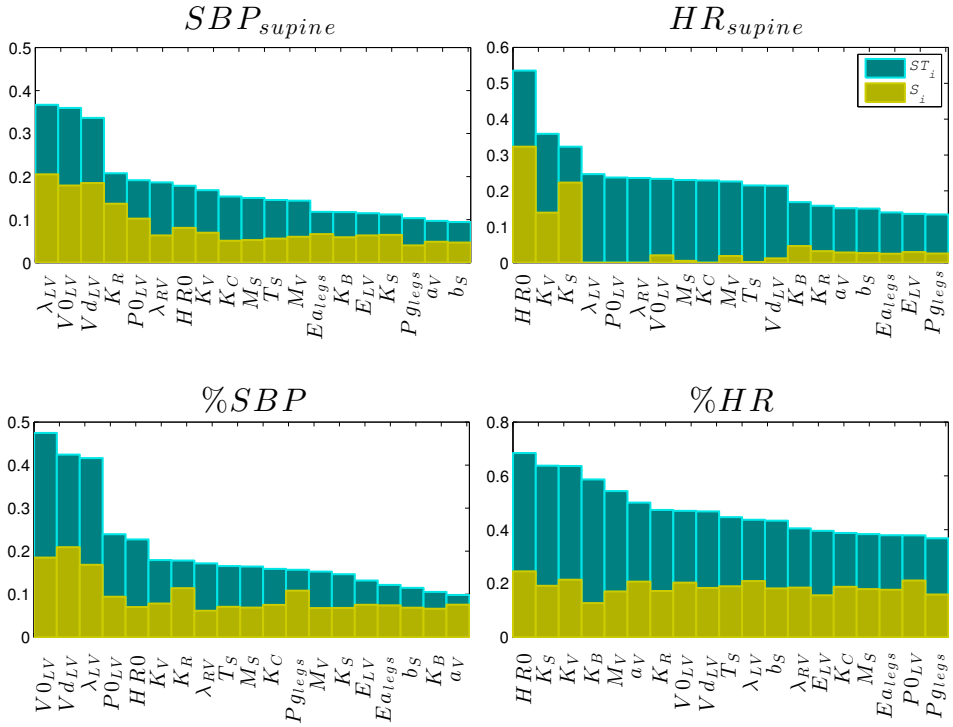

FIGURE 5.10– Results for global sensitivity analysis based on Sobol indices for mean SBP and HR values in supine rest and for the percentage ratio between the mean at supine and tilting positions. Yellow bars indicate first-order effects S_i (sensitivity to parameter variations alone) and green bars indicate total-order effects ST_i (sensitivity to parameter interactions). The parameters are sorted in descending ST_i values.

was estimated for each participant as the mean HR in supine position. Likewise, all normalization centers in the BRS model (M_V, M_S, M_R, M_C, M_{VV}) were estimated as the mean SBP in supine rest, and only one LV zero-pressure volume was identified, assuming $V0_{LV} = Vd_{LV}$.

K_S and K_V were identified for each subject, and due to their non-negligible importance in Sobol's results, λ_{RV}, K_R and K_C were also added to the identification process. Moreover, since Pg_{legs} demonstrated a rather linear effect on SBP_{tilt}, proved by the elevated main index in Sobol analysis for $\%SBP$, this parameter was also included in the estimation step. Finally, since it was experimentally remarked that better estimations of the rebounds caused by postural change were obtained by identifying the sympathetic and vagal time constants, T_S and T_V estimations were added. Similarly, higher and lower systemic time constants (τ_{head} and τ_{legs}) were included to better estimate the progressive adaptation of systemic circulation.

5.1.6.2. Parameter identification

Figure 5.11 displays representative examples of fit between simulated and experimental SBP and HR signals for a control (C1), a symptomatic (S1) and an asymptomatic (A1) BS patient.

In Figure 5.12, boxplots of the resulting parameters for the control (C), asymptomatic (A) and symptomatic (S) groups are represented.

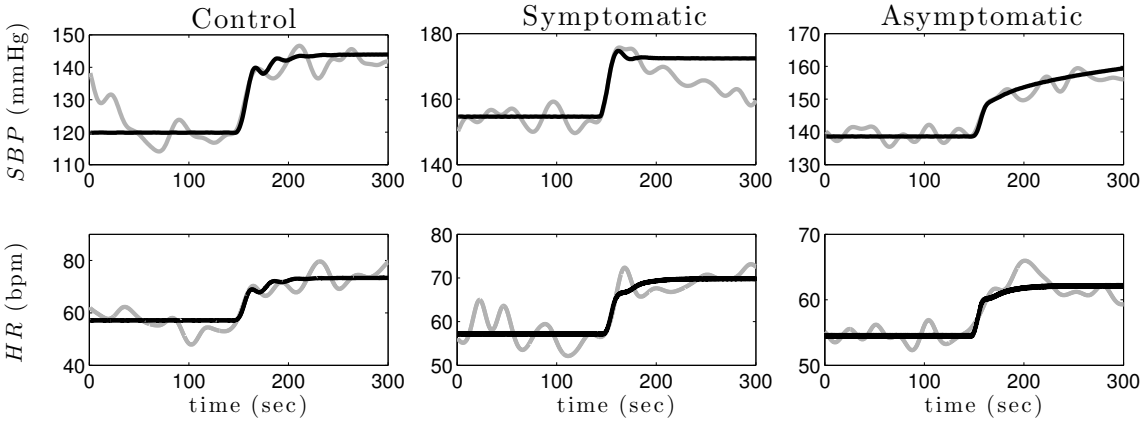

FIGURE 5.11– Representative examples of fit between simulated (black) and experimental (grey) SBP and HR signals for a control, a symptomatic and an asymptomatic BS patients.

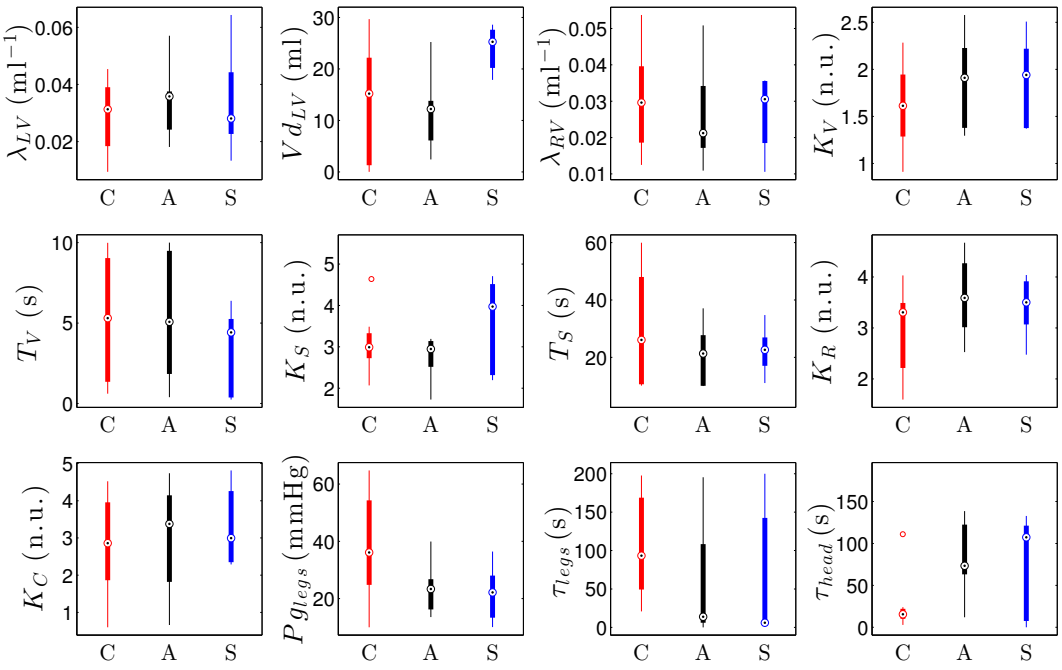

FIGURE 5.12– Boxplots of identified parameters; for controls (C), asymptomatic (A) and symptomatic (S) groups.

Table 5.3 includes the percentage errors of SBP and HR (E_{SBP}, E_{HR}) for each subject. Based on visual inspection and resulting errors ($E_{SBP} = 2.90 \pm 1.63$ %; $E_{HR} = 3.39 \pm 1.00$ %), an acceptable agreement between observed and estimated signals was noted; specially during transitory periods, which demonstrates the capability of the model to reproduce HR and SBP

adaptations to HUT testing. Although some small variations coming from exogenous phenomena, such as temperature, respiration or the central nervous system, could not be simulated, the degree of similarity between signals was significant.

TABLE 5.3– Percentage errors in SBP and HR, for controls (C), symptomatic (S) and asymptomatic (A) BS patients.

	E_{SBP} (%)	E_{HR} (%)
C1	2.46	4.51
C2	5.13	3.51
C3	1.69	2.49
C4	1.98	5.17
C5	1.93	3.70
C6	3.31	3.00
C7	8.37	4.04
C8	3.61	3.32
S1	2.70	3.50
S2	4.15	5.63
S3	2.91	2.56
S4	3.67	2.40
S5	1.68	2.91
A1	1.15	2.02
A2	2.60	3.38
A3	3.22	3.22
A4	1.96	4.77
A5	1.59	2.23
A6	2.06	3.02
A7	1.87	2.49

In addition to identified parameters, the dynamical properties of baroreflex responses to HUT were also assessed and compared between groups. Defining the sympathetic HR regulation difference from baseline as $\Delta S = S_{tilt} - S_{supine}$, we found statistically significant differences between controls and BS patients. Likewise, Vd_{LV}, and thus $V0_{LV}$, were significantly different between symptomatic and asymptomatic patients. Table 5.4 summarizes the mean $\pm$ standard deviation values for each group, as well as the associated p-values.

Vd_{LV} refers to the blood volume at zero pressure, included in the linear relationship between the LV end-systolic pressure and volume. Likewise, since $Vd_{LV} = V0_{LV}$, it also represents the blood volume at zero pressure in the non-linear relationship between the LV end-diastolic pressure and volume. Thus, based on the results of the passive mechanics captured by Vd_{LV} and $V0_{LV}$, symptomatic patients presented significantly higher values of LV volumes at zero pressure than asymptomatic patients. This shifts arterial elastance, end-systolic and end-diastolic relationships describing the pressure-volume (PV) loop to the right; leading to reduced stroke works (SW), measured as the area enclosed by the PV loop. Due to higher Vd_{LV} values, the

Table 5.4– Mean ± standard deviation and p-values for statistically significant variables, for a $p < 0.05$ using Mann-Whitney U tests.

	Controls (n=8)	**BS patients** (n=12)	p-**value**
ΔS	0.19 ± 0.04	0.13 ± 0.06	0.019
	Symptomatic (n=5)	**Asymptomatic** (n=7)	p-**value**
Vd_{LV}	24.00 ± 4.48	11.47 ± 7.46	0.010

cardiac PV cycle is shortened, suggesting a decreased inotropy and an increased compliance in symptomatic patients. Figure 5.13 illustrates changes in the PV loop (and in the SW as the area enclosed) when Vd is increased. Since SW quantifies contractility, the results may suggest a reduced LV pumping function in symptomatic patients.

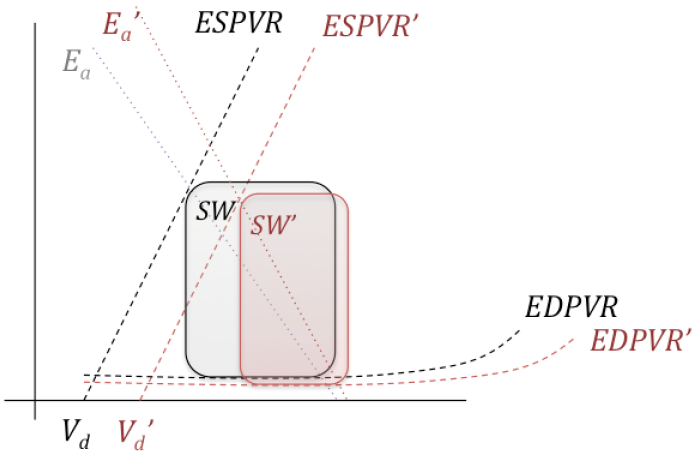

Figure 5.13– PV loop changes (in red) after an increase in blood volume at zero pressure Vd. Ea refers to the arterial elastance, $ESPVR$ and $EDPVR$ are the end-systolic and end-diastolic PV relationships and SW accounts for the stroke work.

Regarding ΔS, BS patients presented a decreased sympathetic HR regulation difference from baseline in relation to healthy subjects. The results are in line with previous studies where sympathetic dysfunctions have been reported in BS patients (Kies et al., 2004; Paul et al., 2011; Wichter et al., 2002). Moreover, the study of (Nakazawa et al., 2003) analyzed the 24-hour autonomic properties of 27 BS patients and 26 healthy subjects, finding higher vagal and reduced sympathetic tones in symptomatic BS patients.

5.2. Recursive model identification of the time-varying autonomic response to exercise

The system-level model proposed in the previous section can only explain the mechanical, circulatory and autonomic sympathetic functions of the cardiovascular system. To tackle this limitation, recursive identifications can simulate the high-frequency oscillations representing the parasympathetic regulation of the ANS. Therefore, in this section, a recursive identification is applied to a simplified version of the previous model in order to estimate the time-varying sympathetic and parasympathetic responses to exertion and subsequent recovery in 44 BS patients.

5.2.1. Experimental data description

Patients' age ranged from 19 to 74 years old (45.07 ± 12.59 years old) and 33 (75%) were males. Thirteen patients had the following documented symptoms: syncope (61.5%), cardiac arrest (38.5%) and dizziness (15.4%). ICD implantation had been performed in 6 of 31 (19.4%) asymptomatic patients, based on a positive EPS test, whereas all symptomatic patients were ICD carriers. Among 31 patients (11 were symptomatic) in whom genetic screening was performed, an *SCN5A* mutation was found in 13 (41.9%), from whom 6 were symptomatic. Table 5.5 summarizes participants' baseline characteristics.

TABLE 5.5– Patients' baseline characteristics.

	Symptomatic (n=13)	**Asymptomatic (n=31)**	***p*-value**
Age, *years old*	43.62 ± 14.51	45.68 ± 11.90	0.322
Male sex, *n (%)*	11 (84.6%)	22 (71%)	0.355
ICD implantation, *n (%)*	13 (100%)	6 (19.4%)	<0.001
Presence of *SCN5A* mutation, *n (%)*	6 (46.2%)	5 (25%)	0.311

Values are mean ± standard deviation or number of observations (%).
All between-groups differences, apart from ICD implantation, are statistically non-significant.

5.2.2. Computational model

Since exertion and post-exercise recovery equivalently influence all body parts, mainly affecting the heart rate, a simplified version of the model proposed in Section 5.1 was implemented. Although it is composed of the same CES submodel, CVS is modeled as in Section 5.1.3.2, but with only one systemic branch, as illustrated in Figure 5.14. Moreover, the baroreflex model, represented in Figure 5.15, only includes chronotropic regulation, adding 2 new time-varying parameters: Z_V and Z_S.

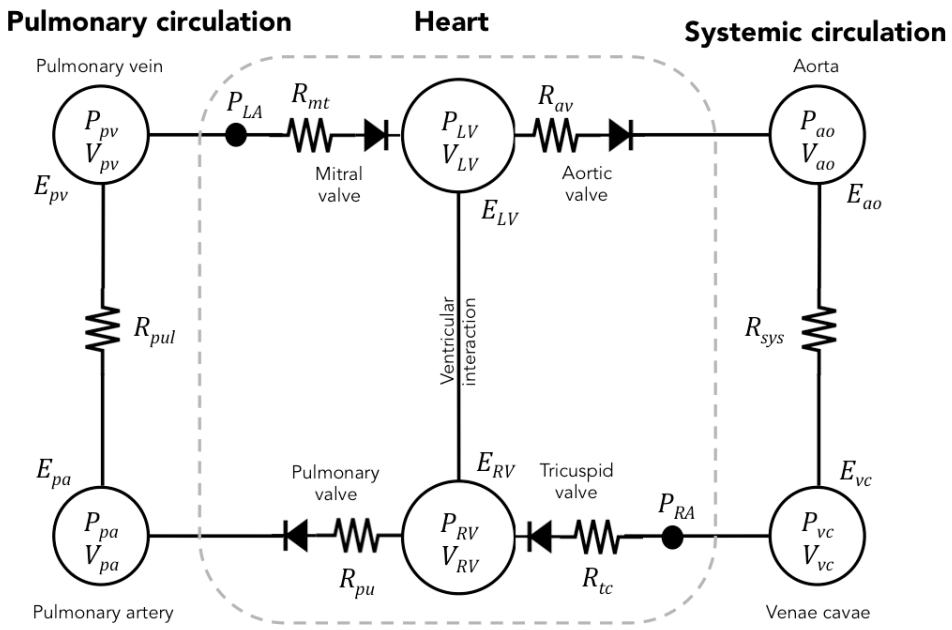

Figure 5.14– Closed-loop model of the simplified cardiovascular system. E: elastance; R: resistance; P: pressure; V: volume; pul: pulmonary; pv: pulmonary vein; pa: pulmonary artery; pu:pulmonary valve; av: aortic valve; ao: aorta; vc: venae cavae; LA: left atrium; LV: left ventricle; RA: right atrium; RV: right ventricle.

As in Section 5.1.3.3, CVS and BRS models are coupled by the systemic arterial pressure. Then, baroreceptors' dynamical properties are represented by a first-order filter, whose gain and time constant are K_B and T_B. The cardiovascular control center is simulated in both sympathetic and vagal branches by a sigmoidal function and delays D_S and D_V, respectively.

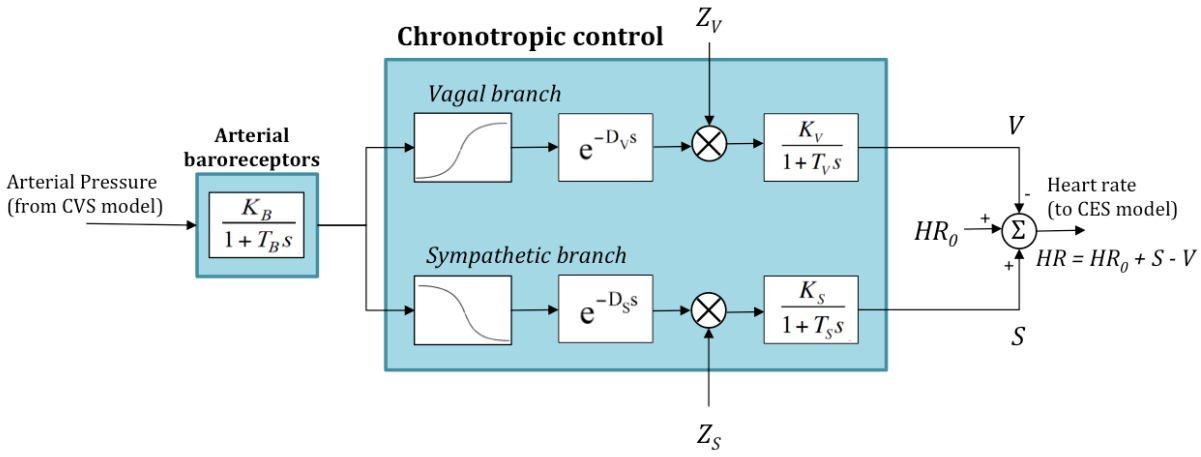

Figure 5.15– Diagram of the baroreflex model for chronotropic regulaton. From the arterial pressure registered at the systemic circulation, the baroreflex system controls heart rate.

Sympathetic and parasympathetic contributions are modulated by two time-varying variables, $Z_S(t)$ and $Z_V(t)$, to account for the influence of exogenous phenomena, such as different brain structures, on both autonomic pathways. Indeed, these two variables collect all the variability caused by sources other than blood pressure fluctuations.

Each efferent pathway is finally modeled with a first-order filter, characterized by a gain (K_V, K_S) and a time constant (T_V, T_S). The output heart rate is the result of adding the contributions of both sympathetic (S) and vagal (V) branches to an intrinsic heart rate (HR_0):

$$HR = HR_0 + S - V \tag{5.28}$$

5.2.3. Recursive identification

All model parameters other than Z_S and Z_V were fixed based on values reported in the litterature (Hernandez Rodriguez, 2000; Le Rolle et al., 2008; Smith et al., 2004). In the recursive identification process, at each step i of the algorithm, parameters Z_S and Z_V were identified on a time interval T_I of duration largely inferior to the RR series length ($T_I << T_{TOT}$). Simulated and experimental signals were compared in order to minimize the error function ϵ_{RR}:

$$\epsilon_{RR}(i) = \sum_{t_e=iT_L}^{(i+1)T_L} |RR_{sim}(t_e) - RR_{exp}(t_e)| + \sum_{t_e=iT_L}^{iT_L+T_I} |RR_{sim}(t_e) - RR_{exp}(t_e)|, \quad i \in [0, \cdots, N] \tag{5.29}$$

where t_e is the time elapsed since the onset of the identification period, T_L corresponds to the overlap time between each interval and $N = \lfloor T_{TOT}/T_L \rfloor$ is the number of identification intervals. Figure 5.16 illustrates the time windows involved in the recursive identification algorithm.

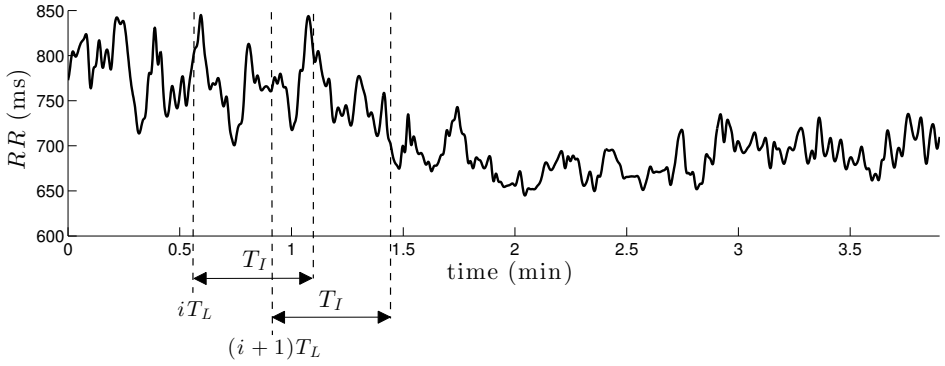

Figure 5.16– Representative time windows involved in the recursive identification of RR series. T_L: overlap window; T_I: identification window.

The overlap time duration T_L was set equal to the parasympathetic time constant (T_V) to capture rapid fluctuations due to the vagal response; whereas interval T_I was set as the sympathetic time constant (T_S) in order to take into account the low frequency component causing RR series slow variations.

The error function was minimized on each interval i through the approach based on evolutionary algorithms described in Section 5.1.5. The initial population, or first set of candidate optimization solutions, was randomly generated. For the following steps, assuming limited parameter variations between intervals, the initial population was set equal to that obtained from the previous interval $i-1$. Although this approach limits parameter variations, mutation probability was set to $p_m = 0.2$ in order to stimulate the exploration of the entire search space and prevent from convergence to local minima.

These recursive identifications were separately performed during exercise and recovery. Since each patient's test differed in the incremental exercise phase duration and the shortest case in our clinical series lasted less than 5 minutes, for exercise analysis, only the warm-up phase and the first 3 minutes of incremental exertion were identified. Moreover, for recovery analysis, the last minute of exertion and the first 3 minutes of recovery, were assessed.

In order to quantify identification performance, the error between simulated and experimental RR series for both exercise and recovery phases was expressed in percentage and computed as:

$$E = \frac{1}{n}\sum_{i=1}^{n} |100 \cdot \frac{RR_{sim}(i) - RR_{exp}(i)}{RR_{exp}(i)}| \tag{5.30}$$

where n is the number of samples being compared. Due to identification errors caused by initialization, the first minute of warm-up was removed from exercise analysis, as well as the first 30 seconds of the last minute of exertion were removed from recovery analysis.

The identified time-varying sympathetic and parasympathetic contributions to exercise and recovery were then compared between symptomatic and asymptomatic patients, by Mann-Whitney U non-parametric tests. In order to compare the last minute of exertion and recovery, all patients had to be synchronized with respect to the peak effort instant.

5.2.4. Results and discussion

Figure 5.17 illustrates an example of simulated and experimental RR series during exercise. Based on visual inspection and error results ($E_{exercise} = 1.10 \pm 0.54\%$, $E_{recovery} = 0.52 \pm 0.16\%$), a satisfactory agreement was observed between simulated signals and real data, leading to errors always inferior to 3.5%.

Figure 5.18 shows the mean vagal and sympathetic contributions of the autonomic response to exertion, for symptomatic and asymptomatic patients. In both groups, vagal tone remained low along the whole exercise phase and decreased as the test progressed. Conversely, sympathetic tone increased during exercise, and specially after warm-up. Moreover, symptomatic patients presented significantly higher parasympathetic values around the second minute of incremental exercise, and mainly at the end of warm-up, where this group also presented significantly higher sympathetic values.

The results show similar trends to those found in the time-frequency analysis performed in chapter 3 (Section 3.3.2), where a higher vagal tone, according to HF_{nu}, was observed in symptomatic patients during the second minute of incremental exercise. Although after recursive

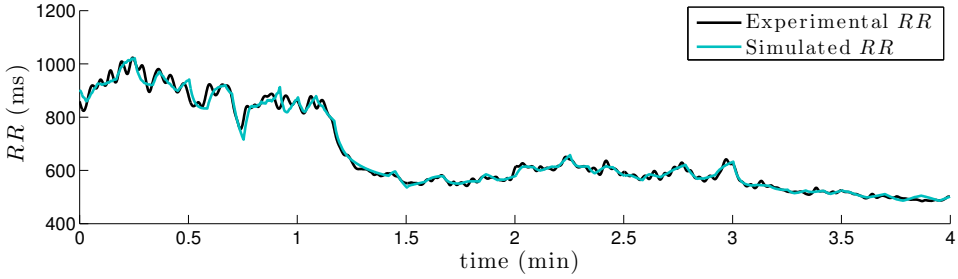

FIGURE 5.17– Simulated (blue) and experimental (black) RR series during the last minute of warm-up and the first 3 minutes of incremental exercise. $E = 1.7\%$.

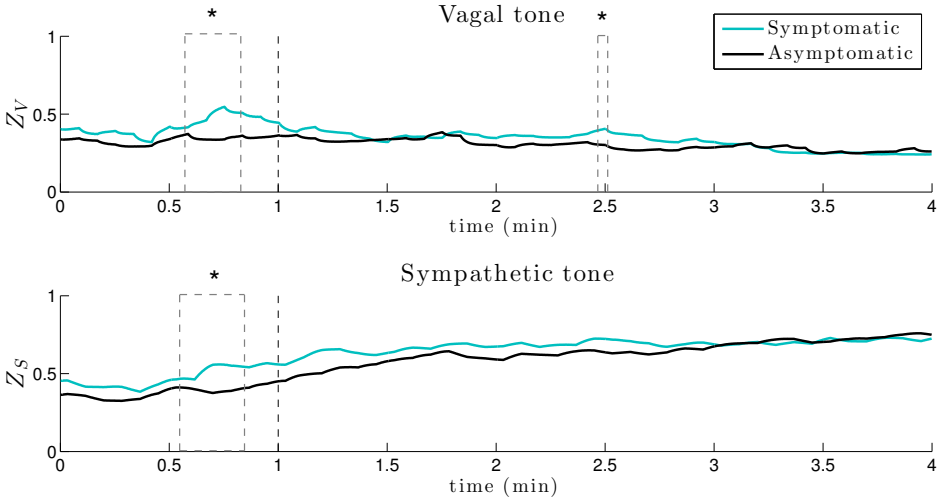

FIGURE 5.18– Mean vagal (Z_V) and sympathetic (Z_S) tones, for symptomatic (blue) and asymptomatic (black) patients, during exercise. Dashed vertical lines delimit the end of warm-up and subsequent incremental exercise onset. Pointed boxes indicate those segments where significant differences between groups ($^*p < 0.05$) were found.

model identification some significant differences were also found in this period, the largest and most significant segment was observed at the end of warm-up. Moreover, sympathetic activity in this phase was also found to be higher in symptomatic patients, contrary to the tendencies found in LF_{nu}. Nevertheless, time-frequency approaches are an approximation of the autonomic function and several works report the influence of both sympathetic and parasympathetic systems on LF_{nu} (MALLIANI et al., 1994; ORI et al., 1992). Nonetheless, results on the vagal tone were found to be consistent with previous studies where symptomatic BS patients showed enhanced parasympathetic activities (BEHAR et al., 2016; NAKAZAWA et al., 2003; TOKUYAMA et al., 2014).

Finally, in Figure 5.19, the mean vagal and sympathetic tones during recovery, for symptomatic and asymptomatic patients, are represented. After the peak effort, an increase in parasympathetic activity, as well as a decrease in the sympathetic tone can be observed for both groups. Although

no statistically significant differences related to symptomatic status were found on the vagal tone, at the end of the second minute of recovery, symptomatic patients presented significantly lower sympathetic values. These findings concur with a previous work where a lower sympathetic activity was reported in symptomatic patients (Nakazawa et al., 2003).

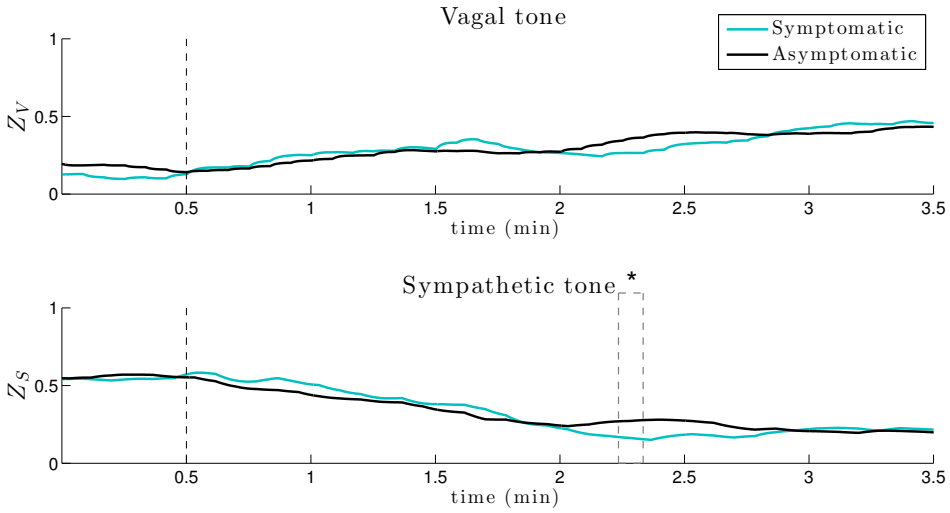

Figure 5.19– Mean vagal (Z_V) and sympathetic (Z_S) tones, for symptomatic (blue) and asymptomatic (black) patients, during post-exercise recovery. Dashed vertical lines delimit the end of exertion and subsequent recovery onset.

5.3. Multivariate model-based classification

A multivariate classifier combining model parameters identified in Section 5.1 was implemented. Although it is based on a small sample of 5 symptomatic and 7 asymptomatic BS patients, it is presented as a first step towards the study of physiological model parameters for risk stratification in BS patients.

5.3.1. Clinical data description

As in Section 5.1.2, five BS patients presented documented symptoms of ventricular origin: cardiac arrest (60%) and syncope (40%). An ICD had been placed in one asymptomatic patient, based on a positive EPS test, whereas all symptomatic patients had ICDs implanted. Three BS patients (2 were symptomatic) presented an SCN5A mutation (25%). Table 5.6 summarizes patients' clinical characteristics.

5.3.2. Multivariate classification method

The LDA-based classifier described in chapter 4 was optimized in order to distinguish symptomatic and asymptomatic groups. However, due to the reduced sample of patients included in this study, all the observations were used for training and performance evaluation.

TABLE 5.6– Patients' baseline characteristics for multivariate model-based classification.

	Symptomatic (n=5)	**Asymptomatic (n=7)**	***p*-value**
Age, *years old*	48.0 ± 11.5	51.6 ± 13.2	0.604
Male sex, *n (%)*	5 (100%)	5 (71.4%)	0.636
ICD implantation, *n (%)*	5 (100%)	1 (14.3%)	0.015
***SCN5A* mutation,** *n (%)*	2 (40%)	1 (14.3%)	0.727

Values are mean ± standard deviation or number of observations (%).
All between-groups differences, apart from ICD implantation, are statistically non-significant.

This LDA classifier was designed as the linear combination of model parameters best distinguishing between symptomatic and asymptomatic patients. Being $x_i \in \{\lambda_{LV}, Vd_{LV}, \lambda_{RV}, K_V, T_V, K_S, T_S, K_R, K_C, Pg_{legs}\}$ the input features, the LDA predictive model was defined as:

$$Z = \beta_1 x_1 + \beta_2 x_2 + \cdots + \beta_{10} x_{10} \tag{5.31}$$

where β_i were the estimated linear model coefficients.

5.3.3. Results and discussion

Table 5.7 summarizes the optimized model coefficients β. According to these coefficients, T_S, K_C and K_V negatively contributed to the classification decision. Thus, higher values in the sympathetic time constant and gains related to cardiac contractility and vagal tone increased the probability of classifying a patient as asymptomatic. Conversely, model parameters more positively contributing to linear classification were K_S, Vd_{LV}, K_R and λ_{RV}, providing further evidence in the combination of CVS and BRS variables for the identification of BS patients at high risk.

As expected from sensitivity analysis, sympathetic and parasympathetic gains (K_S, K_V), as well as the LV volume at zero pressure (Vd_{LV}), had a relevant impact on the classification of BS patients. However, a higher contribution was placed on the end-diastolic exponent of the RV (λ_{RV}) than that of the LV (λ_{LV}). Although sensitivity analysis identified the latter as a more relevant parameter causing a greater influence on model outputs, in the context of Brugada syndrome where patients present ECG patterns of RBBB, λ_{RV} seems to be more conclusive for classification purposes.

Finally, by the application of these coefficients on the entire clinical database, only one symptomatic patient was identified as asymptomatic and, thus, the 91.7% of patients were correctly classified, leading to a sensitivity of the 80% and a specificity of the 100%.

Table 5.7– LDA-model coefficients for each independent variable.

	β
λ_{LV}	0.887
Vd_{LV}	2.139
λ_{RV}	1.074
K_V	-1.397
T_V	0.998
K_S	5.770
T_S	-5.100
K_R	1.096
K_C	-2.019
Pg_{legs}	0.064

5.4. Conclusion

In this chapter, two system-level model-based approaches were proposed in order to study the mechanic, circulatory and autonomic function of BS patients. First, by the integration and evaluation of a computational model capturing the cardiovascular system's dynamics and its autonomic response to HUT testing. After a thorough two-step parameter sensitivity analysis to identify the most relevant variables affecting model outputs, results showed that SBP was mainly modulated by CVS parameters, whereas HR was mostly affected by autonomic variables coming from the BRS model. Then, subject-specific model parameters were estimated by comparing cardiac experimental data and simulated signals through evolutionary algorithms. The results showed significant differences between asymptomatic and symptomatic BS patients in the left ventricle zero-pressure volumes, suggesting a reduced contractility function in the latter. Moreover, controls showed an increased sympathetic regulation after tilting with respect to BS patients.

Since this model can only explain the mechanical, circulatory and autonomic sympathetic function of the cardiovascular system, a second approach based on a recursive identification of the sympathetic and parasympathetic contributions to ANS regulation was proposed. It was applied to a simplified version of the previous model in order to estimate the time-varying autonomic response to exertion and subsequent recovery in 44 BS patients. According to the results, a significantly higher parasympathetic activity in symptomatic patients, with respect to asymptomatic subjects, was observed during exercise; providing further evidence for the role of vagal tone in BS patients' prognosis.

In both approaches, in order to reduce computational cost in parameter identification, a small amount of parameters were selected, probably absorbing changes in other previously fixed variables. For instance, significant results for LV parameters in the first approach may have been affected by RV variations. Thus, a more extensive evaluation including a wider range

of parameters should be performed in the future. Moreover, studies were based on a small population of BS patients and, thus, conclusions on risk stratification cannot be extracted. Nevertheless, the results indicate important trends of clinical relevance in autonomic, circulatory and mechanical variables never studied before in BS that provide new insights into the disease.

Finally, in order to capture the multifactorial etiology of the syndrome, a multivariate approach integrating model-based results was implemented. Although it was performed with an insufficient amount of observations so as to infer conclusions, it is presented as a prospective study introducing the next step in the development of a robust Brugada-based methodology to identify patients at high risk for SCD.

References

Behar, N., B. Petit, V. Probst, F. Sacher, G. Kervio, J. Mansourati, P. Bru, A. Hernandez, and P. Mabo (2016). "Heart rate variability and repolarization characteristics in symptomatic and asymptomatic Brugada syndrome". In: *Europace*, euw224.

Coatrieux, J.-L. and J. Bassingthwaighte (2006). "The physiome and beyond". In: *Proceedings of the IEEE* 94.4, pp. 671–677.

Goldberg, D. E. and J. H. Holland (1988). "Genetic algorithms and machine learning". In: *Machine learning* 3.2, pp. 95–99.

Heldt, T., E. B. Shim, R. D. Kamm, and R. G. Mark (2002). "Computational modeling of cardiovascular response to orthostatic stress". In: *Journal of applied physiology* 92.3, pp. 1239–1254.

Hernandez Rodriguez, A. I. (2000). "Fusion de signaux et de modèles pour la caractérisation d'arythmies cardiaques". PhD thesis. Université Rennes 1.

Hernandez, A. I., V. Le Rolle, D. Ojeda, P. Baconnier, J. Fontecave-Jallon, F. Guillaud, T. Grosse, R. G. Moss, P. Hannaert, and S. R. Thomas (2011). "Integration of detailed modules in a core model of body fluid homeostasis and blood pressure regulation". In: *Progress in Biophysics and Molecular Biology* 107.1, pp. 169–182.

Hernández, A. I., G. Carrault, F. Mora, and A. Bardou (2002). "Model-based interpretation of cardiac beats by evolutionary algorithms: signal and model interaction". In: *Artificial Intelligence in Medicine* 26.3, pp. 211–235.

Hernández, A. I., V. Le Rolle, A. Defontaine, and G. Carrault (2009). "A multiformalism and multiresolution modelling environment: application to the cardiovascular system and its regulation". In: *Philosophical Transactions of the Royal Society of London A: Mathematical, Physical and Engineering Sciences* 367.1908, pp. 4923–4940.

Kies, P., T. Wichter, M. Schäfers, M. Paul, K. P. Schäfers, L. Eckardt, L. Stegger, E. Schulze-Bahr, O. Rimoldi, G. Breithardt, et al. (2004). "Abnormal myocardial presynaptic norepinephrine recycling in patients with Brugada syndrome". In: *Circulation* 110.19, pp. 3017–3022.

Le Rolle, V., A. Beuchee, J.-P. Praud, N. Samson, P. Pladys, and A. I. Hernández (2015). "Recursive identification of an arterial baroreflex model for the evaluation of cardiovascular autonomic modulation". In: *Computers in biology and medicine* 66.287–294.

Le Rolle, V., A. I. Hernández, P.-Y. Richard, and G. Carrault (2008). "An autonomic nervous system model applied to the analysis of orthostatic tests". In: *Modelling and Simulation in Engineering* 2008, p. 2.

Le Rolle, V., D. Ojeda, and A. I. Hernández (2011). "Embedding a cardiac pulsatile model into an integrated model of the cardiovascular regulation for heart failure followup". In: *IEEE transactions on biomedical engineering* 58.10, pp. 2982–2986.

Malliani, A., F. Lombardi, and M. Pagani (Jan. 1994). "Power spectrum analysis of heart rate variability: a tool to explore neural regulatory mechanisms." In: *British Heart Journal* 71.1, pp. 1–2.

McKay, M. D., R. J. Beckman, and W. J. Conover (1979). "Comparison of three methods for selecting values of input variables in the analysis of output from a computer code". In: *Technometrics* 21.2, pp. 239–245.

Morris, M. D. (1991). "Factorial sampling plans for preliminary computational experiments". In: *Technometrics* 33.2, pp. 161–174.

Nakazawa, K., T. Sakurai, A. Takagi, R. Kishi, K. Osada, T. Nanke, F. Miyake, N. Matsumoto, and S. Kobayashi (2003). "Autonomic imbalance as a property of symptomatic Brugada syndrome". In: *Circulation journal* 67.6, pp. 511–514.

Ojeda Avellaneda, D. (2013). "Multi-resolution physiological modeling for the analysis of cardiovascular pathologies". PhD thesis. Université Rennes 1.

Ojeda, D., V. Le Rolle, O. Rossel, N. Karam, A. Hagege, J.-L. Bonnet, P. Mabo, G. Carrault, and A. Hernández (2015). "Analysis of a baroreflex model for the study of the chronotropic response to vagal nerve stimulation". In: *Neural Engineering (NER), 2015 7th International IEEE/EMBS Conference on*, pp. 541–544.

Ojeda, D., V. L. Rolle, K. T. V. Koon, C. Thebault, E. Donal, and A. I. Hernández (2013). "Towards an atrio-ventricular delay optimization assessed by a computer model for cardiac resynchronization therapy". In: *Proc. SPIE 8922, IX International Seminar on Medical Information Processing and Analysis*. Vol. 8922.

Ojeda, D., V. Le Rolle, M. Harmouche, A. Drochon, H. Corbineau, J.-P. Verhoye, and A. I. Hernandez (2014). "Sensitivity analysis and parameter estimation of a coronary circulation model for triple-vessel disease". In: *IEEE Transactions on Biomedical Engineering* 61.4, pp. 1208–1219.

Ori, Z., G. Monir, J. Weiss, X. Sayhouni, and D. Singer (1992). "Heart rate variability. Frequency domain analysis." In: *Cardiology clinics* 10.3, pp. 499–537.

Paul, M., M. Meyborg, P. Boknik, U. Gergs, W. Schmitz, G. Breithardt, T. Wichter, and J. Neumann (2011). "Autonomic dysfunction in patients with Brugada syndrome: further biochemical evidence of altered signaling pathways". In: *Pacing and Clinical Electrophysiology* 34.9, pp. 1147–1153.

Romero-Ugalde, H. M., D. Ojeda, V. L. Rolle, D. Andreu, D. Guiraud, J.-L. Bonnet, C. Henry, N. Karam, A. Hagege, P. Mabo, G. Carrault, and A. I. Hernandez (2015). "Model-based design and experimental validation of control modules for neuromodulation devices". In: *Biomedical Engineering, IEEE Transactions on* 63.7, pp. 1551–1558.

Saltelli, A., P. Annoni, I. Azzini, F. Campolongo, M. Ratto, and S. Tarantola (2010). "Variance based sensitivity analysis of model output. Design and estimator for the total sensitivity index". In: *Computer Physics Communications* 181.2, pp. 259–270.

Saltelli, A., M. Ratto, T. Andres, F. Campolongo, J. Cariboni, D. Gatelli, M. Saisana, and S. Tarantola (2008). *Global sensitivity analysis: the primer*. John Wiley & Sons.

Smith, B. W., J. G. Chase, R. I. Nokes, G. M. Shaw, and G. Wake (2004). "Minimal haemodynamic system model including ventricular interaction and valve dynamics". In: *Medical engineering & physics* 26.2, pp. 131–139.

Sobol, I. M. (2001). "Global sensitivity indices for nonlinear mathematical models and their Monte Carlo estimates". In: *Mathematics and computers in simulation* 55.1, pp. 271–280.

Tokuyama, T., Y. Nakano, A. Awazu, Y. Uchimura-Makita, M. Fujiwra, Y. Watanabe, A. Sairaku, K. Kajihara, C. Motoda, N. Oda, et al. (2014). "Deterioration of the circadian variation of heart rate variability in Brugada syndrome may contribute to the pathogenesis of ventricular fibrillation". In: *Journal of cardiology* 64.2, pp. 133–138.

Ursino, M. and E. Magosso (2000). "Acute cardiovascular response to isocapnic hypoxia. I. A mathematical model". In: *American Journal of Physiology-Heart and Circulatory Physiology* 279.1, H149–4165.

Wichter, T., P. Matheja, L. Eckardt, P. Kies, K. Schäfers, E. Schulze-Bahr, W. Haverkamp, M. Borggrefe, O. Schober, G. Breithardt, et al. (2002). "Cardiac autonomic dysfunction in Brugada syndrome". In: *Circulation* 105.6, pp. 702–706.

CHAPTER 6

Conclusion

Brugada syndrome (BS) is a genetic arrhythmogenic disease associated with a distinctive ECG pattern and an elevated risk for sudden cardiac death (SCD) due to ventricular fibrillation (VF) in absence of structural cardiopathies (Priori et al., 2015). To date, the only proven effective treatment for the prevention of SCD is the implantation of cardioverter defibrillators (ICD). However, since they can present some complications, such as inappropriate shocks or risks related to surgery (Miyazaki et al., 2013), these devices are recommended in patients with documented life-threatening arrhythmias or presenting a spontaneous type 1 ECG and a history of syncope (Priori et al., 2015). Thus, the decision of implanting an ICD on asymptomatic subjects, who represent around 60% of diagnosed patients and present a relatively low risk for cardiac events estimated at less than 1% (Probst et al., 2010), is still complex.

Since autonomic imbalance has been reported to play a determinant role in the pathophysiology, arrhythmogenesis and prognosis of the disease, the characterization of autonomic alterations induced by different ANS stimulations on patients at high risk having already suffered symptoms could provide new insights into the autonomic mechanisms underlying the disease, with a potential impact on risk stratification and, thus, on therapeutic strategies.

In this contex, the thesis was focused on the assessment of the autonomic function in Brugada syndrome through the application of previously described methods for the study of heart rate variability (HRV), heart rate complexity (HRC) and baroreflex sensitivity (BRS); and by the development of novel approaches better accounting for the complexity and multifactorial nature of biomedical signals. They were applied on clinical databases composed of cardiovascular data from subjects at different levels of risk (symptomatic and asymptomatic BS patients), acquired for 24 hours including exercise testing and a head-up tilt (HUT) test. The autonomic function was evaluated by three main approaches:

- Characterization and comparison of HRV, HRC and BRS indices, in order to identify cardiac markers capable of distinguishing between symptomatic and asymptomatic BS patients.

- Development, analysis and comparison of system-level patient-specific models describing interactions between the cardiovascular and autonomic nervous systems, in order to better understand the autonomic mechanisms underlying the disease and find new biomarkers capable of identifying a high-risk group of patients.

- Optimization of a multivariate approach based on a step-based machine learning method built with features extracted from previous approaches, in order to design predictive models improving classification perfomance and, thus, better identifying BS patients at high risk.

According to univariate analysis, symptomatic patients showed lower heart rate variability and complexity, as well as a greater SA node sensitivity at night. During exercise testing, symptomatic patients showed an increased vagal function and a reduced sympathetic activity, with respect to asymptomatic BS patients, under conditions of incremental exercise. Moreover, lower HRC values were noted in symptomatic patients under conditions of post-exercise recovery and rest after recovery. Regarding the autonomic response to HUT testing, symptomatic patients presented an increased parasympathetic tone and a reduced sympathovagal balance with respect to asymptomatic patients during tilting, and specially before the 15^{th} minute in upright posture. After tilting, sympathovagal balance was more rapidly restored to baseline values in the asymptomatic group. The results concur with previous publications reporting higher vagal and lower sympathetic tones, as well as lower HRV values, in symptomatic patients (BEHAR et al., 2016; NAKAZAWA et al., 2003; TOKUYAMA et al., 2014). However, since univariate comparisons can only explain the effect of isolated factors on BS prognosis, a multivariate approach capable of capturing the multifactorial nature of the disease was proposed.

When extracted autonomic features were included in multivariate models designed from a step-based machine learning method, although exercise and HUT testing together lead to better predictive results than when they were assessed separately, the classifier based on autonomic features obtained during nighttime analysis presented the best performance ($AUC = 95\%$), improving previously reported predictive models of risk in BS based on non-invasive parameters (KAWAZOE et al., 2016). Previous studies have reported that most major cardiac events in BS occur at rest and during sleep (KIES et al., 2004; MATSUO et al., 1999), and that the occurrence of Brugada-like ECG changes increases with vagal stimulation (IKEDA et al., 2005). Thus, these findings provide further evidence for the relevant role of autonomic night analysis to identify BS patients at high risk, when parasympathetic activity is predominant.

However, since these multivariate predictive models do not integrate explicit physiological *a priori* knowledge, two system-level model-based methods were proposed in order to study the hemodynamic and autonomic function of BS patients. First, by the integration and evaluation of a computational model capturing the cardiovascular system's dynamics and its autonomic response to HUT testing. After a thorough two-step parameter sensitivity analysis to identify the most relevant variables affecting model outputs, results showed that systolic blood pressure was mainly modulated by cardiovascular parameters, whereas heart rate was mostly affected by autonomic variables coming from the BRS model. Then, subject-specific model parameters

were estimated in 8 controls and 12 BS patients, by comparing cardiac experimental data and simulated signals through evolutionary algorithms. The results showed significant differences between asymptomatic and symptomatic BS patients in the left ventricle zero-pressure volumes, suggesting a reduced contractility function in the latter. Moreover, controls showed an increased sympathetic regulation after tilting with respect to BS patients.

A second model-based approach, integrating an original recursive identification algorithm for the estimation of time-varying sympathetic and parasympathetic activities, was applied to a simplified version of the previous model during exertion and subsequent recovery. A remarkable agreement was noted between experimental and simulated signals (mean error = 0.81%) and estimations of the sympathetic and parasympathetic components were consistent with physiological knowledge. Moreover, a significantly higher parasympathetic activity in symptomatic patients, with respect to asymptomatic subjects, was observed during exercise; providing further evidence for the role of vagal tone in BS patients' prognosis. Regarding sympathetic tone, significantly higher values at the end of warm-up and lower values during recovery were observed in symptomatic patients. To our knowledge, these contributions on recursive model-based autonomic analysis are original and represent one of the main methodological contributions of this work.

Finally, in order to capture the multifactorial etiology of the syndrome, a multivariate classification approach integrating model-based features was proposed. More specifically, parameters identified from the physiological model more accurately representing the cardiovascular and autonomic response to HUT testing were included in a multivariate predictive LDA-based model. Although classification performance could have been improved by means of the complete step-based machine learning method previously proposed, the reduced sample of BS patients available limited the study to a simpler approach.

From a methodological point of view, this work presents some limitations that should be mentioned. On one hand, studies were based on a relatively small population of BS patients and, thus, results should be confirmed by applying the proposed methods on larger clinical series. Moreover, databases under study only included the blood pressure and ECG recordings acquired for a specific moment. Since HRV measures have been reported to depend on day-to-day random variations (Pinna et al., 2007), the repeatibility of computed HRV, HRC and BRS indices should be proved stable and therefore characteristic of each patient, as in (Sinnreich et al., 1998). Measures' reliability is of major importance so as to be proposed as consistent markers of risk. Moreover, since some patients classified as asymptomatic may develop symptoms in the future and thus present high-risk patterns during the analyzed recordings, a more suitable clinical database for risk stratification should include follow-up information so as to relate autonomic changes to the probability of developing symptoms and not to the identification of a high-risk group having already suffered these symptoms.

On the other hand, in order to reduce computational cost in model-based parameter identifications, a small amount of variables were identified, probably absorbing changes in other previously fixed parameters. Thus, a more extensive evaluation including a wider range of parameters should be performed in the future. Moreover, model-based approaches could be

improved by including the effect of respiration on the vagal tone response and by integrating a Brugada-based cardiac electrical system coupling the electrophysiological aspects characterizing the disease with autonomic modulation. Apart from the need of integrating models capable of representing the ionic currents leading to the Brugada-like ECG pattern; according to higher circadian fluctuations found in symptomatic patients (BEHAR et al., 2016), an increased SA node response to ANS seems to be associated with patients at high risk for SCD. Since this increased response can be due to wider fluctuations in autonomic tone, but also due to a greater SA node autonomic receptors sensitivity, improved versions of the integrated cardiac electrical system should include an SA node sensitivity regulation.

Electrophysiological models simulating BS mutations should also be coupled since they cause ionic imbalances heterogeneously affecting ventricular action potentials, which lead to alterations causing Brugada-like ECG manifestations. Parasympathetic stimulation potentiates the ionic imbalance caused by these BS mutations and accentuates the ionic and cellular alterations that underlie the risk for ventricular arrhythmias in BS patients. Indeed, some approaches based on the simulation of Brugada electrophysiological characteristics through mathematical models have been reported (CLANCY et al., 2002; HOOGENDIJK et al., 2011; MIYOSHI et al., 2003; XIA et al., 2006). Nevertheless, the proposed approach would be the first model integrating Brugada electrophysiological knowledge on interactions between the cardiac function and the circulatory and autonomic systems.

Furthermore, as proposed in (LE ROLLE et al., 2015, 2016), identifications should be performed in two steps combining a batch identification of model parameters, followed by a recursive estimation of the time-varying autonomic response. Finally, features extracted from these improved model-based approaches should be included in multivariate classifiers based on machine-learning methods accounting for the multifactorial etiology of the disease. Final predictive models responsible for the detection of patients at high risk should be based on physiological models representing cardiac conditions characterizing the Brugada syndrome.

Nonetheless, the results thus far indicate important trends of clinical relevance that provide new insights into the underlying autonomic mechanisms regulating the cardiovascular system in BS, improving physiopathology and prognosis interpretation, with a potential future impact on therapeutic strategies. The proposed approach is presented as a potential instrument for the identification of those asymptomatic patients at high risk who may benefit from an ICD implantation. Moreover, since the analyzed features can be automatically extracted from cardiac signals, the methodological approach presented in this thesis might be applied to data acquired from ICDs on implanted BS patients, in order to control their risk of SCD occurrence at follow-up.

References

BEHAR, N., B. PETIT, V. PROBST, F. SACHER, G. KERVIO, J. MANSOURATI, P. BRU, A. HERNANDEZ, and P. MABO (2016). "Heart rate variability and repolarization characteristics in symptomatic and asymptomatic Brugada syndrome". In: *Europace*, euw224.

Clancy, C. E. and Y. Rudy (2002). "Na+ channel mutation that causes both Brugada and long-QT syndrome phenotypes". In: *Circulation* 105.10, pp. 1208–1213.

Hoogendijk, M. G., M. Potse, A. Vinet, J. M. de Bakker, and R. Coronel (2011). "ST segment elevation by current-to-load mismatch: an experimental and computational study". In: *Heart Rhythm* 8.1, pp. 111–118.

Ikeda, T., M. Takami, K. Sugi, Y. Mizusawa, H. Sakurada, and H. Yoshino (2005). "Noninvasive Risk Stratification of Subjects with a Brugada-Type Electrocardiogram and No History of Cardiac Arrest". In: *Annals of Noninvasive Electrocardiology* 10.4, pp. 396–403.

Kawazoe, H., Y. Nakano, H. Ochi, M. Takagi, Y. Hayashi, Y. Uchimura, T. Tokuyama, Y. Watanabe, H. Matsumura, S. Tomomori, et al. (2016). "Risk stratification of ventricular fibrillation in Brugada syndrome using noninvasive scoring methods". In: *Heart Rhythm* 13.10, pp. 1947–1954.

Kies, P., T. Wichter, M. Schäfers, M. Paul, K. P. Schäfers, L. Eckardt, L. Stegger, E. Schulze-Bahr, O. Rimoldi, G. Breithardt, et al. (2004). "Abnormal myocardial presynaptic norepinephrine recycling in patients with Brugada syndrome". In: *Circulation* 110.19, pp. 3017–3022.

Le Rolle, V., A. Beuchee, J.-P. Praud, N. Samson, P. Pladys, and A. I. Hernández (2015). "Recursive identification of an arterial baroreflex model for the evaluation of cardiovascular autonomic modulation". In: *Computers in biology and medicine* 66.287–294.

Le Rolle, V., A. Beuchée, J.-P. Praud, N. Samson, P. Pladys, and A. I. Hernández (2016). "Recursive Model Identification for the Evaluation of Baroreflex Sensitivity". In: *Acta biotheoretica* 64.4, pp. 469–478.

Matsuo, K., T. Kurita, M. Inagaki, M. Kakishita, N. Aihara, W. Shimizu, A. Taguchi, K. Suyama, S. Kamakura, and K. Shimomura (1999). "The circadian pattern of the development of ventricular fibrillation in patients with Brugada syndrome". In: *European heart journal* 20.6, pp. 465–470.

Miyazaki, S., T. Uchiyama, Y. Komatsu, H. Taniguchi, S. Kusa, H. Nakamura, H. Hachiya, M. Isobe, K. Hirao, and Y. Iesaka (2013). "Long-term complications of implantable defibrillator therapy in Brugada syndrome". In: *The American journal of cardiology* 111.10, pp. 1448–1451.

Miyoshi, S., H. Mitamura, K. Fujikura, Y. Fukuda, K. Tanimoto, Y. Hagiwara, M. Ita, and S. Ogawa (2003). "A mathematical model of phase 2 reentry: role of L-type Ca current". In: *American Journal of Physiology-Heart and Circulatory Physiology* 284.4, H1285–H1294.

Nakazawa, K., T. Sakurai, A. Takagi, R. Kishi, K. Osada, T. Nanke, F. Miyake, N. Matsumoto, and S. Kobayashi (2003). "Autonomic imbalance as a property of symptomatic Brugada syndrome". In: *Circulation journal* 67.6, pp. 511–514.

Pinna, G. D., R. Maestri, A. Torunski, L. Danilowicz-Szymanowicz, M. Szwoch, M. T. La Rovere, and G. Raczak (2007). "Heart rate variability measures: a fresh look at reliability". In: *Clinical Science* 113.3, pp. 131–140.

PRIORI, S. G., C. BLOMSTRÖM-LUNDQVIST, A. MAZZANTI, N. BLOM, M. BORGGREFE, J. CAMM, P. ELLIOTT, D. FITZSIMONS, R. HATALA, G. HINDRICKS, et al. (2015). "Task Force for the Management of Patients with Ventricular Arrhythmias and the Prevention of Sudden Cardiac Death of the European Society of Cardiology (ESC). 2015 ESC guidelines for the management of patients with ventricular arrhythmias and the prevention of sudden cardiac death: the Task Force for the Management of Patients with Ventricular Arrhythmias and the Prevention of Sudden Cardiac Death of the European Society of Cardiology (ESC) endorsed by: Association for European Paediatric and Congenital Cardiology (AEPC)". In: *Europace* 17, pp. 1601–1687.

PROBST, V., C. VELTMANN, L. ECKARDT, P. MEREGALLI, F. GAITA, H. TAN, D. BABUTY, F. SACHER, C. GIUSTETTO, E. SCHULZE-BAHR, et al. (2010). "Long-term prognosis of patients diagnosed with Brugada syndrome results from the FINGER Brugada Syndrome Registry". In: *Circulation* 121.5, pp. 635–643.

SINNREICH, R., J. KARK, Y. FRIEDLANDER, D. SAPOZNIKOV, and M. LURIA (1998). "Five minute recordings of heart rate variability for population studies: repeatability and age–sex characteristics". In: *Heart* 80.2, pp. 156–162.

TOKUYAMA, T., Y. NAKANO, A. AWAZU, Y. UCHIMURA-MAKITA, M. FUJIWRA, Y. WATANABE, A. SAIRAKU, K. KAJIHARA, C. MOTODA, N. ODA, et al. (2014). "Deterioration of the circadian variation of heart rate variability in Brugada syndrome may contribute to the pathogenesis of ventricular fibrillation". In: *Journal of cardiology* 64.2, pp. 133–138.

XIA, L., Y. ZHANG, H. ZHANG, Q. WEI, F. LIU, and S. CROZIER (2006). "Simulation of Brugada syndrome using cellular and three-dimensional whole-heart modeling approaches". In: *Physiological measurement* 27.11, pp. 1125–1142.

APPENDIX A

List of associated publications

International journals

Calvo, M., P. Gomis, D. Romero, V. Le Rolle, N. Béhar, P. Mabo, and A. Hernández (2017a). "Heart rate complexity analysis in Brugada syndrome during physical stress testing". In: *Physiological measurement* 38.2, pp. 387–396.

Calvo, M., D. Romero, V. Le Rolle, P. Gomis, N. Béhar, P. Mabo, and A. Hernández (2017b). "Multivariate classification of Brugada syndrome patients based on autonomic response to exercise stress testing". In: *Submitted to Plos One*.

International conferences

Calvo, M., P. Gomis, A. Hernández, D. Andreu, E. Arbelo, and P. Caminal (2015b). "Automatic detection of Brugada-like pattern on continuous electrocardiographic monitoring". In: *International Congress on Computational Bioengineering (ICCB), 2015*.

Calvo, M., J. Hernández, S. Vidorreta, J. Brugada, P. Gomis, and E. Arbelo (2017c). "Automatic Brugada pattern detection on continuous electrocardiographic monitoring". In: *EHRA Europace Cardiostim 2017*.

Calvo, M., V. Le Rolle, D. Romero, N. Béhar, P. Gomis, P. Mabo, and A. Hernández (2015c). "Comparison of methods to measure baroreflex sensitivity in Brugada syndrome". In: *Computing in Cardiology Conference (CinC), 2015*, pp. 245–248.

— (2017e). "Recursive model identification for the evaluation of the autonomic response to exercise in Brugada syndrome". In: *International Congress on Computational Bioengineering (ICCB), 2017*.

— (2017f). "Time-frequency Analysis of the Autonomic Response to Head-up Tilt Testing in Brugada Syndrome". In: *Computing in Cardiology Conference (CinC), 2017*.

CALVO, M., V. LE ROLLE, D. ROMERO, N. BÉHAR, P. GOMIS, P. MABO, and A. I. HERNÁNDEZ (2016). "Analysis of a cardiovascular model for the study of the autonomic response of Brugada syndrome patients". In: *Engineering in Medicine and Biology Society (EMBC), 2016 IEEE 38th Annual International Conference of the IEEE*, pp. 5591–5594.

ROMERO, D., M. CALVO, N. BÉHAR, P. MABO, and A. HERNÁNDEZ (2016). "Ensemble classifier based on linear discriminant analysis for distinguishing Brugada syndrome patients according to symptomatology". In: *Computing in Cardiology Conference (CinC), 2016*, pp. 205–208.

National conferences

CALVO, M., P. GOMIS, A. HERNÁNDEZ, D. ANDREU, E. ARBELO, and P. CAMINAL (2014). "Análisis del ECG para la detección automática del patrón característico del síndrome de Brugada". In: *Congreso Anual de la Sociedad Española de Ingeniería Biomédica (CASEIB), 2014*.

CALVO, M., V. LE ROLLE, D. ROMERO, N. BÉHAR, P. GOMIS, P. MABO, and A. HERNÁNDEZ (2017d). "Model-based approach for the study of the autonomic response in Brugada syndrome patients". In: *37ème Colloque de la Société Francophone de Biologie Théorique (SFBT), 2017*.

APPENDIX B

Multivariate classification results

This appendix contains the final feature subsets composing the single-test classifiers presented in Chapter 4. The first section includes the resulting subsets when features extracted during exercise testing were included in the multivariate classification approach, first for the example based on 105 BS patients (Table B.1), and then for the result of applying this method on a reduced clinical database of 44 patients (Table B.2). The next two sections include the final subsets obtained for classifiers built from features extracted during HUT testing (Table B.3) and overnight (Table B.4), in the same database of 44 BS patients.

B.1. Exercise testing

TABLE B.1– Selected features for multivariate classification based on exercise testing in 105 BS patients.

	Feature description
$\overline{HF_{nu}^{WU1}}$	Mean HF_{nu} for the first minute of warm-up
$\overline{HF_{nu}^{EX3}}$	Mean HF_{nu} for the third minute of incremental exercise
$\overline{HF_{nu}^{PE}}$	Mean HF_{nu} for the last minute before peak effort
$\overline{HF_{nu}^{AR1}}$	Mean HF_{nu} for the first minute of active recovery
$\overline{HF_{nu}^{AR3}}$	Mean HF_{nu} for the third minute of active recovery
$\overline{HF_{nu}^{PR1}}$	Mean HF_{nu} for the first minute of passive recovery
$\overline{LF/HF^{AR2}}$	Mean LF/HF for the second minute of active recovery
$\overline{LF^{EX1}}$	Mean LF for the first minute of incremental exercise
$\overline{LF^{EX2}}$	Mean LF for the second minute of incremental exercise
$\overline{LF^{EX3}}$	Mean LF for the third minute of incremental exercise
$\overline{LF^{AR3}}$	Mean LF for the third minute of active recovery
$\overline{LF^{PR2}}$	Mean LF for the second minute of passive recovery
$\overline{LF^{PR3}}$	Mean LF for the third minute of passive recovery
$\overline{HF^{PE}}$	Mean HF for the last minute before peak effort
$\overline{HF^{AR3}}$	Mean HF for the third minute of active recovery
$\overline{HF^{PR2}}$	Mean HF for the second minute of passive recovery
$\overline{HF^{PR3}}$	Mean HF for the third minute of passive recovery
$\overline{LF_{nu}^{EX3}}$	Mean LF_{nu} for the third minute of incremental exercise
$\overline{LF_{nu}^{PE}}$	Mean LF_{nu} for the last minute before peak effort
$\overline{LF_{nu}^{AR1}}$	Mean LF_{nu} for the first minute of active recovery
$\overline{LF_{nu}^{AR2}}$	Mean LF_{nu} for the second minute of active recovery
$\overline{LF_{nu}^{AR3}}$	Mean LF_{nu} for the third minute of active recovery

TABLE B.2– Selected features for multivariate classification based on exercise testing in 44 BS patients.

	Feature description
$\overline{HF_{nu}^{WU1}}$	Mean HF_{nu} for the first minute of warm-up
$\overline{HF_{nu}^{EX1}}$	Mean HF_{nu} for the first minute of incremental exercise
$\overline{HF_{nu}^{PE}}$	Mean HF_{nu} for the last minute before peak effort
$\overline{HF_{nu}^{AR1}}$	Mean HF_{nu} for the first minute of active recovery
$\overline{HF_{nu}^{PR2}}$	Mean HF_{nu} for the second minute of passive recovery
$\overline{HF_{nu}^{PR3}}$	Mean HF_{nu} for the third minute of passive recovery
$\overline{LF/HF^{WU2}}$	Mean LF/HF for the second minute of warm-up
$\overline{LF/HF^{EX1}}$	Mean LF/HF for the first minute of incremental exercise
$\overline{LF/HF^{EX2}}$	Mean LF/HF for the second minute of incremental exercise
$\overline{LF/HF^{EX3}}$	Mean LF/HF for the third minute of incremental exercise
$\overline{LF/HF^{PE}}$	Mean LF/HF for the last minute before peak effort
$\overline{LF/HF^{AR1}}$	Mean LF/HF for the first minute of active recovery
$\overline{LF/HF^{AR2}}$	Mean LF/HF for the second minute of active recovery
$\overline{LF/HF^{AR3}}$	Mean LF/HF for the third minute of active recovery
$\overline{LF/HF^{PR3}}$	Mean LF/HF for the third minute of passive recovery
$\overline{LF^{WU1}}$	Mean LF for the first minute of warm-up
$\overline{LF^{EX1}}$	Mean LF for the first minute of incremental exercise
$\overline{LF^{EX3}}$	Mean LF for the third minute of incremental exercise
$\overline{LF^{PE}}$	Mean LF for the last minute before peak effort
$\overline{LF^{AR1}}$	Mean LF for the first minute of active recovery
$\overline{LF^{AR3}}$	Mean LF for the third minute of active recovery
$\overline{LF^{PR3}}$	Mean LF for the third minute of passive recovery
$\overline{HF^{WU2}}$	Mean HF for the second minute of warm-up
$\overline{HF^{EX1}}$	Mean HF for the first minute of incremental exercise
$\overline{HF^{PE}}$	Mean HF for the last minute before peak effort
$\overline{HF^{AR2}}$	Mean HF for the second minute of active recovery
$\overline{HF^{AR3}}$	Mean HF for the third minute of active recovery
$\overline{LF_{nu}^{WU2}}$	Mean LF_{nu} for the second minute of warm-up
$\overline{LF_{nu}^{EX1}}$	Mean LF_{nu} for the first minute of incremental exercise
$\overline{LF_{nu}^{PR3}}$	Mean LF_{nu} for the third minute of passive recovery
$\beta_{exercise}$	Mean β for the whole exercise period

B.2. HUT testing

TABLE B.3– Selected features for multivariate classification based on HUT testing in 44 BS patients.

	Feature description
$\overline{\Delta HF_{nu}^{T11}}$	Mean ΔHF_{nu} for the eleventh minute of tilting
$\overline{\Delta HF_{nu}^{T12}}$	Mean ΔHF_{nu} for the twelfth minute of tilting
$\overline{\Delta HF_{nu}^{T13}}$	Mean ΔHF_{nu} for the thirteenth minute of tilting
$\overline{\Delta HF_{nu}^{T14}}$	Mean ΔHF_{nu} for the fourteenth minute of tilting
$\overline{\Delta HF_{nu}^{S1}}$	Mean ΔHF_{nu} for the first minute in supine position after tilting
$\overline{\Delta HF_{nu}^{S2}}$	Mean ΔHF_{nu} for the second minute in supine position after tilting
$\overline{\Delta HF_{nu}^{S3}}$	Mean ΔHF_{nu} for the third minute in supine position after tilting
$\overline{\Delta HF_{nu}^{S5}}$	Mean ΔHF_{nu} for the fifth minute in supine position after tilting
$\overline{\Delta LF/HF^{T12}}$	Mean $\Delta LF/HF$ for the twelfth minute of tilting
$\overline{\Delta LF/HF^{S1}}$	Mean $\Delta LF/HF$ for the first minute in supine position after tilting
$\overline{\Delta LF/HF^{S2}}$	Mean $\Delta LF/HF$ for the second minute in supine position after tilting
$\overline{\Delta LF/HF^{S3}}$	Mean $\Delta LF/HF$ for the third minute in supine position after tilting
$\overline{\Delta LF/HF^{S4}}$	Mean $\Delta LF/HF$ for the fourth minute in supine position after tilting
$\overline{\Delta LF^{T11}}$	Mean ΔLF for the eleventh minute of tilting
$\overline{\Delta LF^{T14}}$	Mean ΔLF for the fourteenth minute of tilting
$\overline{\Delta LF^{T15}}$	Mean ΔLF for the fifteenth minute of tilting
$\overline{\Delta HF^{T11}}$	Mean ΔHF for the eleventh minute of tilting
$\overline{\Delta HF^{T12}}$	Mean ΔHF for the twelfth minute of tilting
$\overline{\Delta HF^{T13}}$	Mean ΔHF for the thirteenth minute of tilting
$\overline{\Delta HF^{T14}}$	Mean ΔHF for the fourteenth minute of tilting
$\overline{\Delta HF^{T15}}$	Mean ΔHF for the fifteenth minute of tilting
$\overline{\Delta HF^{S1}}$	Mean ΔHF for the first minute in supine position after tilting
$\overline{\Delta HF^{S2}}$	Mean ΔHF for the second minute in supine position after tilting
$\overline{\Delta HF^{S4}}$	Mean ΔHF for the fourth minute in supine position after tilting
$\overline{\Delta HF^{S5}}$	Mean ΔHF for the fifth minute in supine position after tilting
$\overline{\Delta LF_{nu}^{T11}}$	Mean ΔLF_{nu} for the eleventh minute of tilting
$\overline{\Delta LF_{nu}^{T12}}$	Mean ΔLF_{nu} for the twelfth minute of tilting
$\overline{\Delta LF_{nu}^{T13}}$	Mean ΔLF_{nu} for the thirteenth minute of tilting
$\overline{\Delta LF_{nu}^{T14}}$	Mean ΔLF_{nu} for the fourteenth minute of tilting
$\overline{\Delta LF_{nu}^{S2}}$	Mean ΔLF_{nu} for the second minute in supine position after tilting
$\overline{\Delta LF_{nu}^{S5}}$	Mean ΔLF_{nu} for the fifth minute in supine position after tilting

B.3. Night analysis

TABLE B.4– Selected features for multivariate classification based on overnight analysis in 44 BS patients.

Feature description	
$SDNN^{01}$	$SDNN$ between midnight and 1 a.m.
$rMSSD^{01}$	$rMSSD$ between midnight and 1 a.m.
LF_{nu}^{01}	LF_{nu} between midnight and 1 a.m.
HF_{nu}^{01}	HF_{nu} between midnight and 1 a.m.
LF/HF^{01}	LF/HF between midnight and 1 a.m.
$\overline{RR}^{12}$	$\overline{RR}$ between 1 a.m. and 2 a.m.
$SDNN^{12}$	$SDNN$ between 1 a.m. and 2 a.m.
$rMSSD^{12}$	$rMSSD$ between 1 a.m. and 2 a.m.
$SDNN5min^{12}$	$SDNN5min$ between 1 a.m. and 2 a.m.
HF_{nu}^{12}	HF_{nu} between 1 a.m. and 2 a.m.
$\overline{RR}^{23}$	$\overline{RR}$ between 2 a.m. and 3 a.m.
$SDNN^{23}$	$SDNN$ between 2 a.m. and 3 a.m.
$NN50^{23}$	$NN50$ between 2 a.m. and 3 a.m.
$rMSSD^{34}$	$rMSSD$ between 3 a.m. and 4 a.m.
$MIRR^{34}$	$MIRR$ between 3 a.m. and 4 a.m.
HF_{nu}^{34}	HF_{nu} between 3 a.m. and 4 a.m.
LF/HF^{34}	LF/HF between 3 a.m. and 4 a.m.
$rMSSD^{45}$	$rMSSD$ between 4 a.m. and 5 a.m.
$SDANN^{45}$	$SDANN$ between 4 a.m. and 5 a.m.
$SDNN5min^{45}$	$SDNN5min$ between 4 a.m. and 5 a.m.
$NN50^{45}$	$NN50$ between 4 a.m. and 5 a.m.
$MIRR^{45}$	$MIRR$ between 4 a.m. and 5 a.m.
$SampEn^{45}$	$SampEn$ between 4 a.m. and 5 a.m.
$SDNN^{56}$	$SDNN$ between 5 a.m. and 6 a.m.
$rMSSD^{56}$	$rMSSD$ between 5 a.m. and 6 a.m.
$SDNN5min^{56}$	$SDNN5min$ between 5 a.m. and 6 a.m.

APPENDIX C

Parameter values of baroreflex and cardiovascular models

In this appendix, a detailed list of the model parameters used in sensitivity analysis is provided. Their values have been adapted from cited publications. Table C.1 includes model parameters coming from the BRS submodel, while Table C.2 specifies the CVS submodel parameter ranges employed.

TABLE C.1– Ranges of BRS parameters used for sensitivity analysis. When parameters are unitless, units are expressed as n.u.

Parameter	**Units**	**Norminal value**	**Min**	**Max**	**Reference**
HR_0	Hz	1.72	0.7667	2.667	(ROOSSIEN et al., 1997; URSINO et al., 2000) (HELDT, 2004; KORAKIANITIS et al., 2006)
K_B	n.u.	1	0.5	2	(URSINO et al., 2000)
T_B	s	2	0.1	2.5	(VAN ROON et al., 2004)
K_V	n.u.	1	0.5	2	(LU et al., 2001)
T_V	s	1.8	1.5	2.2	(LU et al., 2001; URSINO et al., 2000) (VAN ROON et al., 2004)
a_V	n.u.	0.7	0.56	0.84	(LU et al., 2001)
b_V	n.u.	1	0.8	1.2	(LU et al., 2001)
M_V	n.u.	110	60	140	(LU et al., 2001)
λ_V	n.u.	-0.04	-0.048	-0.032	(LU et al., 2001)
D_V	s	0.2	0.16	0.24	(LU et al., 2001; URSINO et al., 2000) (VAN ROON et al., 2004)
K_S	n.u.	1	0.5	2	(LU et al., 2001)
T_S	s	10	2	12	(LU et al., 2001; URSINO et al., 2000) (VAN ROON et al., 2004)
a_S	n.u.	0.3	0.24	0.36	(LU et al., 2001)
b_S	n.u.	0.7	0.56	0.84	(LU et al., 2001)
M_S	n.u.	100	60	140	(LU et al., 2001)
λ_S	n.u.	0.09	0.072	0.108	(LU et al., 2001)
D_S	s	3	2	3.6	(LU et al., 2001; URSINO et al., 2000) (VAN ROON et al., 2004)
K_R	n.u.	1	0.5	2	(LU et al., 2001)
T_R	s	6	4.8	7.2	(LU et al., 2001; VAN ROON et al., 2004)
a_R	n.u.	0.3	0.24	0.36	(LU et al., 2001)
b_R	n.u.	0.7	0.56	0.84	(LU et al., 2001)
M_R	n.u.	110	60	140	(LU et al., 2001)
λ_R	n.u.	0.04	0.032	0.048	(LU et al., 2001)
D_R	s	3	2.4	3.6	(LU et al., 2001; VAN ROON et al., 2004)
K_{VV}	n.u.	1	0.5	2	(LU et al., 2001)
T_{VV}	s	6	4.8	7.2	(LU et al., 2001; VAN ROON et al., 2004)
a_{VV}	n.u.	0.3	0.24	0.36	(LU et al., 2001)
b_{VV}	n.u.	0.7	0.56	0.84	(LU et al., 2001)
M_{VV}	n.u.	110	60	140	(LU et al., 2001)
λ_{VV}	n.u.	0.04	0.032	0.048	(LU et al., 2001)
D_{VV}	s	3	2.4	3.6	(LU et al., 2001; VAN ROON et al., 2004)
K_C	n.u.	1	0.5	2	(LU et al., 2001)
T_C	s	10	8	12	(LU et al., 2001; VAN ROON et al., 2004)
a_C	n.u.	0.3	0.24	0.36	(LU et al., 2001)
b_C	n.u.	0.7	0.56	0.84	(LU et al., 2001)
M_C	n.u.	110	60	140	(LU et al., 2001)
λ_C	n.u.	0.04	0.032	0.048	(LU et al., 2001)
D_C	s	3	2.4	3.6	(LU et al., 2001; VAN ROON et al., 2004)

TABLE C.2– Ranges of CVS parameters used for sensitivity analysis.

Parameter	**Units**	**Norminal value**	**Min**	**Max**	**Reference**
Ea_{head}	mmHg· ml^{-1}	0.7051	0.62	3.246	(DAVIS, 1991) (SMITH et al., 2004)
Ev_{head}	mmHg·ml^{-1}	0.0113	0.01	0.015	(DAVIS, 1991) (SMITH et al., 2004)
$Vd_{a,head}$	ml	240	192	288	(VAN ROON et al., 2004)
$Vd_{v,head}$	ml	650	520	780	(VAN ROON et al., 2004)
R_{head}	mmHg·s·ml^{-1}	0.125	0.1	0.15	(VAN ROON et al., 2004)
$V0_{head}$	ml	1250	1000	1500	(VAN ROON et al., 2004)
Pg_{head}	mmHg	-20	-30	-10	(LE ROLLE et al., 2008)
Ea_{legs}	mmHg·ml^{-1}	0.7051	0.62	3.246	(DAVIS, 1991) (SMITH et al., 2004)
Ev_{legs}	mmHg·ml^{-1}	0.0113	0.01	0.015	(DAVIS, 1991) (SMITH et al., 2004)
$Vd_{a,legs}$	ml	240	192	288	(VAN ROON et al., 2004)
$Vd_{v,legs}$	ml	350	280	420	(VAN ROON et al., 2004)
R_{legs}	mmHg·s·ml^{-1}	0.0526	0.042	0.063	(VAN ROON et al., 2004)
$V0_{legs}$	ml	850	680	1020	(VAN ROON et al., 2004)
Pg_{legs}	mmHg	60	40	80	(LE ROLLE et al., 2008)
E_{LV}	mmHg·ml^{-1}	3.4053	0.1	8	(CHUNG et al., 1997) (DAVIS, 1991)
Vd_{LV}	ml	5	0	71.44	(BURKHOFF et al., 1993) (LU et al., 2001)
$V0_{LV}$	ml	5	0	71.44	(LU et al., 2001) (URSINO et al., 2000)
λ_{LV}	ml^{-1}	0.015	0.014	0.1	(LUO et al., 2011) (URSINO et al., 2000)
$P0_{LV}$	mmHg	1.2751	0.2	4	(BURKHOFF et al., 1993) (LUO et al., 2011)
E_{RV}	mmHg·ml^{-1}	0.6526	0.34	2.87	(DAVIS, 1991) (DELL'ITALIA et al., 1988)
Vd_{RV}	ml	5	0	89	(BURKHOFF et al., 1993) (HELDT, 2004)
$V0_{RV}$	ml	5	0	89	(LU et al., 2001) (URSINO et al., 2000)
λ_{RV}	ml^{-1}	0.015	0.01	0.06	(CHUNG et al., 1997)
$P0_{RV}$	mmHg	1	0.35	1.2	(BURKHOFF et al., 1993) (SMITH et al., 2004)

References

Burkhoff, D. and J. V. Tyberg (1993). "Why does pulmonary venous pressure rise after onset of LV dysfunction: a theoretical analysis". In: *American Journal of Physiology-Heart and Circulatory Physiology* 265.5, H1819–H1828.

Chung, D., S. Niranjan, J. Clark, A. Bidani, W. Johnston, J. Zwischenberger, and D. Traber (1997). "A dynamic model of ventricular interaction and pericardial influence". In: *American Journal of Physiology-Heart and Circulatory Physiology* 272.6, H2942–H2962.

Davis, T. L. (1991). "Teaching physiology through interactive simulation of hemodynamics". PhD thesis. Massachusetts Institute of Technology.

Dell'italia, L. J. and R. A. WALSH (1988). "Application of a time varying elastance model to right ventricular performance in man". In: *Cardiovascular research* 22.12, pp. 864–874.

Heldt, T. (2004). "Computational models of cardiovascular response to orthostatic stress". PhD thesis. Massachusetts Institute of Technology.

Korakianitis, T. and Y. Shi (2006). "A concentrated parameter model for the human cardiovascular system including heart valve dynamics and atrioventricular interaction". In: *Medical engineering & physics* 28.7, pp. 613–628.

Le Rolle, V., A. I. Hernández, P.-Y. Richard, and G. Carrault (2008). "An autonomic nervous system model applied to the analysis of orthostatic tests". In: *Modelling and Simulation in Engineering* 2008, p. 2.

Lu, K., J. Clark, F. Ghorbel, D. Ware, and A. Bidani (2001). "A human cardiopulmonary system model applied to the analysis of the Valsalva maneuver". In: *American Journal of Physiology-Heart and Circulatory Physiology* 50.6, H2661.

Luo, C., D. Ramachandran, D. L. Ware, T. S. Ma, and J. W. Clark (2011). "Modeling left ventricular diastolic dysfunction: classification and key indicators". In: *Theoretical Biology and Medical Modelling* 8.1, p. 14.

Roossien, A., J. R. Brunsting, A. Nijmeijer, J. Zaagsma, and W. G. Zijlstra (1997). "Effects of vasoactive intestinal polypeptide on heart rate in relation to vagal cardioacceleration in conscious dogs". In: *Cardiovascular research* 33.2, pp. 392–399.

Smith, B. W., J. G. Chase, R. I. Nokes, G. M. Shaw, and G. Wake (2004). "Minimal haemodynamic system model including ventricular interaction and valve dynamics". In: *Medical engineering & physics* 26.2, pp. 131–139.

Ursino, M. and E. Magosso (2000). "Acute cardiovascular response to isocapnic hypoxia. I. A mathematical model". In: *American Journal of Physiology-Heart and Circulatory Physiology* 279.1, H149–4165.

Van Roon, A. M., L. J. Mulder, M. Althaus, and G. Mulder (2004). "Introducing a baroreflex model for studying cardiovascular effects of mental workload". In: *Psychophysiology* 41.6, pp. 961–981.

List of Figures

List of Tables